Cosmic Origins Spectrograph (COS)
Science Operations Requirements Document
(OP-01)

Date:	March 17, 2004
Document Number:	COS-01-0001
Revision:	Initial Release
Contract No.:	NAS5-98043
CDRL No.:	OP-01

Prepared By: ______________________________ ____________
J. Morse, COS Project Scientist, CU/CASA — Date

Reviewed By: ______________________________ ____________
E. Wilkinson, COS Instrument Scientis, CU/CASA — Date

Reviewed By: ______________________________ ____________
K. Brownsberger, COS Experiment Manager, CU/CASA — Date

Approved By: ______________________________ ____________
T. Keyes,COS Instrument Scientist, STScI — Date

Approved By: ______________________________ ____________
J. Green, COS Principal Investigator, CU/CASA — Date

Approved By: ______________________________ ____________
T. LaJeunesse, Cos Program Manager, BATC — Date

Center for Astrophysics & Space Astronomy
University of Colorado
Campus Box 593
Boulder, Colorado 80309

REVISIONS

Letter	ECO No.	Description	Check	Approved	Date
1	COS-042	Pre-release ECO changes.		EW	10-10-00
2	COS-044	Pre-release ECO changes.		EW	10-23-00
3	COS-047	Pre-release ECO changes.		EW	1-2-01
4	COS-048	Pre-release ECO changes.		EW	1-3-01
5	COS-049	Pre-release ECO changes.		EW	1-9-01
6	COS-050	Pre-release ECO changes.		EW	1-12-01
7	COS-051	Pre-release ECO changes.		EW	1-17-01
8	COS-055	Pre-release ECO changes.		EW	1-24-01
9	COS-056	Pre-release ECO changes.		EW	2-7-01
10	COS-057	Pre-release ECO changes.		EW	2-13-01
11	COS-058	Pre-release ECO changes.		EW	3-6-01
12	COS-059	Pre-release ECO changes.		EW	3-13-01
13	COS-061	Pre-release ECO changes.		EW	4-5-01
14	COS-062	Pre-release ECO changes.		EW	5-3-01
15	COS-063	Pre-release ECO changes.		EW	6-4-01
16	COS-069	Pre-release ECO changes.		EW	10-2-01
17	COS-070	Pre-release ECO changes.		EW	2-7-02
18	COS-075	Pre-release ECO changes.		EW	7-18-02
19	COS-081	Pre-release ECO changes		EW	11-21-02
20	COS-082	Pre-release ECO changes		EW	1-14-03

Original Release Name	Date
Drawn: J. Morse	8-1-00
Reviewed:	
Approved:	

THE UNIVERSITY OF COLORADO
At Boulder
The Center for Astrophysics and Space Astronomy

Cosmic Origins Spectrograph (COS)
Science Operations Requirements Document
(OP-01)

Size	Code Indent No.	Document No.	Rev
A		COS-01-0001	-
Scale: N/A			

REVISIONS					
Letter	ECO No.	Description	Check	Approved	Date
21	COS-083	Pre-release ECO changes		EW	2-12-03
22	COS-083	Pre-release ECO changes		EW	2-24-03
23	COS-086	Pre-release ECO changes		EW	5-23-03
-	COS-087	Initial Release with ECO changes			

Original Release Name	Date	
Drawn: J. Morse	8-1-00	
Reviewed:		
Approved:		

THE UNIVERSITY OF COLORADO

At Boulder

The Center for Astrophysics and Space Astronomy

Cosmic Origins Spectrograph (COS)
Science Operations Requirements Document
(OP-01)

Size	Code Indent No.	Document No.	Rev
A		COS-01-0001	-
Scale: N/A			

Table of Contents

1. INSTRUMENT OVERVIEW 1
1.1 Science Overview 1
1.2 HST after SM4 2
1.3 Operational Design Characteristics 3
1.3.1 Science Operations Summary 7
1.3.2 COS FUV Channel 7
1.3.3 COS NUV Channel 11
1.3.4 Science and Calibration Apertures 16
1.3.5 Sensitivities, Coordinate Systems, and Plate Scale Summary 20
2. MECHANISMS AND LAMPS 28
2.1 Mechanisms 28
2.1.1 External Shutter 28
2.1.1.1 External Shutter Motor Drive and Position Sensing 28
2.1.1.2 External Shutter FSW Macro Control 30
2.1.2 Aperture Mechanism (ApM) 31
2.1.2.1 Aperture Mechanism Motor Drive and Position Sensing 32
2.1.2.2 ApM Motor Operating Constraints 34
2.1.2.3 APM FSW Macro Control 34
2.1.2.3.1 Initialize Aperture Mechanism Macro 34
2.1.2.3.2 Move Aperture Mechanism to Relative Position Macro 35
2.1.2.3.3 Move ApM to Absolute Position Macro 35
2.1.2.4 ApM Home Commanding 36
2.1.3 Optics Select Mechanism 1 (OSM1) 36
2.1.4 Optics Select Mechanism 2 (OSM2) 38
2.1.5 OSM Motor Drive and Position Sensing 40
2.1.5.1 OSM Motor Operating Constraints 42
2.1.5.2 OSM FSW Macro Control 42
2.1.5.2.1 Initialize Optic Select Mechanism Macro 43
2.1.5.2.2 Move Optic Select Mechanism to Relative Position Macro 44
2.1.5.2.3 Move OSM to Absolute Position Macro 44
2.1.5.3 OSM Home Commanding 44
2.1.6 Overheat Protection 44
2.1.6.1 Overheat Protection Provided by the Electronics 45
2.1.6.2 FSW Interface 46
2.1.6.3 Special Overheat Protection Notes 46
2.1.6.4 Motor Winding Relays 46
2.2 On-board Calibration Lamps 47
2.2.1 Safe and Efficient Operations 50
2.2.2 Wavelength Calibration Lamp 51

2.2.3 Flat-Field Calibration Lamp 56
2.3 Vacuum Sensing System 60
3. ELECTRONICS AND FLIGHT SOFTWARE 61
3.1 Overview 61
3.1.1 Block Diagrams of the FSW and Electronics 61
3.1.2 High Level Description of Functions 65
3.1.2.1 COS AP (Application Processor) FSW 65
3.1.2.2 CS (Control Section) FSW 65
3.1.2.3 MCE (MAMA Control Electronics) FSW 65
3.1.2.4 DCE (XDL Detector Control Electronics) FSW 66
3.1.3 DIB (Detector Interface Board) FSW 66
3.2 Science Data Buffer Management 66
3.2.1 Buffer Management during Time-Tag Exposures 68
3.2.1.1 Flight Software Processing 68
3.2.1.2 Ground System Modeling and Dump Commanding 69
3.2.2 Science Data Header Format 71
3.3 Memory Dumps 73
3.4 Engineering Diagnostic Data 73
3.5 Doppler Correction 73
3.6 Bright Object Protection 74
4. DETECTORS 74
4.1 FUV XDL Detector 74
4.1.1 Overview of FUV Detector 74
4.1.2 Detector Subsystem Components 78
4.1.2.1 Detector Vacuum Assembly (DVA) 78
4.1.2.1.1 Detector Body Assembly 78
4.1.2.1.2 Brazed Detector Body 78
4.1.2.1.3 Photocathode Material 78
4.1.2.1.4 Microchannel Plates 78
4.1.2.1.5 Quantum Detection Efficiency Grid 79
4.1.2.1.6 Delay Line Anodes 80
4.1.2.1.7 Detector Door Mechanism 80
4.1.2.1.8 Ion Repeller Grid 80
4.1.2.1.9 High Voltage Filter Module (HVFM) 80
4.1.2.2 Detector Electronics Box (DEB) 81
4.1.2.2.1 Detector Control Electronics (DCE) 81
4.1.2.2.2 Time to Digital Converters (TDCs) and Stim Pulses 81
4.1.2.2.3 Low Voltage Power Converter (LVPC) 82
4.1.2.2.4 High Voltage Power Supply (HVPS) 83
4.1.3 Normal Detector Operations 83
4.1.3.1 Operating Parameters 85

4.1.3.2 Housekeeping Data ... 85
4.1.4 Autonomous Operations ... 87
4.1.4.1 Power-on Reset (POR) ... 87
4.1.4.2 Watchdog Reset (WDR) ... 87
4.1.4.3 Other Resets ... 87
4.1.4.4 HV Overcurrent Protection ... 87
4.1.4.5 Count Rate Protection ... 88
4.1.4.6 Other Autonomous Operations ... 89
4.1.4.6.1 Autonomous Door Operations ... 89
4.1.4.6.2 Background memory checking ... 90
4.1.5 Bright Object Protection ... 90
4.1.6 Thermal Runaway of Microchannel Plate Detectors ... 92
4.1.7 Detector Pulse Height Diagnostic Data ... 93
4.1.7.1 Ground processing of pulse height data in time tag science data ... 93
4.1.7.2 Ground processing of pulse height histograms ... 94
4.2 NUV MAMA Detector ... 94
4.2.1 Detector Overview ... 94
4.2.2 Detector Subsystem Components ... 96
4.2.2.1 MAMA Detector Tube ... 96
4.2.2.1.1 Microchannel Plate ... 96
4.2.2.1.2 Coded Anode Array and Multi-layer Ceramic Header ... 97
4.2.2.1.3 MgF_2 Window and Photocathode ... 98
4.2.2.1.4 Ceramic-Kovar Tube Body ... 98
4.2.2.2 Detector Electronics ... 99
4.2.2.2.1 Charge Amplifier-Discriminator Assembly ... 99
4.2.2.2.2 LVPS ... 100
4.2.2.2.3 HVPS ... 100
4.2.2.2.4 Decoder ... 100
4.2.2.2.5 MAMA Control Electronics (MCE) ... 101
4.2.3 Operational Modes and Transition Sequences ... 101
4.2.3.1 MAMA Mode: HOLD ... 102
4.2.3.2 MAMA Mode: LVON ... 102
4.2.3.3 MAMA Mode: HVON ... 102
4.2.3.4 MAMA Mode: HVSAA ... 103
4.2.3.5 First Time On-orbit Turn-on ... 104
4.2.3.6 Anomalous Recovery Turn-on ... 104
4.2.3.7 Precautions ... 105
4.2.3.8 Bright Object Protection ... 105
5. OBSERVING STRATEGIES ... 106
5.1 On-orbit Alignments and Calibrations ... 106
5.1.1 Initial Alignment aboard HST ... 106

5.1.1.1 NUV Initial Alignment 107
5.1.1.2 FUV Initial Alignment 111
5.1.1.2.1 Confirm OSM1 Positions Using Internal Pt-Ne lamps 111
5.1.1.2.2 Calibrate V2,V3 Coordinates of PSA 111
5.1.1.2.3 Refine Target Position for Optimum FUV Performance 111
5.1.1.2.4 Refine OSM1 "Δz" Position for Optimum FUV Resolution 112
5.1.1.2.5 Verify Alignment of the Aperture Mechanism 112
5.1.2 HST Secondary Mirror Adjustments 114
5.2 Target Acquisition Procedures 114
5.2.1 COS Autonomous Target Acquisition 114
5.2.1.1 Dispersed Light Target Acquisition 119
5.2.1.2 Imaging Target Acquisition with the TA1 Mirror 121
5.2.2 Sub-arrays for Target Acquisition 125
5.2.2.1 FUV TA Sub-arrays 125
5.2.2.2 NUV TA Sub-arrays 130
5.2.2.3 NUV TA1 Imaging TA Sub-arrays 132
5.2.3 Camera Assisted Acquisitions 134
5.3 Science Observations 134
5.3.1 Time-tag Mode 134
5.3.1.1 Doppler Correction for Time-tag Science Observations 135
5.3.1.2 Sub-arrays for Time-tag Exposures 135
5.3.1.3 Pulse-Height Distribution Data for Time-tag Mode Observations 136
5.3.2 Accum Mode 136
5.3.2.1 Doppler Correction for Accum Mode Science Observations 136
5.3.2.2 Sub-arrays for Accum Mode Science Observations 137
5.3.2.3 Pulse-Height Distribution Data for Accum Mode Observations 138
5.3.3 FUV Gap Coverage 139
5.3.4 Selectable Stim Pulse Rates for the FUV Detector 139
5.3.5 Detector Lifetime Adjustments 140
5.3.5.1 Microchannel Plate Gain Diagnostics & Spectral Adjustment Strategies141
5.3.6 Aperture Mechanism Motions when Using the BOA 145
5.3.7 FUV Single Segment Operational Scenarios 146
5.3.8 FP-SPLITs 147
5.3.9 NUV Imaging Observations 148
5.4 Calibrations 152
5.4.1 Wavelength Calibration 152
5.4.2 Flat-field Calibration 153
5.4.3 Signal-to-Noise Ratio 153
5.4.4 Sensitivity Calibration 154
5.4.5 Dark Count Rates 154

1. INSTRUMENT OVERVIEW

1.1 SCIENCE OVERVIEW

COS will bring the diagnostic power of ultraviolet spectroscopy to bear on such fundamental issues as the ionization and baryon content of the intergalactic medium and the origin of large-scale structure in the Universe; the ages, dynamics, and chemical enrichment of galaxies; and stellar and planetary origins. This frontier science program critically depends on having the capability to obtain moderate resolution ($R \geq 20{,}000$) spectroscopic observations of faint UV sources, such as distant quasars. Hence, the driving priority behind the COS instrument design is to optimize the spectrograph for maximum throughput.

COS will be, by a large factor, the most sensitive UV spectrograph ever flown aboard HST. Compared to modes of comparable spectral resolution on previous HST UV spectrographs, COS is ~8-10 times more sensitive in the wavelength range 1150 - 1775Å, and ~2 times more sensitive over the wavelength range 1750 - 3200Å. In the ultraviolet, maximizing sensitivity implies minimizing the number of optical components, and leads to an inherently simple design. The unique capabilities of COS derive from a fundamentally different design approach, and not from new technology. COS will build on the legacies of previous UV missions and instruments, such as Copernicus, IUE, GHRS, FOS, STIS, and FUSE, giving HST the greatest possible grasp of faint UV targets and ensuring that Hubble maintains a powerful UV spectroscopic capability from SM4 until the end of its mission.

The COS scientific investigation addresses questions of fundamental importance in astrophysics and cosmology which require the moderate spectral resolution and high throughput of COS, and four unique capabilities of HST: access to ultraviolet wavelengths, large collecting area, precise pointing stability, and excellent image quality. Our study is organized into three broad categories, united by the theme of cosmic origins: (1) the origin of large-scale structure and the intergalactic medium (IGM); (2) the formation, evolution, and ages of galaxies; and (3) the origins of stellar and planetary systems.

Models for the formation of large-scale structure and the reionization of the IGM will be constrained by observing distant quasars to measure the He II Gunn-Peterson effect, the structure of the Lyman α forest, and the D/H ratio and metallicity in primordial clouds. COS will be capable of obtaining moderate-resolution UV spectra of hundreds more quasars and AGNs than existing UV instruments. The COS database of absorption-line systems will have sufficient spectral resolution and signal-to-noise to determine accurate column densities, abundances, and kinematics of intergalactic matter at epochs when the first galaxies were formed and the first heavy elements were synthesized.

COS will be used to determine abundances and kinematics of hot gas in galaxy halos, gauge the impact of violent starbursts and supernovae on interstellar and intergalactic environments, and refine the ages of globular clusters. The numerous quasar sight-lines accessible to COS will intersect hot galaxy halos over a large redshift range. COS spectra will constrain galaxy evolution models by mapping the production of metal-enriched gas through time. We will also observe nearby starbursting systems over a range of metallicity. These spectra will be used to model the chemical enrichment of the interstellar medium (ISM), and will serve as templates for deriving the properties of high-z galaxies. COS UV spectra of horizontal-branch stars in globular clusters will allow significant refinement of globular cluster age estimates. We will attempt to reconcile the ages of the oldest stars in galaxies with the age of the Universe derived from recent measurements of the Hubble constant and closure parameter.

The origins of stellar and planetary systems will be investigated by studying the physical processes and chemical abundances in the cold ISM. For the first time in the UV, COS will observe sight-lines toward hot, embedded stars that probe dense, molecular regions where the star formation process begins. COS data will also provide clues to the conditions and composition of the outer solar nebula. The high sensitivity of COS will allow an order of magnitude more background stars to be observed in stellar occultation studies of planetary and cometary atmospheres. COS will break new ground with direct moderate-resolution UV observations of Pluto and Triton that will be used to detect fluorescence emission from volatile gases, as these bodies both undergo rare seasonal changes during the first decade of the next century.

Our investigation requires observations of very faint targets, taking full advantage of HST capabilities (large aperture, UV coatings, excellent pointing, and image quality). COS is optimized to observe faint UV sources with spectral resolution high enough to determine the physical conditions in a broad range of astrophysical environments. Its design meets programmatic requirements for reliability and redundancy, and its simplicity and efficient operation ensure a high science return. With these capabilities, we anticipate a high degree of interest in using COS throughout the worldwide astronomical community.

1.2 HST after SM4

The HST servicing missions of 1993, 1997, 1999, and 2001 (SM1, SM2, SM3a, and SM3b) met with great success. New instruments (WFPC2, STIS, NICMOS, ACS) have replaced first generation instruments (WF/PC, FOS, GHRS, FOC); the wavelength domain covered by HST has been extended into the near-IR; and several other improvements such as new solar arrays, gyros, FGS units, and a Solid State Recorder that has dramatically increased the data storage capacity of HST, have been implemented.

The final planned HST servicing mission (SM4) is currently scheduled for 2005, when COS and the Wide Field Camera 3 (WFC3) will be installed. COS will be placed into the axial bay currently occupied by COSTAR, which, after SM3b, will no longer be in use. WFC3 will replace WFPC2 in a radial bay, and will provide a back-up imaging capability to ACS as well as unique narrow-band and near-UV imaging science. WFC3's near-IR channel will also provide a unique imaging capability in the *J* and *H* bands. From SM4 until 2010 (the projected end of the HST mission), the HST focal plane will include the following instruments for imaging and spectroscopic studies of the universe: ACS, WFC3, NICMOS, STIS, and COS.

STIS provides a powerful spectroscopic capability for investigating point-like and extended objects over UV and visible wavelengths. At this time, STIS is functioning as expected (better than expected in some areas), except for the following items: (1) the opto-isolator relays suffer resets due to cosmic ray hits (the same is true for the relays on NICMOS; these relays will be fixed on COS in the same manner as they were fixed for ACS); and (2) the near-UV (NUV) MAMA detector has a higher than expected background rate, due to phosphorescence of impurities in the detector window in the on-orbit radiation environment. (The back-up STIS NUV MAMA flight unit will be used in COS as the NUV detector. This Band 2 MAMA is expected to have a background count rate ~ 1/4 of the STIS NUV MAMA.) COS will provide some redundancy to STIS spectroscopic modes, and will restore scientific capability that may be compromised by the high background rate of the STIS NUV MAMA. But mostly COS will represent the frontier instrument aboard HST for UV spectroscopy of faint sources in the most distant reaches of the Universe.

1.3 Operational Design Characteristics

COS offers dramatic improvement in sensitivity to faint objects over previous UV spectroscopic instruments flown aboard HST. COS achieves high sensitivity, particularly in the FUV, by minimizing the number of reflections, which leads to an inherently simple design. Because the unique capabilities of COS derive from a fundamentally different design approach, and not from new technology, we are able to provide an instrument with flight heritage in all of its critical areas: optics, detectors, electronics, software, etc.

In designing COS, we have assumed that STIS will continue to work well. COS is not intended to duplicate the powerful capabilities of STIS for observing bright or extended sources. COS does not have many "bells and whistles," but the capabilities of COS are unique. The order-of-magnitude gains in UV sensitivity over STIS and previous UV spectrographs will open a huge volume of discovery space. Figure 1.3-1 shows an isometric drawing of the COS instrument and Fig. 1.3-2 shows the optical bench assembly, each with important features and mechanisms labeled.

The mechanisms and lamps are described in detail in Sec. 2, and the detectors are described in Sec. 4. Briefly, a cross-delay line (XDL) detector is used in the FUV channel, and a MAMA in the NUV channel. The aperture mechanism translates in two degrees of freedom for positioning the COS apertures in the HST focal plane. The OSM1 mechanism contains the FUV gratings and a mirror that feeds the NUV channel. The OSM1 rotates to position the desired optic in the optical beam path. Small rotations move the spectrum in the dispersion direction on the FUV detector. The OSM1 also translates toward or away from the HST secondary in order to provide focus and alignment. The OSM2 mechanism holds the NUV gratings and a target-alignment mirror. The OSM2 has one degree of freedom (rotation) for selecting the desired optic and for moving the spectrum in the dispersion direction on the NUV detector.

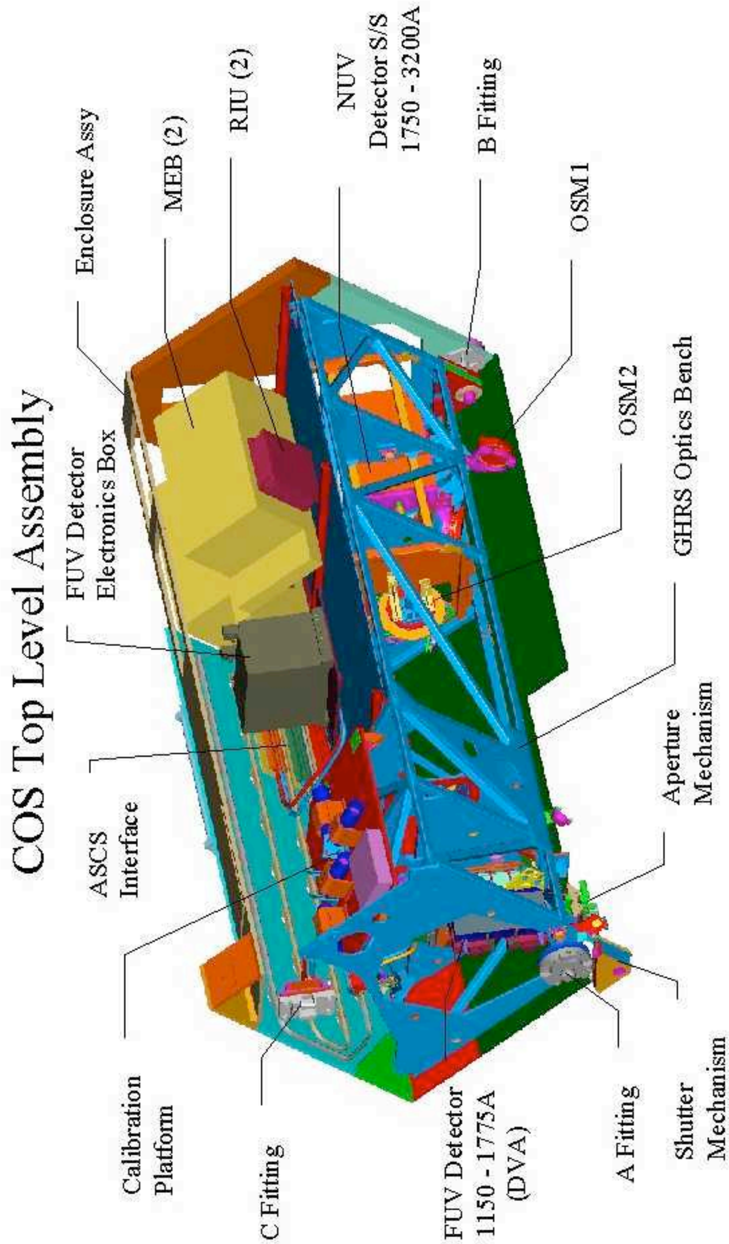

Figure 1.3-1: *Isometric drawing of the COS top level assembly. The various mechanisms, detector and calibration sub-systems, electronic boxes, and fittings are labeled.*

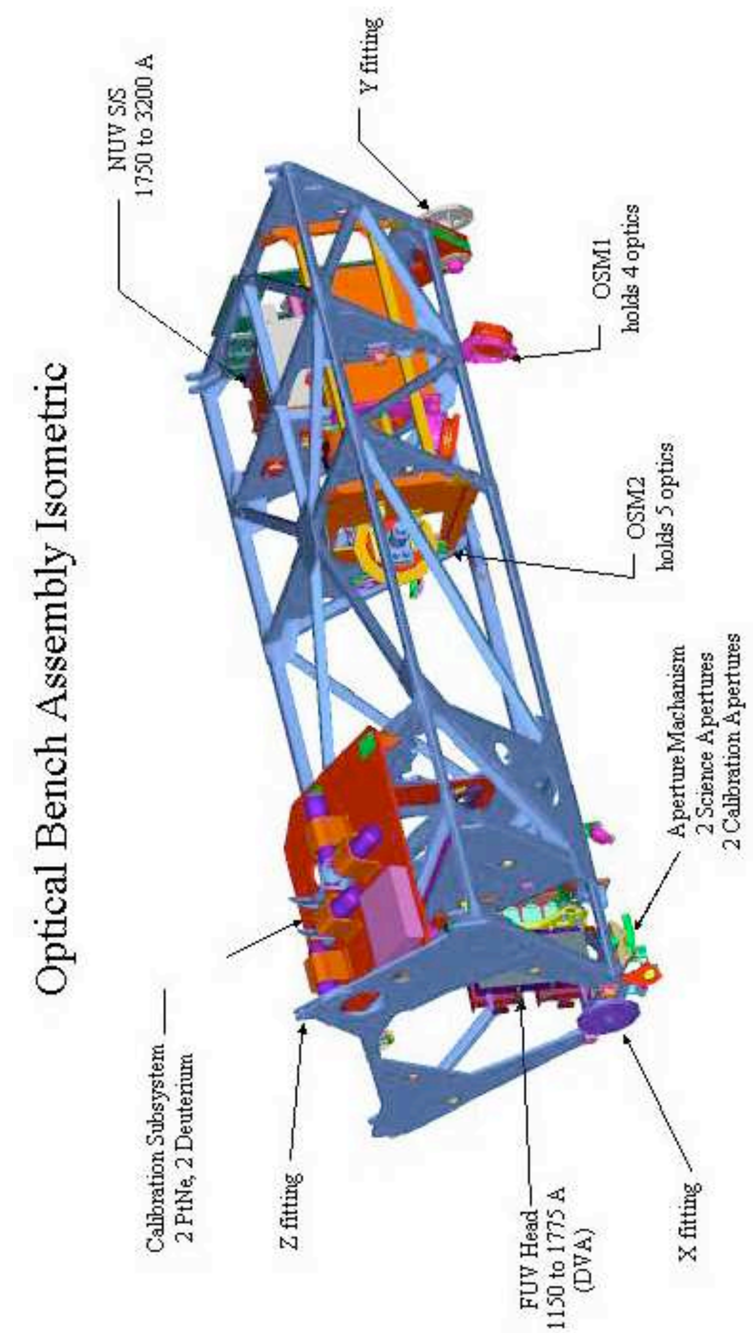

Figure 1.3-2: *Isometric drawing of the COS optical bench assembly. The FUV and NUV detector sub-systems, calibration platform sub-system, and mechanisms are labeled.*

1.3.1 Science Operations Summary

COS has two channels: a far-UV (FUV) channel that covers (at R ≥ 20,000 spectral resolution) the 1150 - 1775Å wavelength region, and a near-UV (NUV) channel that covers the 1750 - 3200Å wavelength region. Each channel has its own detector and selection of gratings (see Sections 1.3.2 and 1.3.3). The two channels cannot make parallel observations, as the NUV channel is fed by an optic on the FUV optics select mechanism. In general, an observer will specify a target, its coordinates, an exposure time, and then select which channel (COS/FUV or COS/NUV), which aperture (PSA or BOA), and which grating (G130M, G160M, G140L; G185M, G225M, G285M, G230L) to use.

The observer will also specify the central wavelength of the exposure. The central wavelength will be chosen from a table of pre-set values designated for each grating. These values will allow any region of interest in the entire 1150 – 3200 Å wavelength region to be covered. The NUV gratings, in particular, are flat gratings mounted in a collimated beam that are meant to be scanned in order to achieve wide wavelength coverage (due to the Czerny-Turner optical design). The FUV gratings, on the other hand, each cover about 300Å per exposure. They will operate at only a few central wavelength settings. Some wavelengths fall within the FUV "detector gap" (see Sections 2, 4, and 5.3) at a particular setting and are lost. So the FUV gratings will have a limited set of alternate central wavelength positions that make it possible to shift the spectrum on the detector in order to recover the needed wavelengths.

1.3.2 COS FUV Channel

The COS FUV channel covers the wavelength range 1150 – 1775Å at moderate spectral resolution. The FUV channel employs concave diffraction gratings and a curved detector. It is fundamentally a Rowland spectrograph, modified to meet the specific needs of HST. There is one reflection between the aperture and the detector. The gratings have aspheric concave surface figures specified to compensate for spherical aberration. Holographically generated grooves provide dispersion and correct the astigmatism. Ion-etching creates a blaze that optimizes the grating efficiency over a narrow range of wavelengths. Two gratings, G130M and G160M, are used to cover the range 1150 – 1775Å wavelength range at medium resolution ($R = \lambda/\Delta\lambda$ = 20,000 – 24,000). Each medium-dispersion grating covers roughly 300Å in one exposure. A third grating, G140L, can be used to observe the 1230 – 2050Å region at lower resolution (R = 2500 – 3500). The short wavelength cut-off of the low-dispersion grating is designed to avoid bright geocoronal Lyman α emission at 1216Å by placing it on the XDL detector gap.

The three FUV gratings are mounted on a rotating mechanism, designated Optics Select Mechanism 1 (OSM1). The full spectrum from each grating mode appears on the XDL as a single stripe across the two detector segments. Although the nominal wavelength range of the G140L spectrum is 1230 – 2050Å, this spectrum takes up only part of one detector segment. The grating actually directs light out to 2400Å onto this detector segment, but the XDL sensitivity to these longer wavelengths is extremely low. On the other detector segment, the G140L grating disperses light between ~100 – 1100Å. Again the sensitivity to these wavelengths is very low, limited in this case by the reflectance of the OTA mirrors and COS optics. Calculations predict that the effective area below 1150Å plummets rapidly but is not zero.

The detector is a windowless microchannel-plate (MCP) array, with an opaque CsI photocathode, and a cross delay-line (XDL) readout that has been adapted from the FUSE mission detectors (see Section 4). Figure 1.3-3 shows the optical light path of the COS FUV channel within the instrument, Fig. 1.3-4 shows a stick-figure layout of the FUV optical path, and Table 1.3-1 summarizes the FUV spectroscopic modes.

Figure 1.3-3: *The COS FUV optical light path. The light received from the HST OTA through the aperture (lower left in the figure) is dispersed and focused by a concave diffraction grating (lower right) to the FUV XDL detector.*

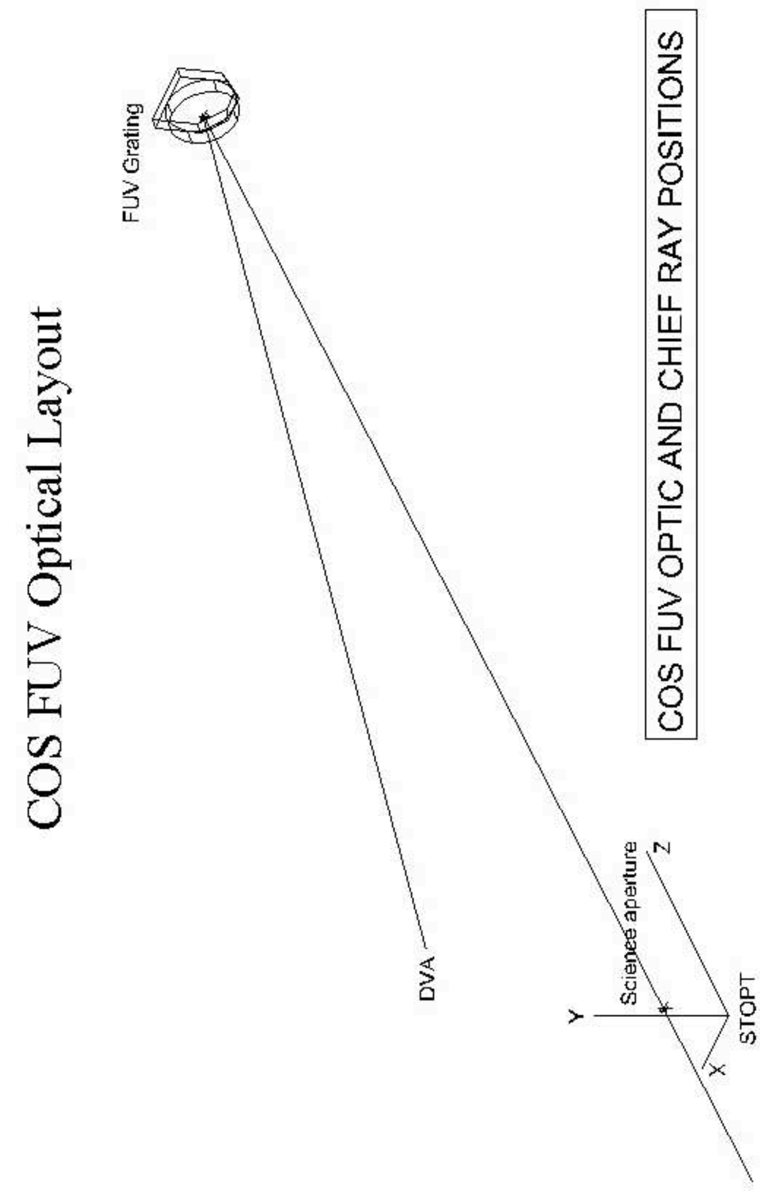

Figure 1.3-4: *Layout of the COS FUV optical light path. "DVA" stands for Detector Vacuum Assembly, which is the FUV detector head that records the photon events.*

Table 1.3-1: COS FUV Spectroscopic Modes

Grating	Nominal Wavelength Range[a]	λ Coverage per Exposure	Dispersion (Å/pixel)	Resolving Power ($R = \lambda/\Delta\lambda$)[b]
G130M	1150 – 1450 Å	300 Å	~0.0094	20,000 – 24,000
G160M	1405 – 1775 Å	370 Å	~0.0118	20,000 – 24,000
G140L	1230 – 2050 Å	> 820 Å	~0.0865	2500 – 3500

[a] Nominal Wavelength Coverage is the expected usable spectral range delivered by each grating mode. As describe in the text, the G140L disperses the ~100 – 1100Å region onto one segment and 1230 – 2400Å onto the other. The sensitivity to wavelengths outside the 1230 – 2050Å region will be very low.
[b] The lower values of the Resolving Power are delivered at the shortest wavelengths covered, and the higher values at longer wavelengths. The resolution increases roughly linearly between the short and long extremes of the nominal wavelength range covered by each grating mode.

1.3.3 COS NUV Channel

The COS NUV channel covers the wavelength range 1700 – 3200 Å at moderate spectral resolution. The NUV channel is fundamentally a Czerny-Turner design, fed by a mirror (NCM1) mounted on the OSM1. The NCM1 corrects the input beam for spherical aberration, magnifies it by a factor of ~4, and directs it to a collimating optic, NCM2. The collimated beam is then directed to one of several gratings mounted in the Optics Select Mechanism 2 (OSM2). The OSM2 contains several flat, first-order gratings and a mirror (TA1). Three medium-dispersion gratings, G185M, G225M, and G285M, deliver resolutions R ≥ 16,000 over the wavelength range 1700 – 3200 Å. The dispersed light from the gratings is imaged onto a CsTe MAMA detector by three camera optics (NCM3a, b, c). The spectra appear as three non-contiguous ~35-40Å stripes on the MAMA detector, allowing ~105-120Å wavelength coverage per exposure. The gratings can be scanned with slight rotations of the OSM2 to cover the entire NUV wavelength band. The NCM3a,b,c mirrors are spaced such that three exposures will produce a continuous spectrum from the beginning of the short wavelength stripe in the first exposure to the end of the long wavelength stripe in the third exposure. In other words, two intermediate grating settings will cover the wavelength gap between the stripes in the first exposure, as depicted in Fig. 1.3-5.

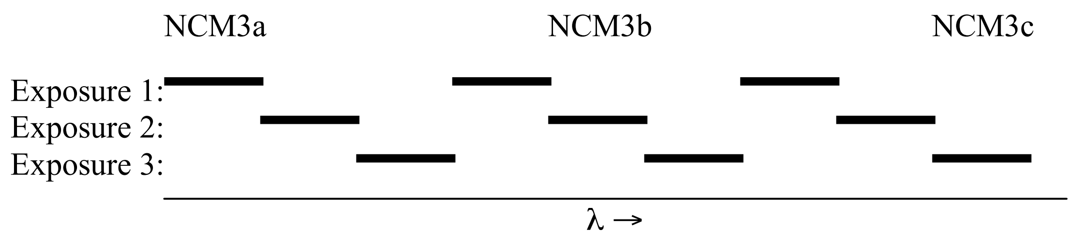

Figure 1.3-5: *An illustration of the wavelength coverage of the R = 20,000 spectral modes of the COS NUV channel. Three spectral stripes are recorded per exposure. (The actual format of the stripes on the detector is shown in Fig. 1.3-15.) Two additional exposures at intermediate grating scan positions cover the wavelength gap between the stripes in the first exposure (with some overlap).*

A low-dispersion grating, G230L, delivers ~398Å coverage per stripe with a resolution of ~1.1Å (R = 1550 – 2900). The 1st-order science spectrum from G230L over the 1700 – 3200Å region is captured in three separate exposures using four spectral stripes on the detector. The optical design places 1700Å at the beginning of the first stripe A and 3200Å at the end of the second stripe B of a single exposure. Three exposures will be required for complete, contiguous coverage of the 1700-3200 Å region, with some overlap between each exposure. Wavelengths covered by the G230L exposures are shown in Table 1.3-2.

Table 1.3-2: COS G230L Wavelength Coverage

Central Wavelength Of Stripe B	**Stripe A**	**Stripe B**	**Stripe C (2nd order)**
2635 Å	1334 – 1733 Å	**2435 – 2834 Å**	(1768 – 1967 Å)
2950 Å	**1650-2050 Å**	**2750-3150 Å**	(1900 – 2100 **Å)**
3000 Å	**1700 – 2100 Å**	**2800 – 3200 Å**	(1950 – 2150 Å)
3360 Å	**2059 – 2458 Å**	3161 – 3560 Å (2nd order: 1580 – 1780 Å)	(2164 – 2361 Å)

Note: Wavelengths in bold type are the nominal first-order wavelengths of interest. The “2635”, “3000”, and “3360” wavelength settings together provide a contiguous first-order spectrum covering 1700-3200Å.

Over the FUV wavelengths the NUV MAMA detector actually has a QE of several percent, and 2nd-order light from the FUV could appear on the detector with some gratings. To eliminate this 2nd-order light, the coatings on the NUV optics are optimized for wavelengths >1600Å, but will have poor throughput at FUV wavelengths. The four optical bounces in the NUV channel will therefore effectively reduce unwanted 2nd-order light, such as from Lyman α airglow. In addition, the G285M and G230L gratings will have order blocking filters mounted directly to the gratings in order to block the 2^{nd}-order blue spectra below ~1700Å. Even so, Table 1.3-2 shows the G230L 2^{nd}-order light that will appear on the NUV detector in each of the G230L exposures, especially in the long wavelength stripe C. The 2^{nd}-order spectra will have low sensitivity due to the detected wavelengths being so far off the 2^{nd}-order blaze, but the spectral resolution will be twice as high and may yield useful data in some circumstances. The 2^{nd}-order throughput should be measured during ground calibration and SMOV, and the extra photons should be included in count rate estimates during bright object screening. Wavelengths longer than 3200Å that project onto the detector will have very low throughput due to the poor sensitivity of the CsTe photocathode in the NUV MAMA detector.

Figure 1.3-6 shows the COS NUV optical light path within the instrument, and Fig. 1.3-7 displays a stick-figure layout of the NUV light path. Table 1.3-3 summarizes the NUV spectroscopic modes. The NUV MAMA operations are further discussed in Section 4.2.

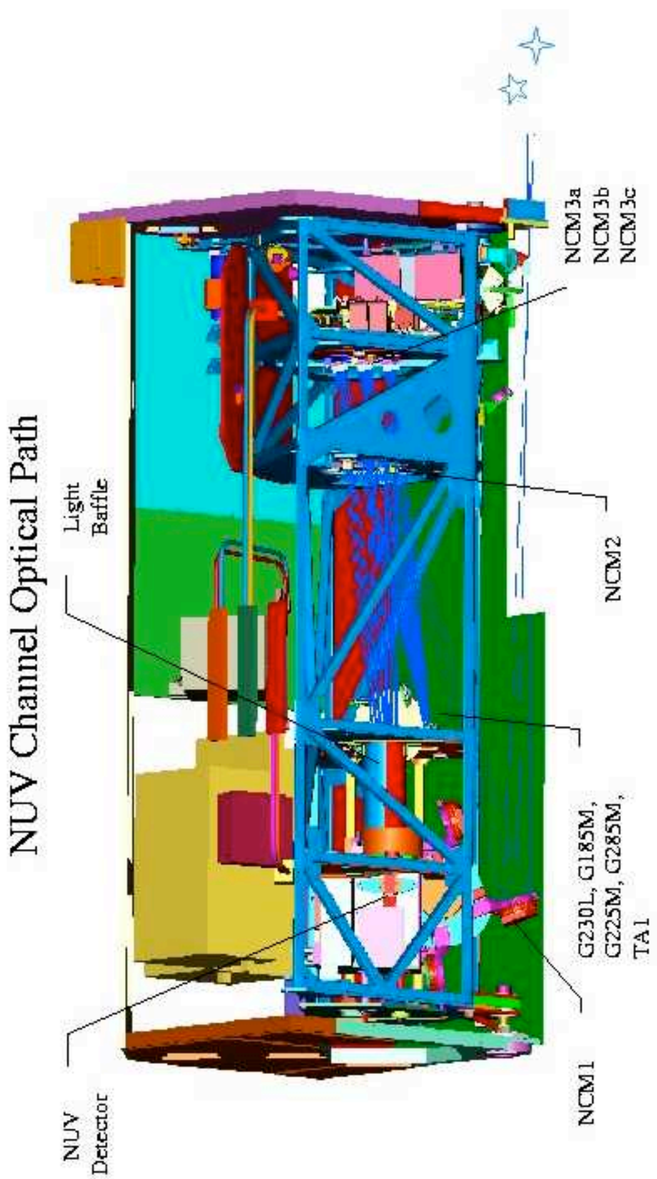

Figure 1.3-6: *The COS NUV optical light path. Light is received through the aperture (lower right in the figure; reverse view from Fig. 1.3-3) from the HST OTA and is reflected and magnified by the NCM1 mirror on OSM1 (lower left). The light then strikes the NCM2 collimating mirror mounted on a bulkhead ~1-ft in front of the XDL detector head. The collimated light is directed to the flat gratings on the OSM2 (near center). The dispersed light is captured by three camera optics (NCM3a,b,c) and focused onto the NUV MAMA detector.*

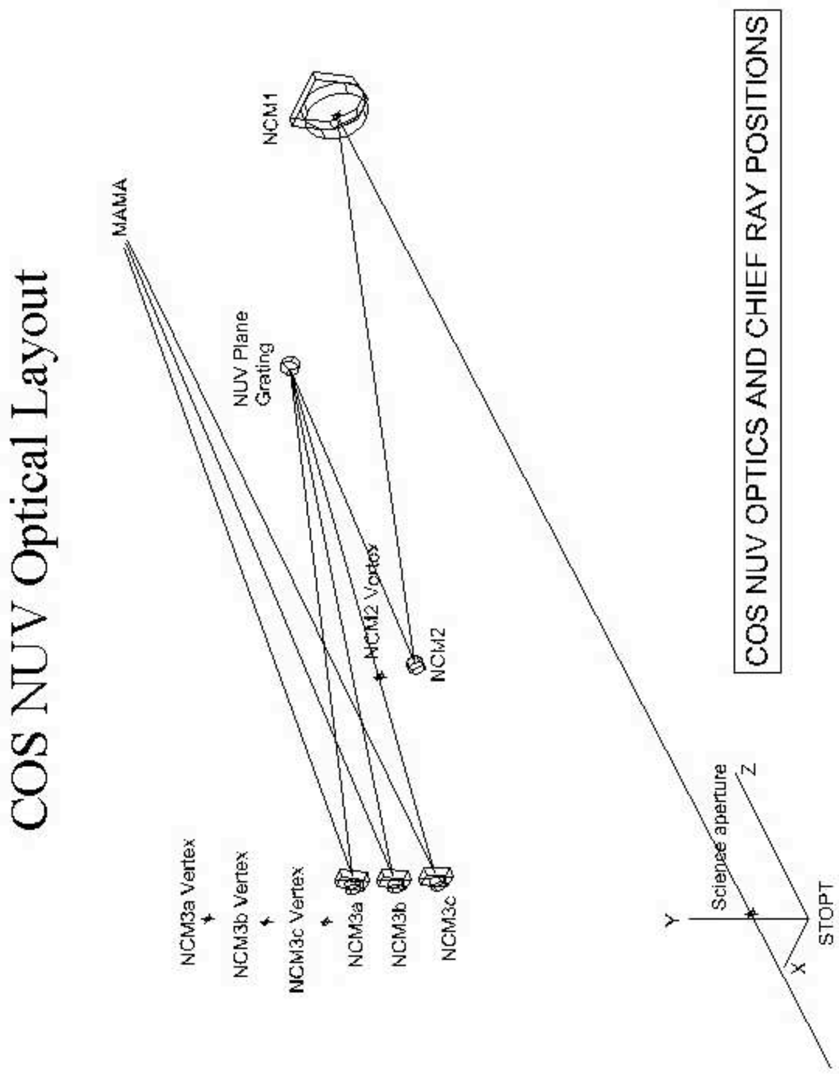

Figure 1.3-7: *Layout of the COS NUV optical light path.*

Table 1.3-3: COS NUV Spectroscopic Modes

Grating	Nominal Wavelength Range[a]	λ Coverage per Exposure	Dispersion (Å/pixel)	Resolving Power ($R = \lambda/\Delta\lambda$)[b]
G185M	1700 – 2100 Å	3 × 35 Å	~0.0342	16,000 – 20,000
G225M	2100 – 2500 Å	3 × 35 Å	~0.0342	20,000 – 24,000
G285M	2500 – 3200 Å	3 × 41 Å	~0.0400	20,000 – 24,000
G230L	1700 – 3200 Å	(1 or 2) × 398 Å	~0.3887	1550 – 2900

[a] Nominal Wavelength Coverage is the expected usable spectral range delivered by each grating mode, in three non-contiguous stripes for the medium-resolution modes. See text for a discussion of the G230L wavelength coverage and detection of 2nd-order spectra.
[b] The lower values of the Resolving Power are delivered at the shortest wavelengths covered, and the higher values at longer wavelengths. The resolution increases roughly linearly between the short and long extremes of the nominal wavelength range covered by each grating mode.

1.3.4 Science and Calibration Apertures

COS is optimized for observing faint UV point sources. There are two science apertures and two calibration apertures on the aperture plate, which can be translated in two dimensions with the Aperture Mechanism (ApM) to optimize the throughput and determine the detector region to be used. Two points regarding the aperture are important to note. One, the PSA and the BOA are both active, i.e. light can pass through each of the apertures onto the detector, albeit that each aperture is viewing a different portion of the sky. This has ramifications for target acquisition (ref. Section 5.2) and target pre-screening. Second, the science apertures are NOT re-imaged by the spectrograph (as with STIS); the apertures are slightly out of focus and do not project sharp edges on the detectors. Because COS is a slitless spectrograph, the spectral resolution depends on the nature of the target. The medium-dispersion gratings deliver resolutions R ~ 20,000 for unresolved sources (intrinsic size ≤ 0.1” FWHM). However, for an extended source, for example, ~0.5” in diameter, the spectral resolution is degraded to R ~ 5000. Though not optimized for extended objects, COS can be used to detect faint, diffuse sources with lower spectral resolution.

Primary Science Aperture: The Primary Science Aperture (PSA) is a 2.5-arcsecond (700 μm) diameter field stop located on the HST focal surface near the point of maximum encircled energy. This aperture transmits essentially all of the light from a well-centered aberrated stellar image delivered by the HST OTA. The PSA is expected to be used for most COS observations.

Bright Object Aperture: We also provide a Bright Object Aperture (BOA) of 2.5-arcsecond (700 μm) diameter with a neutral density (ND2) filter that permits COS to observe targets five magnitudes (factor of 100) brighter than the Bright Object Protection limits allow through the PSA. The BOA is offset 3.7 mm in the cross-dispersion direction from the PSA on the aperture plate. The BOA must be moved with the Aperture Mechanism to the (currently used) position of the PSA for science observations. This is necessary because (1) flat fields obtained with the internal flat-field calibration lamp can only access a limited region on the detectors (see discussion below), and (2) severe aberrations at small off-axis positions in the NUV channel require that the BOA be translated to the nominal position of the PSA for taking NUV spectra of bright targets. Thus, science spectra obtained through either the PSA or BOA will utilize the same detector region (for a given channel) and may employ the same flat-field calibration.

Wavelength Calibration Aperture: The Wavelength Calibration Aperture (WCA) is offset from the PSA by 2.5 mm in the cross-dispersion direction, on the opposite side of the PSA from the BOA. The wavelength calibration spectrum can be used to assign wavelengths to pixel coordinates for science spectra obtained through either the PSA or BOA. The size of the WCA is 20 microns in the dispersion direction by 100 microns in the cross-dispersion direction. The wavelength calibration spectra will be obtained at WCA's nominal offset position from the PSA on both the NUV and FUV detectors. If the BOA is moved to the PSA position and used for science observations, the WCA aperture will be moved 3 mm away from its nominal position. Hence, in order to obtain wave cal spectra for BOA observations, the WCA must be moved back into its nominal position before the wave cal exposure is taken. Not only does this place the wave cal spectrum in the correct location on the detector, but it ensures that the Flat-field Calibration Aperture is masked from transmitting any photons from the wave cal lamps during the wave cal exposure.

Flat-field Calibration Aperture: A Flat-field Calibration Aperture (FCA) is offset by ~2 mm in the dispersion direction and by 3.7 mm in the cross-dispersion direction from the PSA. The size of the FCA is 0.75 mm by 1.75 mm. External light can only go through the PSA and BOA science apertures; light from the internal calibration lamps can only go through the WCA and FCA apertures. The FCA must be moved to project the flat-field continuum spectrum along the desired detector rows (e.g., at the PSA position). While not in use, the FCA is stowed at a position that does not transmit any light from an internal (or external) light source – e.g., the wavelength calibration lamp. After moving the FCA to the desired position, the flat-field spectrum falls along the same detector rows as the PSA or BOA science spectra (though is displaced in wavelength).

Table 1.3-4 shows the sizes of the COS science and calibration apertures, and Fig. 1.3-8 shows their placement on the aperture plate. Figure 1.3-8 also shows the relative placement of the apertures for the different observing modes, including 5 potential placements for FUV detector lifetime adjustments. Because both science apertures always view the sky when the external shutter is open, the STScI target screening procedure must ensure that no bright targets are within a ~4” radius of either aperture for all observations. Since the spacecraft orientation may not be known and either of the science apertures could be specified, it may be prudent to screen the entire region within a ~17” radius of the nominal aperture position.

Table 1.3-4: COS Science and Calibration Apertures

Aperture	Size (Arcseconds)	Size (mm)
PSA	2.5 (Diam.)	0.700 (Diam.)
BOA	2.5 (Diam.)	0.700 (Diam.)
WCA	N/A	0.020 x 0.100
FCA	N/A	0.750 x 1.750

Table 1.3-5 specifies the number of aperture positions to be used with each channel. Twelve total ApM positions are needed for science and calibration observations.

Table 1.3-5: Number of Aperture Positions For Detector Lifetime Adjustments

Aperture	FUV *	NUV **
PSA	5	1
BOA	5	1

* **Note:** The five FUV detector lifetime adjustment positions for the PSA are shown in the middle panel of Fig. 1.3-8. The BOA accesses the same regions of the FUV detector as the PSA, but using five additional ApM step positions. The WCA accesses five unique FUV detector regions using the same ApM settings as the PSA. The FCA accesses the same regions of the detector as the PSA and BOA using the same ApM settings as the BOA.

** **Note:** Only one PSA aperture position is used for the NUV channel that accesses a particular region on the MAMA detector. The BOA is moved to access this same detector region.

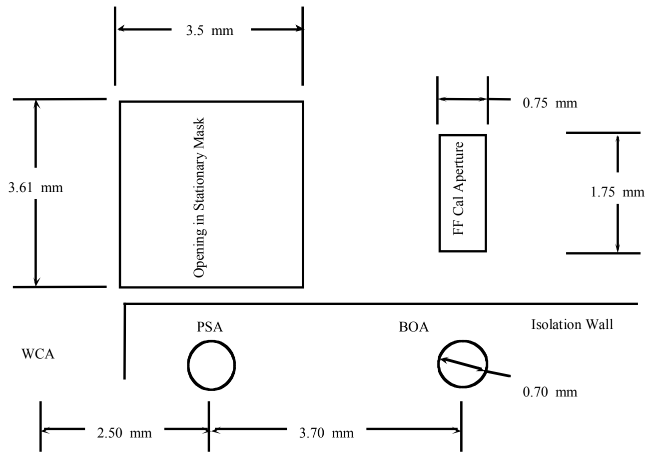

Nominal Aperture Configuration: This panel shows the basic layout of the COS aperture plate. The WCA, PSA, BOA, and FCA are fabricated as part of a single piece and thus move together as a unit. The opening in the stationary mask is fixed with respect to the instrument, so light cannot pass through the FCA without it first being placed over the opening in the stationary mask. The isolation wall separates the science apertures from the FCA and WCA, thus ensuring light from the calibration lamps cannot pass through the science aperture during calibration operations.

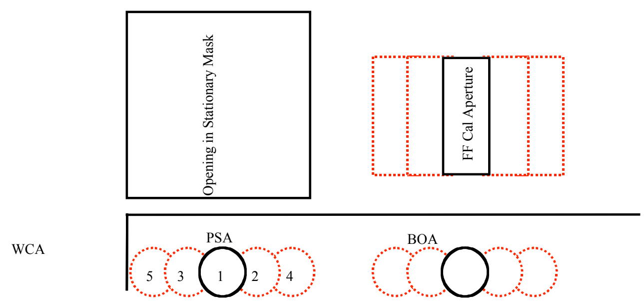

Aperture Motion to Accommodate Detector Lifetime: This panel shows how the WCA, PSA, BOA, and FCA will move to accommodate detector lifetime adjustments. The numbers in the PSA and BOA circles denote separate positions of the PSA. Note how the FCA does not overlap the opening in the stationary mask, so light from the wavelength calibration lamp cannot pass through the FCA during wavelength calibration activities, which will occur far more frequently than flat field calibrations.

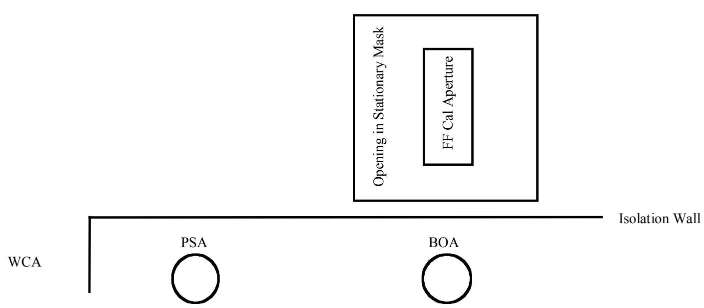

Aperture Configuration for Flat Field Calibration of Position 1 of the PSA: This figure shows how the WCA, PSA, BOA, and FCA will be positioned to acquire a flat field calibration of the PSA position 1 shown in the upper panel.

Figure 1.3-8: *Layout of the COS apertures on the aperture plate. The dispersion and cross-dispersion directions are indicated. See the notes for each panel.*

1.3.5 Sensitivities, Coordinate Systems, and Plate Scale Summary

Point source sensitivities through the PSA for each grating mode are shown in Fig. 1.3-9 as count rates per spectral resolution element (summing over dispersion and cross-dispersion pixels; see Table 1.3-6) per incident unit flux density to the HST OTA. (The extended source sensitivity curves will be shown at a later time.)

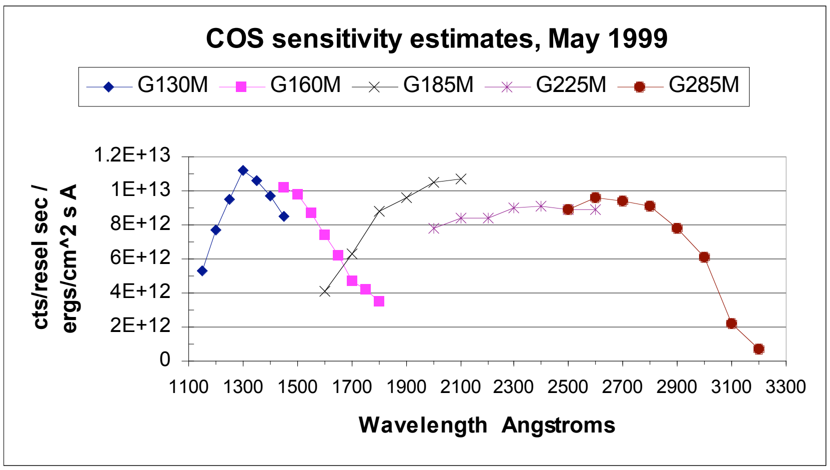

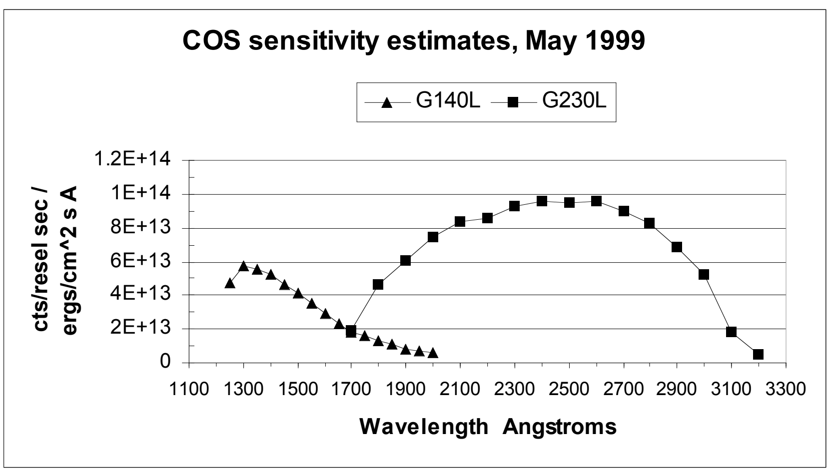

Figure 1.3-9: *Sensitivity curves for all of the COS grating modes. The curves are for point sources observed through the PSA. Sources observed through the BOA will have count rates ~100 times lower for a given incident flux. The upper plot shows the sensitivity curves for the medium-resolution M gratings and the lower plot shows curves for the low-resolution L gratings.*

The detector science data coordinate systems which currently exist in the COS instrument, the relative placement of the FUV and NUV detectors within the COS instrument in relation to those coordinate systems, and the dispersion and cross-dispersion directions of spectra on those detectors are now addressed. Figures 1.3-10 to

1.3-13 show different views of the detector coordinate systems with respect to looking forward or aft into the instrument.

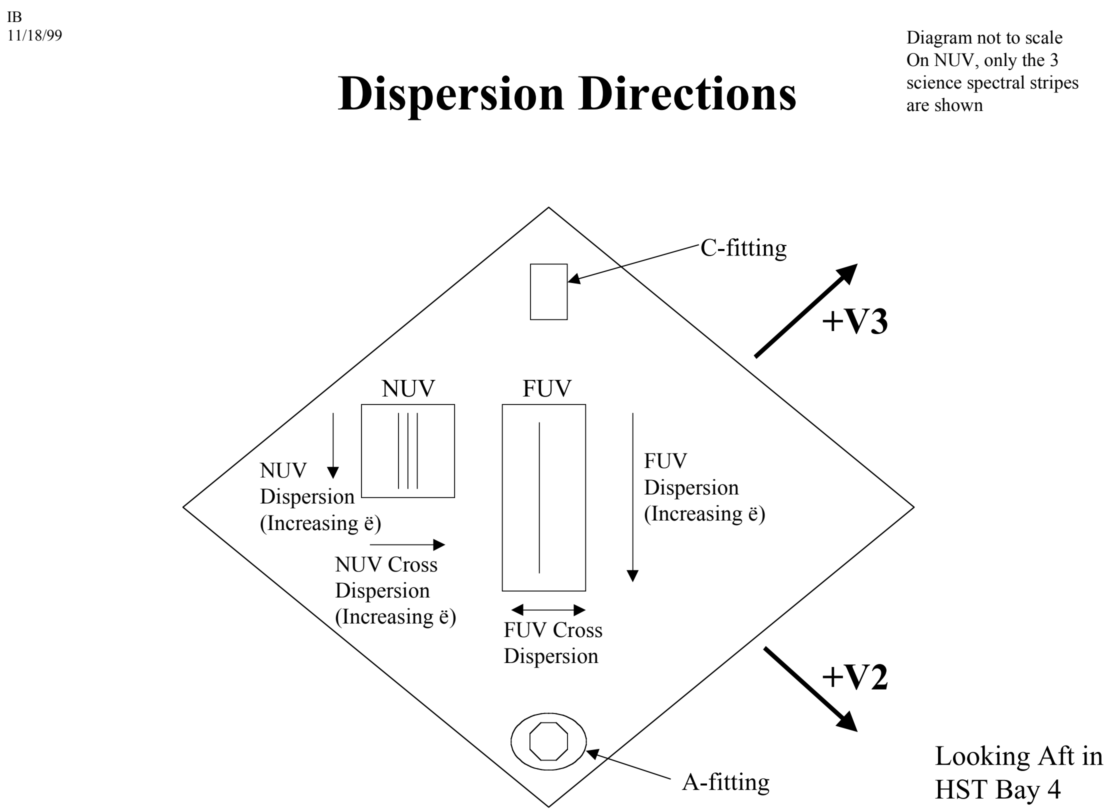

Figure 1.3-10: *Looking in the aft direction into the front of the instrument in HST Bay 4, the C-fitting is at the top and the A-fitting is at the bottom, the FUV detector is more or less in the middle of the instrument, and the NUV detector is to the left.*

For the FUV detector, the light path goes through one bounce and into the FUV detector, so the view in Fig. 1.3-10 is looking at the back of the FUV detector. For the NUV detector, the light path goes through four bounces and into the NUV detector, so the view in Fig. 1.3-10 is looking at the front of the NUV detector. The HST V2/V3 axes are shown as increasing down and to the right (V2) and up and to the right (V3). For both detectors, the dispersion direction toward increasing wavelengths is down.

For the FUV detector, which will contain one spectrum (assuming all cal-lamps are off), the cross-dispersion direction is horizontal, with no preferred direction for increasing cross-dispersion. However, for the NUV detector, which will contain three science spectra (assuming all cal-lamps are off), the preferred positive direction of cross-dispersion is to the right, since the spectra to the right will contain higher wavelengths.

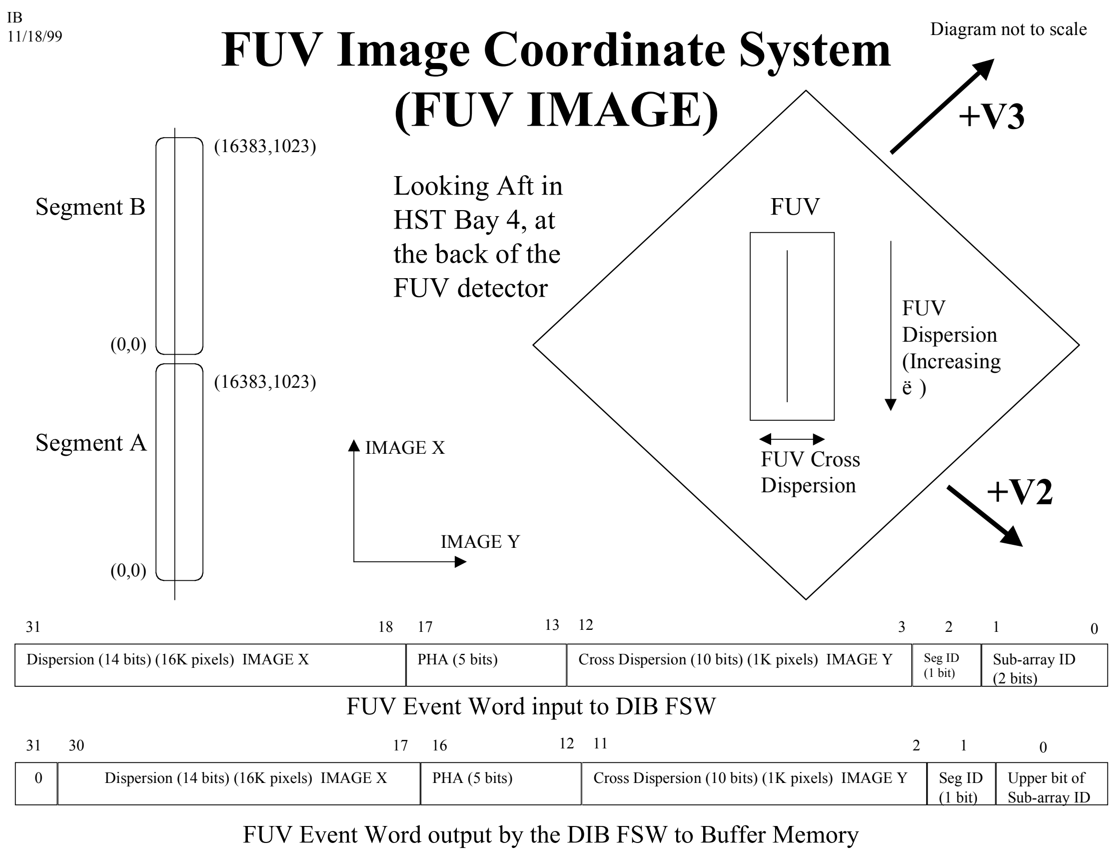

Figure 1.3-11: *The FUV Detector Image Coordinate System.*

The FUV Detector Image Coordinate System (IMAGE) is shown on the diagram in Fig. 1.3-11. The relative placement and orientation of the FUV detector within COS is duplicated from the diagram in Fig. 1.3-10 on the right side. The two segments A and B within the FUV detector are shown on the left side, with Segment A on the bottom and Segment B on the top (i.e., *shorter wavelengths fall on Segment* B). A photon event which occurs on the FUV detector is reported to the DIB FSW in IMAGE coordinates, with IMAGE X increasing upward (in the direction of decreasing wavelength), and IMAGE Y (cross-dispersion) increasing to the right. As shown at the bottom of Fig. 1.3-11, these IMAGE event coordinates are reported to the DIB FSW with the IMAGE X coordinate in bits 18-31, and the IMAGE Y coordinate in bits 3-12. In time-tag mode, the FUV event words will be shifted one bit to the right and then placed into CS buffer memory for eventual downlinking, as also shown at the bottom of Fig. 1.3-11. The shifting forces the upper bit of the 32-bit word to be 0, so that the ground system can distinguish these event-words from time-words, in which the upper bit is 1. Events occurring at geometrically identical spots on the two segments will have slightly different IMAGE X/Y coordinates, due to slightly differing electronic plate-scales on the two segments. Keep in mind that Fig. 1.3-11 is looking aft, at the back of the FUV detector. A more conventional view is looking into the front of the detector as shown in Fig. 1.3-12.

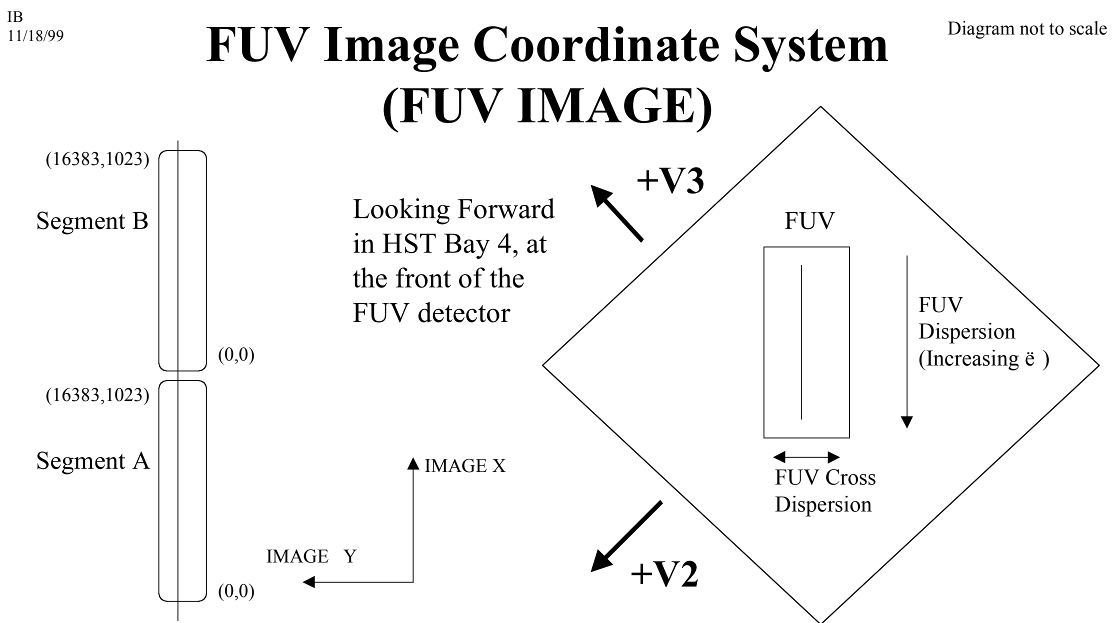

31 – 18	17 – 13	12 – 3	2	1 – 0
Dispersion (14 bits) (16K pixels) IMAGE X	PHA (5 bits)	Cross Dispersion (10 bits) (1K pixels) IMAGE Y	Seg ID (1 bit)	Sub-array ID (2 bits)

FUV Event Word input to DIB FSW

31	30 – 17	16 – 12	11 – 2	1	0
0	Dispersion (14 bits) (16K pixels) IMAGE X	PHA (5 bits)	Cross Dispersion (10 bits) (1K pixels) IMAGE Y	Seg ID (1 bit)	Upper bit of Sub-array ID

FUV Event Word output by the DIB FSW to Buffer Memory

Figure 1.3-12: *The FUV Detector Image Coordinate System (IMAGE) as seen looking into the front of the FUV detector, looking forward in HST Bay 4.*

The diagram in Fig. 1.3-12 shows the FUV Detector Image Coordinate System (IMAGE) as seen looking into the front of the FUV detector, looking forward in HST Bay 4. The two segments A and B within the FUV detector are again shown on the left side of this diagram, with Segment A still on the bottom and Segment B still on the top. A photon event which occurs on the FUV detector is still reported to the DIB FSW in IMAGE coordinates, with IMAGE X still increasing upward (still in the direction of decreasing wavelength), but with IMAGE Y (cross-dispersion) increasing now to the left. Note that the pixel at (0,0) is now at the lower right of the segment, and the pixel at (16383,1023) is now at the upper left of the segment. The directions of the HST V2/V3 axes are also different now that the view is forward rather than aft in HST Bay 4.

The NUV Detector Coordinate System (MAMA) is shown on the diagram in Fig. 1.3-13. The relative placement and orientation of the NUV detector within COS is duplicated from Fig. 1.3-10 on the right side of this diagram. The mechanical orientation of the MAMA detector is shown at the upper right of this diagram to aid the mechanical and detector engineers. A photon event which occurs on the NUV detector is reported to the DIB FSW in MAMA coordinates, with MAMA X (cross-dispersion) increasing to the left, and MAMA Y (decreasing wavelength) increasing up. Thus, neither MAMA X nor MAMA Y are coincident (or even in the same direction) as COS X and COS Y. As shown at the bottom of Fig. 1.3-13, these MAMA event coordinates are reported to the DIB FSW with the MAMA X coordinate in bits 18-27, and the MAMA Y coordinate in bits 3-12. In time-tag mode, the NUV event words will be reformatted by the DIB FSW and placed into CS buffer memory for eventual downlinking in the second format shown at the bottom of Fig. 1.3-13. The unused 9 bits in bit-positions 22-30 are the bits in which the STIS fine-time was inserted. There are no COS requirements for this fine-time; therefore this field becomes 'Unused' for COS. Moreover, bits 21 and 10 were used on STIS for the upper bit of the high-resolution 11-bits of X and Y, respectively. The COS MAMA will not be operated in high-resolution mode and thus these bits will be 0 for COS. Note also that the upper bit of the re-formatted event word is 0, allowing the customary distinction to be maintained between event words and time-words.

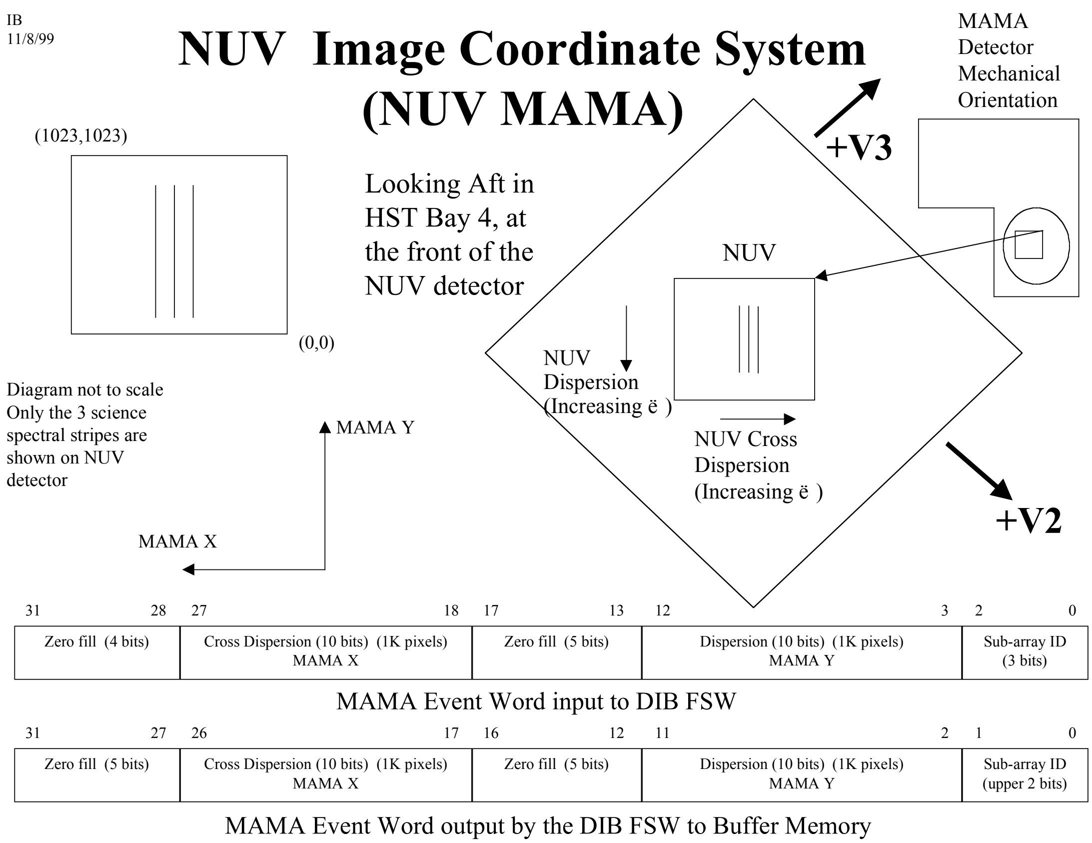

Figure 1.3-13: *The NUV Detector Coordinate System (MAMA) is shown.*

Plate scales and pixel formats on both COS detectors are summarized in Table 1.3-6. The "2 x" designation for the FUV detector indicates that there are 2 detector segments, each with the dimensions given in parentheses.

Table 1.3-6: COS Detector Plate Scale and Pixel Format

Detector	**Plate Scale (µm/arcsec)**	**Active Area (mm)**	**Active Area (pixels)**	**Pixel Size (µm)**	**Resel Size (pixels)**
XDL (FUV)	~265	2 x (85 x 10)	2 x (~14160x~400)	6 x 24	7 x 10
MAMA (NUV)	~970	25.6 x 25.6	1024 x 1024	25 x 25	3 x 3

Figures 1.3-14 and 1.3-15 show the projection of the science and wavelength calibration spectra onto the FUV XDL and NUV MAMA detectors.

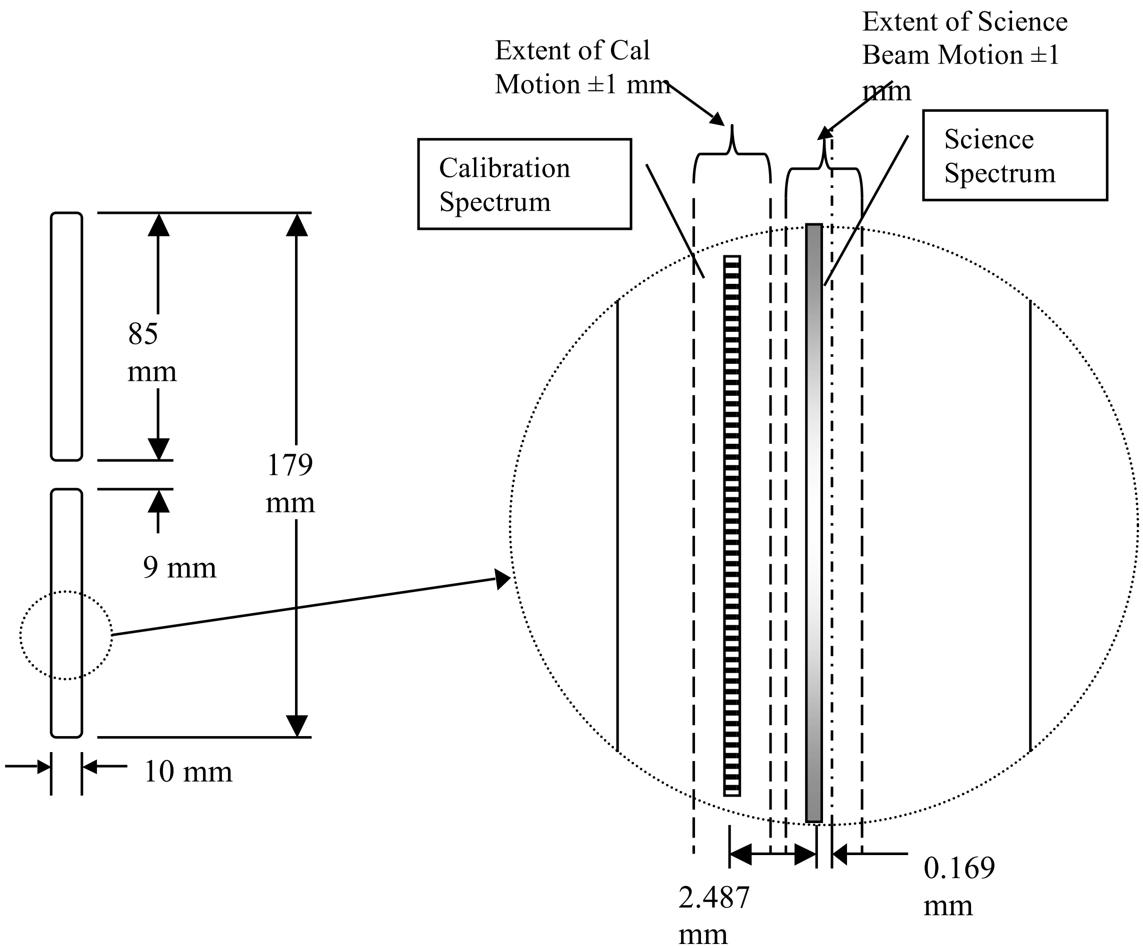

Figure 1.3-14: *Projection of the science and wavelength calibration spectra onto the FUV XDL detector.*

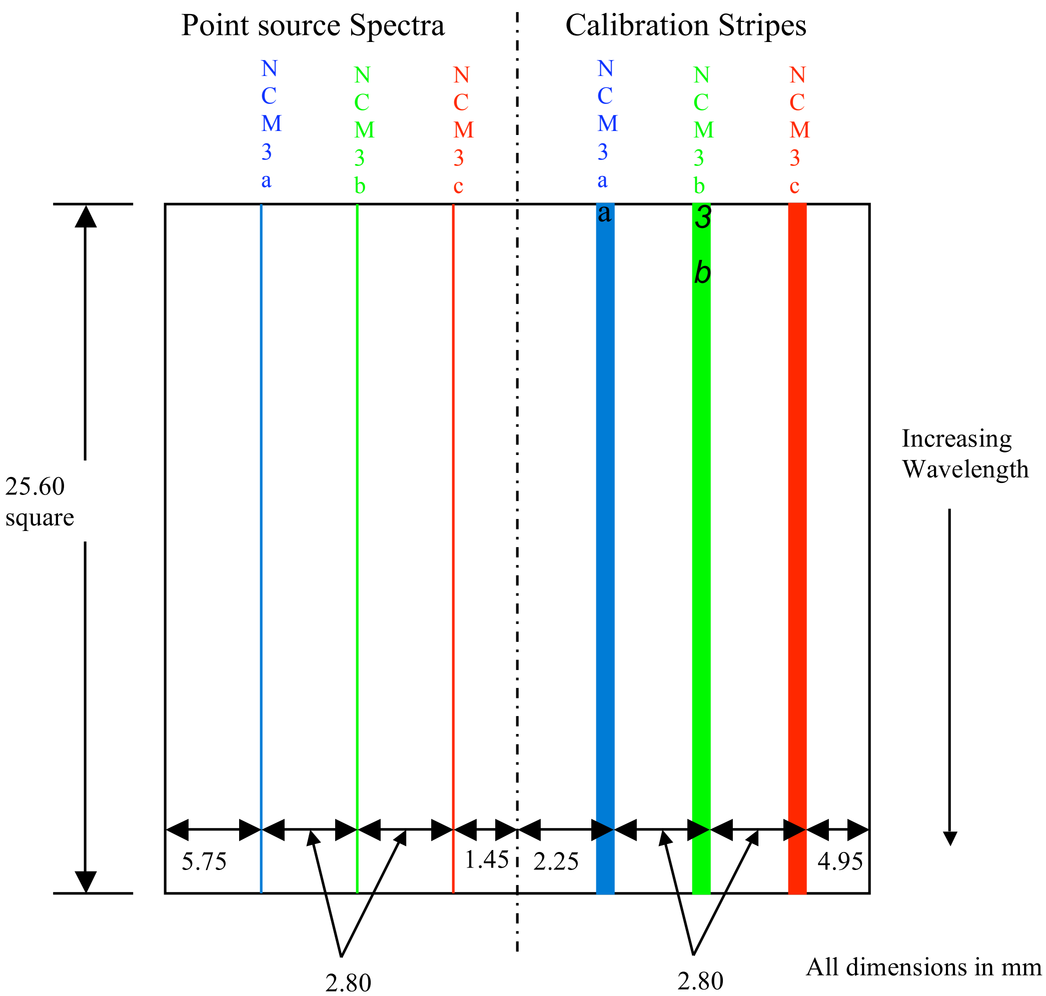

Figure 1.3-15: *Projection of the science and wavelength calibration spectra onto the NUV MAMA detector. The color coding shows that NCM3A projects the shortest wavelength stripe, and NCM3C projects the longest wavelength stripe. The arrow at right shows the direction of increasing wavelength along each stripe.*

2. MECHANISMS AND LAMPS

This section describes the purpose and operations of the COS on-board mechanisms and lamps.

2.1 MECHANISMS

COS uses four moving mechanisms to carry out its normal science observations: an external shutter, the Aperture Mechanism (ApM), the Optics Select Mechanism 1 (OSM1), and the Optics Select Mechanism 2 (OSM2). (An additional moving door on the front of the FUV XDL detector is described in Section 4.2.)

2.1.1 External Shutter

The external shutter is a paddle shaped arm, with a shutter blade made up of a thin, circular disc approximately 1.5 inches in diameter. It is located at the front of the COS enclosure in the optical path before the aperture mechanism. When closed, the shutter blocks all external light from entering the COS instrument and light from the COS internal lamps from exiting the instrument. The shutter is commanded through the FSW. The shutter travel-time is <500 milliseconds. The opening and closing of the external shutter is not used to determine the duration of an exposure. Due to bright object concerns, the external shutter will only be opened by ground command at the beginning of every external exposure. It will be closed by ground command at the end of every external exposure, with the possible exception of one or more phases of target acquisition. The external shutter will be closed autonomously by the COS FSW whenever any over-light condition is triggered by an external or internal source or when the HST take-data-flag goes down indicating loss of fine lock (both for Bright Object Protection concerns).

2.1.1.1 External Shutter Motor Drive and Position Sensing

The external shutter motor assembly has quadruple redundancy. There are two single phase, redundantly-wound stepper motors available to drive the external shutter. The primary motor has the ability to open or close the external shutter. The secondary motor can only move the shutter out of the optical path (open) and leave it there. Either MEB can command either motor since they are each wired to separate sets of windings.

The primary winding of each motor is driven by the side 1 Support Electronics Section (SES) electronics; the redundant windings of each motor are driven by the side 2 SES electronics. The control of the windings cannot be cross-strapped (e.g., the side 1 SES electronics cannot control the redundant motor windings of the external shutter). A failure in either the side 1 SES electronics or the primary motor winding would require the operator to change to side 2 of the instrument to operate this mechanism.

The primary motor moves the shutter to the Open or Closed position in one 30 degree step via a 28 volt pulse from the SES electronics. The motor is held in place by the motor's detent torque and by additional permanent magnets. One magnet is located in the middle of the shutter's travel range, and the other permanent magnet is located on the shutter itself. The magnets are equally polarized which forces the shutter to either the Open or Closed position, even if power is removed. When the shutter is commanded to move, it must overcome motor detent torque as well as the force of the magnets.

The secondary motor is a fail-safe used to move the entire external shutter assembly out of the optical path in the event of a primary motor failure that would leave the shutter in the closed position. To move the increased mass, the secondary motor has a 100:1 gear ratio associated with it, and the flight software will command the motor to move 946 steps, the full range of the mechanism, to open the shutter. At the nominal rate of 78 steps per second, the move with the secondary motor takes approximately 12 seconds to complete.

An isometric drawing of the external shutter is shown in Figure 2.1-1. Properties of the external shutter, and parameters supplied to the FSW to operate it, are listed in the LSHUTTER macro sheet of DM-05. Additional information may be found in Appendix A of the Flight Software User's Manual (Control Section Hardware/Software Interface).

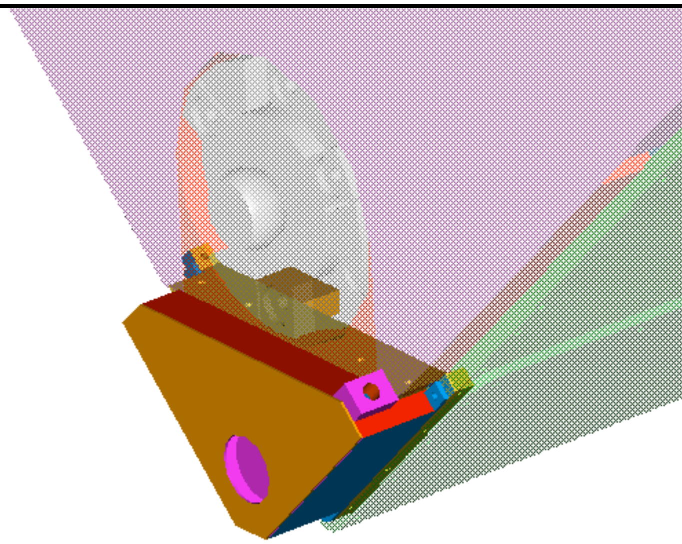

Figure 2.1-1: *Isometric drawing of the COS external shutter, located at the lower front region of the enclosure, similar to where the STIS shutter is located.*

The external shutter's position is sensed via non-redundant Reed switches. There is a Reed switch in both the Open and Closed shutter positions. When the shutter moves into position, the permanent magnet on the shutter comes in close proximity with the Reed switch. The magnet's field closes the switch contacts indicating the shutter is in that position. Since the Reed switches are not redundant, the sense signals must be relay switched to the MEB that is on. The relays reside in MEB1 but the relays can be commanded via a macro using either MEB. Both the open and closed switch positions are stored in a latch as a separate digital 1 or 0 to be read by the FSW. A digital value of one indicates that the switch is in position. A digital value of zero indicates that the switch is not in position. Therefore, a one value for the open bit indicates that the shutter is open and a one value for the closed bit indicates that the shutter is closed. A value of zero in both locations is invalid and a value of one in both locations would indicate that the shutter is positioned somewhere in-between open and shut (possibly via a motor 2 move).

2.1.1.2 External Shutter FSW Macro Control

The "Move External Shutter" macro commands the External Shutter to either the Open or Closed position. If the mechanism fails to move to the commanded position, the FSW will detect this and report the status.

If the External Shutter is already in the requested position, the move will be set up, the position will be updated in the current value table, and then the motor will be disabled, all without moving the mechanism. The final position will be verified, and the status will reflect achieving the commanded position.

For a typical COS target with flux between 1-5 × 10^{-15} ergs/cm^2/s/Å, it is estimated that 4-10 external shutter moves may be necessary during a COS science orbit. The predicted mechanism lifetime is therefore: 10 external shutter movements/orbit × ~1200 COS orbits/yr × 5 year COS lifetime = 60,000 total movements.

2.1.2 Aperture Mechanism (ApM)

Normal ApM adjustments for science and calibration: The ApM is located near the HST focal surface in the forward, lower portion of the COS enclosure (see Fig. 1.3-2). The ApM positions the aperture block which contains the Primary Science Aperture (PSA), Bright Object Aperture (BOA), Wavelength Calibration Aperture (WCA), and Flat-field Calibration Aperture (FCA). The ApM is used to position the PSA at the optimum position along the optical beam to maximize throughput of a focussed aberrated point source (see Section 5.1.1), and to move the spectra in the cross-dispersion direction on the FUV detector to distribute the photoelectrons and lengthen detector lifetime (see Section 5.3.5). The ApM is used to move the BOA to the position of the PSA for observations of bright targets (for both the FUV and NUV channels). Finally, the ApM is used to move the FCA to the desired position for obtaining flat-field exposures for PSA or BOA science spectra. The WCA need not be moved for wavelength calibration exposures associated with PSA science spectra. The WCA spectrum is displaced at an off-axis position relative to the PSA, projected ~2.5 mm away from the PSA spectrum on the FUV detector. On the NUV detector, the corresponding WCA spectral stripe lies ~9.3 mm away from the associated PSA science strip (see Fig. 1.3-15). When the ApM is moved in the cross-dispersion direction for BOA science exposures, it must be commanded back to its nominal (PSA) position to project the WCA spectrum in the appropriate place for wavelength calibrations.

The detailed on-orbit procedure for aligning the science apertures with the best focus position for each grating and detector is described in Sec. 5.1. This alignment procedure will establish absolute positions for the ApM to be used for each optic on the OSM1. Offset positioning of the ApM will be used for the FUV detector lifetime adjustments. The ApM is not to be moved for FP-SPLITs, which will be accomplished by scanning the gratings. The baseline plan is that the three FUV gratings on the OSM1 will be at the same focus position and, hence, will require no movement of the ApM when switching between optics. However, we expect that the ApM *will* generally need to be moved when switching between the FUV and NUV channels (using the NCM1 optic on OSM1). This will especially be true after the first FUV detector lifetime adjustment is made.

Since most moves of the ApM are anticipated to be small, periodic large moves need to be scheduled, once a year, to redistribute the gear lubricants to prevent long-term wear and changes in mechanism behavior. Dedicated move sequences should be scheduled for the ApM X and ApM Y motors that move them beyond their normal ranges for science operations, but not to their soft or hard limits. (Similar occasional large moves should also be scheduled once a year for the OSM1 focus motor.)

2.1.2.1 Aperture Mechanism Motor Drive and Position Sensing

The ApM is driven by two motors that are used to position the PSA in the main optical beam such that the point source throughput is optimized. One motor drives the ApM in the cross-dispersion direction, and has a range of motion of ≥7 mm (~25 arcsecs) that allows aperture selection and accommodates possible COS installation errors, plus the capability to access enough pristine regions of the detectors to ensure long detector life (± 1 mm). The other motor drives the ApM in the dispersion direction with a range of motion of 2 mm, sufficient to accommodate installation errors (+/- ~0.3 mm). The ApM needs to be positioned with a repeatable accuracy of +/- 0.1" (= ~30 μm) in both directions, and is required to remain stable through one HST orbit to within +/- ~3 μm.

There are two double phase, redundantly-wound stepper motors available to drive the aperture mechanism. Either MEB can command either motor since they are each wired to separate sets of windings.

The primary winding of each motor is driven by the side 1 Support Electronics Section (SES) electronics; the redundant windings of each motor are driven by the side 2 SES electronics. The control of the windings cannot be cross-strapped (e.g., the side 1 SES electronics cannot control the redundant motor windings of the aperture mechanism). A failure in either the side 1 SES electronics or the primary motor winding would require the operator to change to side 2 of the instrument to operate this mechanism.

The aperture mechanism is shown in Figure 2.1-2, and the placement of the science and calibration apertures on the aperture block is portrayed in Figure 1.3-8. Properties of the aperture mechanism, and parameters supplied to the FSW to operate it, are listed in the macro sheets LAPERINI, LAPERREL, and LAPER and Section 6.1 (Mechanism Limits and Settings) of DM-05.Additional information may be found in Appendix A of the Flight Software User's Manual (Control Section Hardware/Software Interface).

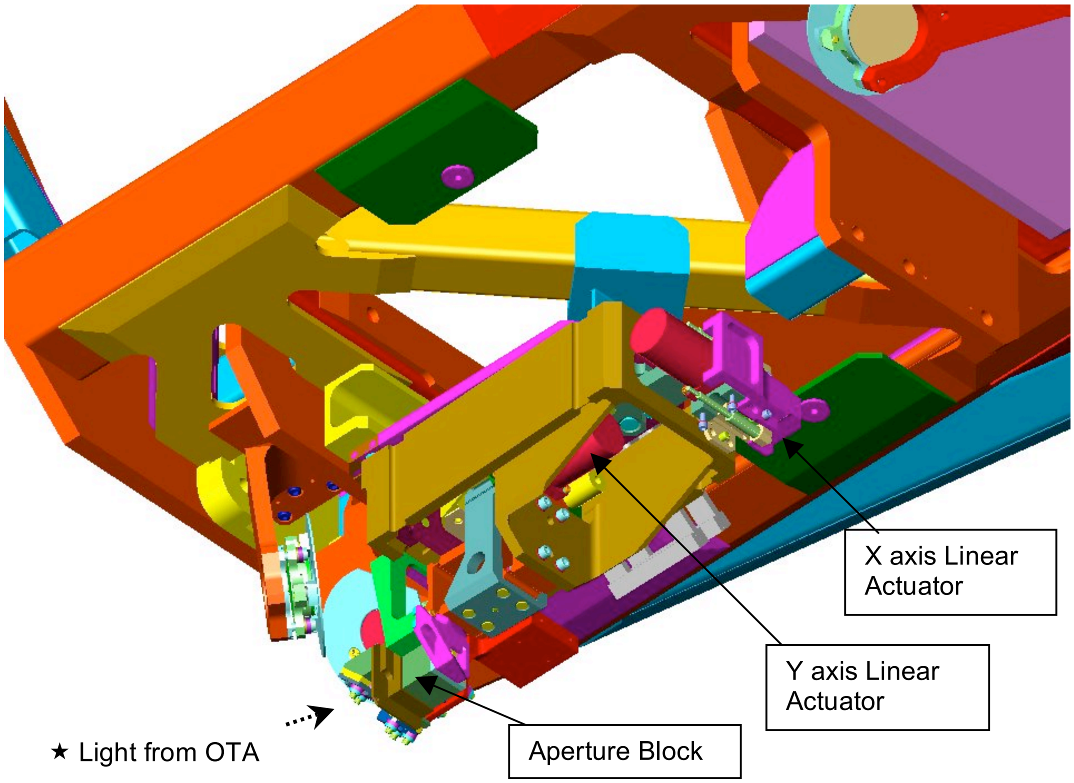

Figure 2.1-2: *Isometric drawing of the Aperture Mechanism (ApM).*

Position sensing is done with a Linear Variable Differential Transformer (LVDT). The LVDT is basically a series of inductors in a hollow cylindrical shaft and a solid cylindrical core (see Figure 2.1-3 below).

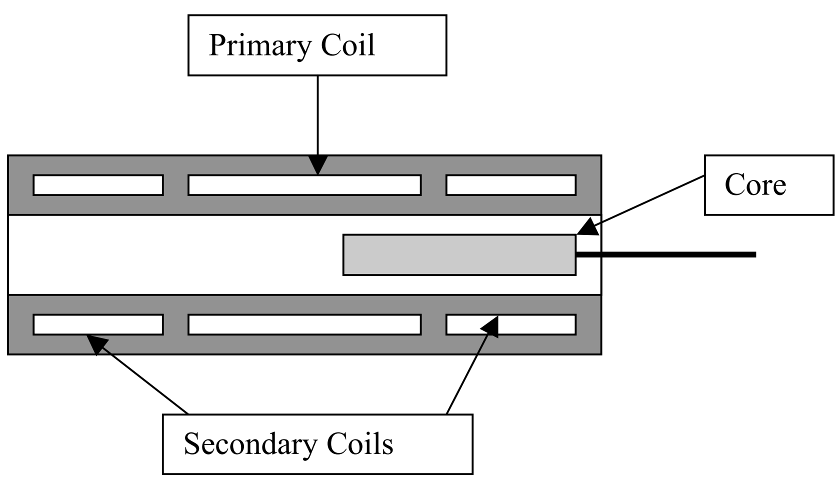

Figure 2.1-3: *Cross section of an LVDT.*

The LVDT produces an electrical output proportional to the position of the core. The lack of friction between the hollow shaft and the core prolongs the life of the LVDT. The LVDT is constructed with two secondary coils placed symmetrically on either side of a primary coil contained within the hollow cylindrical shaft. Movement of the magnetic core causes the mutual inductance of each secondary coil to vary relative to the primary, and thus the relative voltage induced from the primary coil to the secondary coil will vary as well. These LVDTs are calibrated by varying the position of the core and measuring the corresponding output voltages. Then a calibration curve is determined and applied to arrive at the engineering units of position. Motion in the dispersion and cross-dispersion directions are measured with separate LVDTs.

2.1.2.2 ApM Motor Operating Constraints

Although the motor has unlimited rotation, there are both hardware and software travel limits. Software limits are checked by the FSW. If a move command would send the aperture block beyond its software limits, the move is not performed and an error is reported with a status buffer message.

The COS ApM motors should not be overheated. A detailed discussion of overheating is given in section 2.1.6.

2.1.2.3 APM FSW Macro Control

The ApM is operated by three FSW macros:

1) Initialize ApM;
2) Move ApM to Absolute Position;
3) Move ApM to Relative Position.

2.1.2.3.1 Initialize Aperture Mechanism Macro

The "Initialize Aperture Mechanism " macro is used to initialize the ApM motor parameters. Each ApM motor must be initialized at least once after power-on before it can be moved. The macro parameters are:

- Motor selection;
- Whether to return to the home position during motor initialization;
- Motor speed selection;

- Motor hold-off count.

The **motor selection** indicates which mechanism motor is being initialized. Each motor has to be initialized separately.

The **home position option**, when enabled, returns the selected motor to a home position during motor initialization. Under normal operations this option will be enabled. The home position is a patchable constant, and will initially be defined for each motor so that the PSA is in its optimized science position.

The **motor speed selection** selects the stepping speed of the selected motor. The same motor speed will be used in all subsequent moves of that motor, until it is redefined via a new "Initialize ApM" macro. Laboratory testing shows that the ApM motors should be operated at a preferred speed, therefore the LAPERINI macro has a CARD item which states that the preferred speed for both ApM motors is TWOTHIRD (52.08 steps/second).

The **motor hold-off count** defines the length of time to keep the selected motor enabled after completion of the commanded number of steps, to allow for electrical braking of the motor. To determine the total time to complete the move, the hold-off count is added to the time needed to move the commanded number of steps. The same motor hold-off count will be used in all subsequent moves of that motor, until it is redefined via a new "Initialize ApM" macro.

2.1.2.3.2 Move Aperture Mechanism to Relative Position Macro

The "Move ApM to Relative Position" macro specifies the motor (X, Y), the number of motor steps to move, and the direction of travel. For both ApM motors, it is desirable that moves in the non-preferred direction overshoot and return to the desired destination in the preferred direction to eliminate mechanism backlash. The relative move macro does not perform this overshoot, therefore, for relative moves in the non-preferred direction, the STScI ground system will need to perform overshoot processing by adding the overshoot to the number of steps in the non-preferred direction and commanding a separate relative move macro for the return move.

2.1.2.3.3 Move ApM to Absolute Position Macro

The "Move ApM to Absolute Position" macro specifies the motor and the desired aperture. With absolute moves, overshoot processing is performed by the FSW. This is the macro that will be used during normal operations to position the aperture block correctly in the optical path. The absolute step position of each aperture is stored in a

FSW look-up table. Each aperture has two look-up table entries, one for each detector. See DM-05 (macro sheet LAPER) for the name of the flight software look-up table patchable constant.

2.1.2.4 ApM Home Commanding

The PSA is the operational home position of the ApM. If the last exposure of a visit uses the BOA, the ApM will be moved back to the PSA position at the end of the visit. This is independent of whether the home position option described in section 2.1.2.3.1 is used for motor initialization.

2.1.3 Optics Select Mechanism 1 (OSM1)

The function of the OSM1 is to position an optic into the optical beam of the COS instrument. The optics mounted on OSM1 receive the input light beam from the HST OTA through the ApM and direct it to the FUV detector or the NUV channel, depending on which optic is rotated into place. The optic positioned by this mechanism will be the first reflecting surface that the light encounters once it enters the instrument. The mechanism will position any one of four different optics into the beam. The OSM1 contains the G130M, G160M, and G140L gratings, and the NCM1 mirror. The gratings direct light to the FUV detector while the mirror directs light to the NUV channel. Because of soft stops which limit the range of motion of the OSM1 to just under 360 degrees, the OSM1 rotates up to ~270 degrees to place the desired optic in the beam path.. The four optics mounted on OSM1 are arranged at 90-degree intervals. The rotational position of each optic will be stored in a FSW table which will be updated during SMOV (see Section 5.1) to correct any angular misalignments which occur due to instrument insertion error (i.e., those misalignments due to uncertainties in the instrument/HST interface).

Once an optic is positioned by OSM1, the mechanism must allow for small adjustments in 2 degrees of freedom. Rotational adjustments are required to move the spectra on the FUV detector in the dispersion direction for FP-SPLITs in the FUV channel and for recovering wavelengths that fall on the FUV detector gap (see Section 5.3). Translational adjustments are required to refocus the instrument on orbit in order to optimize the focus of each of the FUV gratings and the NCM1 mirror, and to accommodate any instrument installation misalignments or any modifications to the location of the HST secondary mirror. The translational motions are in the z-direction (towards or away from the HST secondary).

The location of the mechanism is driven by the required location of the selected optic. The absolute location of the optic is dictated by the optical design. The current optical design locates the selected optic at the lower aft end of the instrument (see Figure

1.3-2). Since most moves of the OSM1 focus mechanism are anticipated to be small, periodic large moves need to be scheduled, once a year, to redistribute the gear lubricants to prevent long-term wear and changes in mechanism behavior. A dedicated move sequence should be scheduled for the OSM1 focus motor that moves it somewhat beyond its normal range for science operations, but not to its soft or hard limits.

The optic positioning requirements are contained in Ball SER COS-SYS-006, and will not be repeated here. For detailed positioning requirements, refer to that document.

Table 2.1-1 lists the central wavelengths for each FUV grating mode. Note that a central wavelength is commanded and the FSW knows how to convert the commanded wavelength to the appropriate OSM1 steps.

Table 2.1-1: Central Wavelengths for OSM1 Optics

Optic	Central λ* (Å)	Observed Wavelengths (Å)
G130M	1291	1132-1274,1291-1433
	1300	1141-1283,1300-1442
	1309	**1150-1292,1309-1451**
	1318	1159-1301,1318-1460
	1327	1168-1310,1327-1469
G160M	1577	1382-1556,1577-1752
	1589	1394-1568,1589-1764
	1600	**1405-1579,1600-1775**
	1611	1416-1590,1611-1786
	1623	1428-1602,1623-1798
G140L	1105**	<300-970,1105-2253
	1230	**<300-1095,1230-2378**
NCM1	NUV Channel	N/A
NCM1-FF***	NUV Flat-Field	N/A

* The "Central Wavelength" designated for the FUV grating modes is actually the first wavelength that falls onto the long wavelength segment of the FUV detector (segment A), under the premise that the specified wavelength should be one that can actually be observed rather than one that falls in the middle of the "detector gap." The multiple wavelength settings for the G130M and G160M gratings are designed to be offset by multiples of 4 OSM1 rotary steps, and the G140L settings are designed to be offset by 6 OSM1 rotary steps. Wavelength settings in bold-face are the nominal settings that are expected to be utilized most. The NCM1 positions are those that yield the best alignment and focus for the NUV channel optical path.
** The G140L "1105" setting moves the zero-order image onto segment B of the FUV detector, while the useful first-order spectrum falls onto segment A. This setting should be only used in "single-segment operation," with HVNOMA and segment B high-voltage set to low.
*** NCM1-FF is the OSM1 position (rotation and focus) for NCM1 used to perform the NUV flat-field exposures. Due to the offset in the dispersion direction of the flat-field aperture (FCA) from the science apertures (PSA or BOA), much of the light in the flat-field calibration beam would miss the NUV grating on OSM2 with NCM1 placed in its normal position for NUV science operations. The NCM1-FF position is 5 rotation steps reverse of the nominal NCM1 (NUV Channel) science position, which restores the alignment to the NUV gratings and maximizes the throughput.

2.1.4 Optics Select Mechanism 2 (OSM2)

The NUV optics mounted on OSM2 receive light from the NCM2 collimating mirror and direct the spectrum or image to the three camera mirrors (NCM3a,b,c). The OSM2 contains the G185M, G225M, G285M, and G230L gratings, and the TA1 mirror. OSM2 rotates but does not translate. Rotations move the spectrum or image in the dispersion direction on the NUV detector. The gratings are flat and each medium-resolution grating must be positioned at ~6 discrete positions in order to achieve full wavelength coverage. Small rotational adjustments will also be used for FP-SPLITs.

The five optics on OSM2 are distributed at 72-degree intervals, thus each rotational transition is at least ~72 degrees. Because of soft stops which limit the range of motion of the OSM2 to just under 360 degrees, the OSM2 rotates up to ~288 degrees to place the desired optic in the beam path. Table 2.1-2 lists the central wavelengths for each NUV grating mode. Note that a central wavelength is commanded and the FSW knows how to convert the commanded wavelength to the appropriate OSM2 step.

Table 2.1-2: Central Wavelengths for OSM2 Optics

Channel	Central λ* (Å)	Observed Wavelengths (Å)		
		Stripe A	Stripe B	Stripe C
G185M	1786	1670-1705	1769-1804	1868-1903
	1817	1701-1736	1800-1835	1899-1934
	1835	1719-1754	1818-1853	1916-1951
	1850	**1734-1769**	**1833-1868**	**1931-1966 ** **
	1864	1748-1783	1847-1882	1945-1980
	1882	1766-1801	1865-190	1964-1999
	1890	1774-1809	1872-1907	1971-2006
	1900	**1783-1818**	**1882-1917**	**1981-2016**
	1913	1796-1831	1895-1930	1993-2028
	1921	**1804-1839**	**1903-1938**	**2002-2037**
	1941	1825-1860	1924-1959	2023-2058
	1953	**1837-1872**	**1936-1971**	**2034-2069**
	1971	1854-1889	1953-1988	2052-2087
	1986	1870-1905	1969-2004	2068-210
	2010	1894-1929	1993-2028	2092-2127
G225M	2186	2070-2105	2169-2204	2268-2303
	2217	2101-2136	2200-2235	2299-2334
	2233	**2117-2152**	**2215-2250**	**2314-2349**
	2250	2134-2169	2233-2268	2332-2367 **
	2268	2152-2187	2251-2286	2350-2385
	2283	2167-2202	2266-2301	2364-2399
	2306	2190-2225	2288-2323	2387-2422
	2325	**2208-2243**	**2307-2342**	**2406-2441**
	2339	2223-2258	2322-2357	2421-2456
	2357	2241-2276	2340-2375	2439-2474
	2373	**2256-2291**	**2355-2390**	**2454-2489**
	2390	2274-2309	2373-2408	2472-2507
	2410	2294-2329	2393-2428	2492-2527
G285M	2617	2480-2521	2596-2637	2711-2752
	2637	**2500-2541**	**2616-2657**	**2731-2772**
	2657	2520-2561	2636-2677	2751-2792
	2676	2539-2580	2655-2696	2770-2811
	2695	**2558-2599**	**2674-2715**	**2789-2830**
	2709	2572-2613	2688-2729	2803-2844
	2719	**2582-2623**	**2698-2739**	**2813-2854**
	2739	2602-2643	2718-2763	2837-2878

Channel	**Central λ* (Å)**	**Observed Wavelengths (Å)**		
		Stripe A	**Stripe B**	**Stripe C**
	2850	2714-2755	2829-2870	2945-2986 **
	2952	**2815-2856**	**2931-2972**	**3046-3087**
	2979	2842-2883	2958-2999	3073-3114
	2996	2859-2900	2975-3016	3090-3131
	3018	2881-2922	2997-3038	3112-3153
	3035	2898-2939	3014-3055	3129-3170
	3057	2920-2961	3036-3077	3151-3192
	3074	**2937-2978**	**3053-3094**	**3168-3209**
	3094	2957-2998	3073-3114	3188-3229
G230L	**2635**			**2435 – 2834**
	2950		1650-2050	2750-3150
	3000		**1700 – 2100**	**2800 – 3200**
	3360		**2059 – 2458**	
TA1	**Faint target** **Bright target**	**~1700-3200** **~1700-3200 (order sorter reflection)**		

* The "Central Wavelength" designated for the NUV grating modes is the central wavelength of the middle spectral stripe (stripe B) on the NUV detector. Wavelength settings depicted in bold type are expected to be utilized most often. See Table 1.3-2 for complete G230L wavelength coverage.
** The "Center Optic Position" is 72 degrees in rotation from the adjacent optic centers.

2.1.5 OSM Motor Drive and Position Sensing

The OSM1 has two motors, one to drive rotational motion and one to drive translational motion. OSM2 only has one motor to drive rotation. The motor and drive for OSM2 rotation is identical to that of OSM1. Each motor is a two phase, redundantly-wound stepper motor. Either MEB can command either motor since they are each wired to separate sets of windings. The primary winding of each motor is driven by the side 1 SES electronics; the redundant windings of each motor are driven by the side 2 SES electronics. The control of the windings cannot be cross-strapped (e.g., the side 1 SES electronics cannot control the redundant motor windings of the external shutter. A failure in either the side 1 SES electronics or the primary motor winding would require the operator to change to side 2 of the instrument to operate this mechanism.

Drawings of the optics select mechanisms are shown in Figs. 2.1-4 and 2.1-5. Properties of the optical select mechanisms and parameters supplied to the FSW to operate them are listed in the LOSMINIT, LOSMREL, AND LOSM macro sheets and Section 6.1 (Mechanism Limits and Settings) of DM-05.

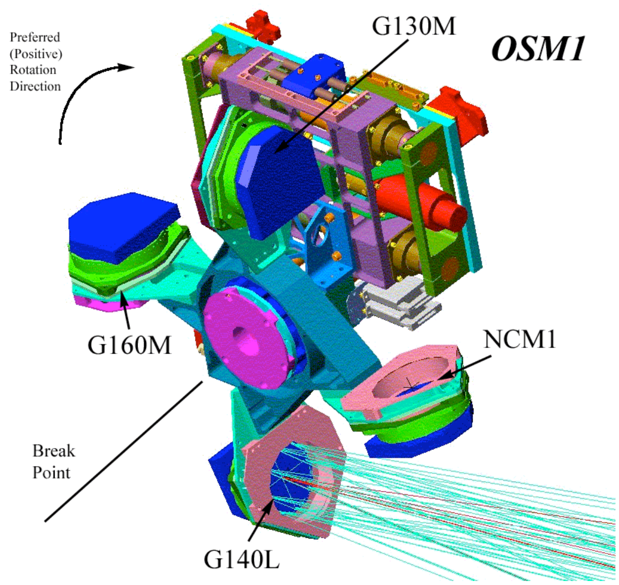

Figure 2.1-4: *Isometric drawing of the OSM1 mechanism. The optics are labeled and the preferred direction of rotation (increasing step numbers) is indicated. The "Break Point" between G140L and G160M is the position through which the OSM1 is not rotated in order to remain on the same motor "track" – i.e., moving between G140L and G160M requires a 270-degree rotation..*

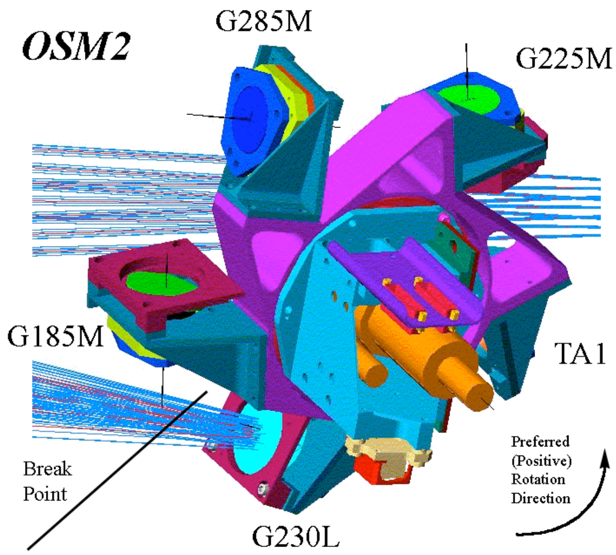

Figure 2.1-5*: Isometric drawing of the OSM2 mechanism. The optics are labeled and the preferred direction of rotation (increasing step numbers) is indicated. The "Break Point" between G230L and G185M is the position through which the OSM2 is not rotated in order to remain on the same motor "track" – i.e., moving between G230L and G185M requires a 288-degree rotation.*

Rotational position sensing is done with coarse and fine resolvers. A resolver is an absolute position senser with an analog output. The resolver is composed of a rotor with one winding and a stator with two windings at right angles to each other. The winding of the rotor is excited with an AC reference voltage. This voltage induces a current in the two windings of the stator. As the rotor spins the voltage that will be induced in the stator will vary. When the windings are parallel to each other, the voltage will be at a maximum. When they are perpendicular to each other, it will be at a minimum. Thus the induced voltage of one stator winding depends on the rotor position and is governed by the equation $V=V_{input}$ SinØ. Because the second rotor winding is at a right angle to the first, its voltage signal can be calculated using the cosine. In the valley and peak of the sine wave there is only a slight slope, so position variations are difficult to pick up. This is the reason the second winding is needed: to provide clearer position signals at these points. The analog signal is translated to a digital signal for the system to process it. The OSM1 focus motor uses an LVDT (discussed above for the ApM) to sense position. This focus motor requires a large (~2 mm) movement to be scheduled once a year to redistribute the gear lubricants to prevent long-term wear and changes in the mechanism behavior.

2.1.5.1 OSM Motor Operating Constraints

Although the rotational motors on the optics select mechanisms have unlimited rotation, soft stops have been implemented to limit the motion to slightly under 360 degrees. The soft stop (or “breakpoint”) for OSM1 is between the G140L and G160M optics, and for OSM2 between the G185M and G230L optics. There are both hardware and software travel limits for the OSM1 focus drive. These limits are listed in Section 6.1 (Mechanism Limits and Settings) of DM-05. Software limits are checked by the FSW. I f a move command would send a motor beyond its software limits, the move is not performed and an error is reported with a status buffer message.

The COS OSM motors may not be overheated. A detailed discussion of overheat protection is given in section 2.1.6.

2.1.5.2 OSM FSW Macro Control

The OSM1 is operated by means of the following FSW macros:

1) Initialize OSM;
2) Move OSM to Absolute Position;
3) Move OSM to Relative Position.

2.1.5.2.1 Initialize Optic Select Mechanism Macro

The "Initialize Optics Select Mechanism " macro is used to initialize the OSM motor parameters. Each OSM motor must be initialized at least once after power-on before it can be moved. The macro parameters are:

- Motor selection;
- Whether to return to the home position during motor initialization;
- Motor speed selection;
- Motor hold-off count.

The **motor selection** indicates which mechanism motor is being initialized. Each motor has to be initialized separately.

The **motor home position** option, when enabled, returns the selected motor to a home position during motor initialization. Under normal operations this option will be enabled. The home position for each motor is a patchable constant. The home position for OSM1 rotation will be the 1230Å central wavelength position of G140L. The home position of the OSM1 focus motor will be the optimized focus position for NCM1. The home position for the OSM2 rotational motor will be the TA1 mirror. Note that the home option must be enabled for the OSM rotational axes to accurately determine the motor position. Subsequent absolute moves will not be allowed of the rotational motors were not sent to their home position during initialization.

The **motor speed selection** selects the stepping speed of the selected motor. The same motor speed will be used in all subsequent moves of that motor, until it is redefined via a new "Initialize OSM" macro. The speed of the rotational motors may not match the speed of the OSM1 focus motor. Laboratory testing shows that the OSM1 and OSM2 motors should be operated at preferred speeds, therefore the macro sheet for LOSMINIT has a CARD item which states that the preferred speed for the rotational motors is ROTFULL (78.12 steps/second), and that the preferred speed for the OSM1 translational (focus) motor is FOC2THRD (52.08 steps/second).

The **motor hold-off count** defines the length of time to keep the selected motor enabled after completion of the commanded number of steps, to allow for electrical braking of the motor. To determine the total time to complete the move, the hold-off count is added to the time needed to move the commanded number of steps. The same motor hold-off count will be used in all subsequent moves of that motor, until it is redefined via a new "Initialize OSM" macro.

2.1.5.2.2 Move Optic Select Mechanism to Relative Position Macro

The "Move OSM to Relative Position" macro specifies the motor (rotational, focus), the number of motor steps to move, and the direction of travel. For all OSM motors, it is desirable that moves in the non-preferred direction overshoot and return to the desired destination in the preferred direction to eliminate mechanism backlash. The relative move macro does not perform this overshoot, therefore, for relative moves in the non-preferred direction, the STScI ground system will need to perform overshoot processing by adding the overshoot to the number of steps in the non-preferred direction and commanding a separate relative move macro for the return move.

2.1.5.2.3 Move OSM to Absolute Position Macro

The "Move OSM to Absolute Position" macro specifies the motor and the desired optical element. The FSW will move to the desired optical element taking into consideration the soft stop motion limits. With absolute moves, overshoot processing is incorporated into a multi-step move sequence performed by the FSW in order to increase mechanism stability and repeatability. This is the macro that will be used during normal operations to control the motors. Absolute moves of the OSM are done using look-up tables for each optical element on the OSM (see Tables 2.1-1 and 2.1-2). The table has separate entries for FUV and NUV optics positions.

2.1.5.3 OSM Home Commanding

The operational home position of OSM1 is the 1309 Å central wavelength position of G130M. The operational home position of OSM2 is the 1850 Å central wavelength position of G185M. The OSMs are commanded to these positions at the end of a COS visit. This is done because the STScI ground system does not keep track of the state of the OSMs between visits, so an operational home position is necessary to ensure the OSMs are in a known state at the start of a visit, which saves time when commanding the initial motions. Another reason is to leave the OSMs in the most scientifically useful state should a mechanism fail between observations. This procedure is independent of whether the home position option described in section 2.1.5.2.1 is used for motor initialization.

2.1.6 Overheat Protection

The COS ApM and OSM motors should not be overheated. Overheat protection is incorporated in all COS mechanisms except for the External Shutter. The purpose of overheat protection is to protect the optics. The lubricant used will outgas above a certain temperature and could damage the optics. The overheat protection circuitry will shut a motor off before the motor reaches that temperature. There are two levels of overheat protection:

1) The first level of overheat protection comes in the form of limits monitoring. All motor temperatures are regularly collected by the normal engineering data collection software and checked by the limits monitoring software about every 2 seconds. The limits monitoring software will safe COS if any of the ApM or OSM motor temperatures is determined to be above 55° C. Both the action taken and the temperature limit are patchable constants.

2) As a second level of protection, the hardware overheat protection circuitry automatically disables an ApM or OSM motor when its temperature rises above 62° C by opening its motor winding relay. Any attempt to move the motor when in a hardware overheat condition will be ignored by the FSW. Before a motor that is in an overheat condition can be re-enabled, the LOVHTCLR macro must be issued followed by the LRELAY macro. The "Clear Overheat" macro will not be allowed to clear the overheat status bit until the motor has cooled to a temperature which is lower than the shutdown threshold. This automatic overheat protection is enabled upon power-on, but may be disabled via a ground macro. Under normal conditions, it will remain enabled.

2.1.6.1 Overheat Protection Provided by the Electronics

1) If the motor temperature of a mechanism exceeds a hardware threshold, the electronics will disable the motor driver for the mechanism and trip the motor winding relay.

2) The motor driver will remain disabled until the overheat bit is cleared and the relay is closed.

3) The overheat protection has temperature hysteresis; the temperature must fall below a lower threshold than the shutdown threshold before the relay can be closed.

4) There is an override overheat control bit which can be used to disable overheat protection.

5) The COS mechanism motor relay control electronics use a pulse circuit to close the relay for any given motor. The relay pulse circuit is edge-triggered. This means that for a pulse to be sent to close the relay, the pulse circuit must see a transition from 0 to 1. The inputs to a pulse circuit are the overheat status bits for a group of motors all OR'd with the nominal relay control bit. This means that all the OR'd overheat status bits must be cleared for the nominal control bit (for any

of the motor relays) to close any relay controlled by that pulse circuit. So, if motor A and motor B are both in an overheat condition, an attempt to clear the motor A overheat condition will not be successful because the motor B overheat status bit will prevent the input to the pulse circuit from going to 0 to later create the rising edge to close the selected relay. For COS, the two OSM rotational axes motors are part of one pulse circuit (SES#2) and the OSM1 focus and aperture cross-dispersion and dispersion motors are part of the other pulse circuit (SES#3).

2.1.6.2 FSW Interface

1) The FSW can detect an overheat condition from status registers.
2) The FSW can clear the overheat bit and close the winding relay after the motor temperature has dropped below the overheat recovery threshold temperature. To successfully close the winding relay, any other overheat bits on the same pulse circuit that have been set must be cleared first.
3) The FSW can set and clear the override overheat bit.
4) FSW must clear the overheat bit at initialization because of potential false overheat protection after a reset.

2.1.6.3 Special Overheat Protection Notes

1) The overheat status bit is the output of a flip-flop which is set by the output of a temperature/threshold comparator. The flip-flop can be reset while the output of the comparator still shows an overheat condition. The output of the comparator would have to go down and back up again for the flip-flop to recognize the overheat condition (edge triggered).
2) In S/W terms, the overheat status bit can be cleared even if the current temperature is still above the threshold. If this occurs, the overheat status will continue show “no overheat” until the temperature goes low enough so that the circuitry will see the transition back up to the overheat threshold.
3) Since the overheat circuits are identical for each mechanism, common thresholds could be used by the FSW.

2.1.6.4 Motor Winding Relays

Each stepper motor has two sets of windings that are configured via the motor winding relays. An MEB sees the motor winding relays as a primary and a redundant motor winding relay. An MEB can only close its own primary motor winding relay and open its redundant relay. The relay seen as the primary relay by MEB 1 is seen as the redundant relay by MEB 2 and *vice versa*. The following diagram attempts to depict this:

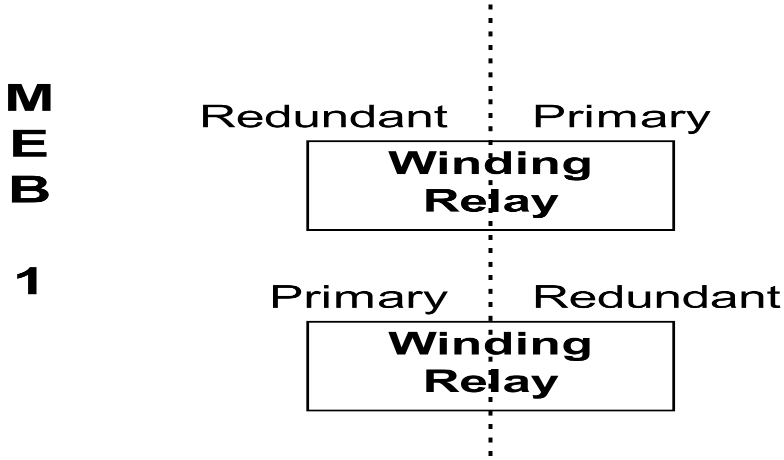

Figure 2.1-5: *Winding relays viewed by the COS MEBs.*

The motor relays are "protection" relays. The implication is that the relays are setup during initialization and are never changed unless there has been a hardware failure, or an overheat condition. Flipping relays is not a part of normal operations.

The steps required to flip a motor winding relay are simple; write a "1" to the relay register bit associated with the specific relay, pause, then clear the same bit (clearing the bit is simply preparation for the next time the relay will be set since the relays detect a rising edge, not a level signal).

Note that it is important that *the relay latch bit be set to a zero after setting the relay bit*, in order to allow the overheat circuitry to operate correctly. Also note that the motor winding relays should be set one at a time. Although the hardware design allows multiple relays to be set simultaneously, this is not recommended since they have not been tested this way.

2.2 ON-BOARD CALIBRATION LAMPS

COS shall be able to produce performance and calibration data using only sources and capabilities which are internal to the instrument (CEI Sec. 4.3.2). The purpose of this capability is to provide a convenient means to obtain routine information that is needed to prepare COS for an upcoming observation (i.e., useful for target acquisition), to reduce and interpret science data properly, and to monitor the functioning of the instrument. The calibration lamps are mounted on the calibration subsystem platform above the thermal shelf (see Figs. 1.3-1 and 2.2-1). Light is directed from the lamps to the ApM through a series of beam-splitters and fold mirrors (Fig. 2.2-2).

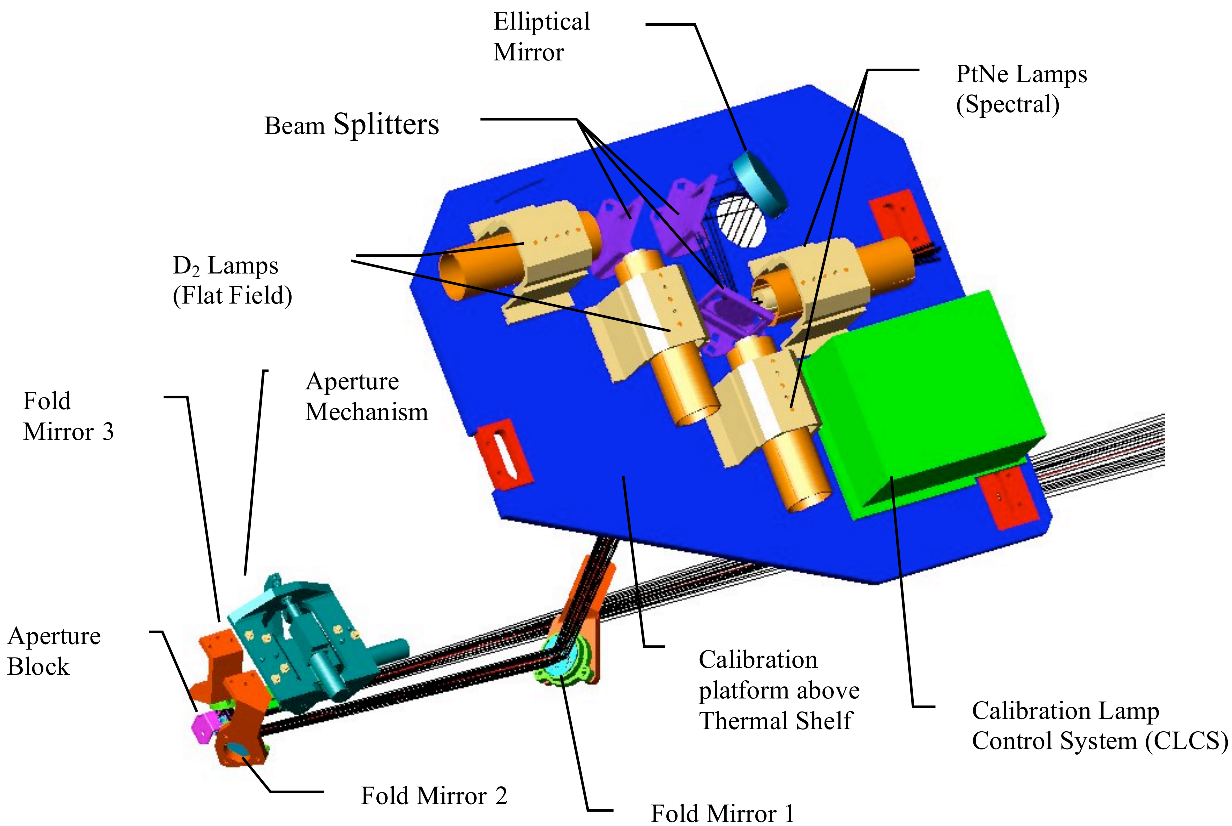

Figure 2.2-1: *Schematic of the Calibration Subsystem. Light from redundant wavelength and flat-field calibration lamps is directed through several beam splitters to an elliptical mirror, then down to the aperture block via several fold mirrors.*

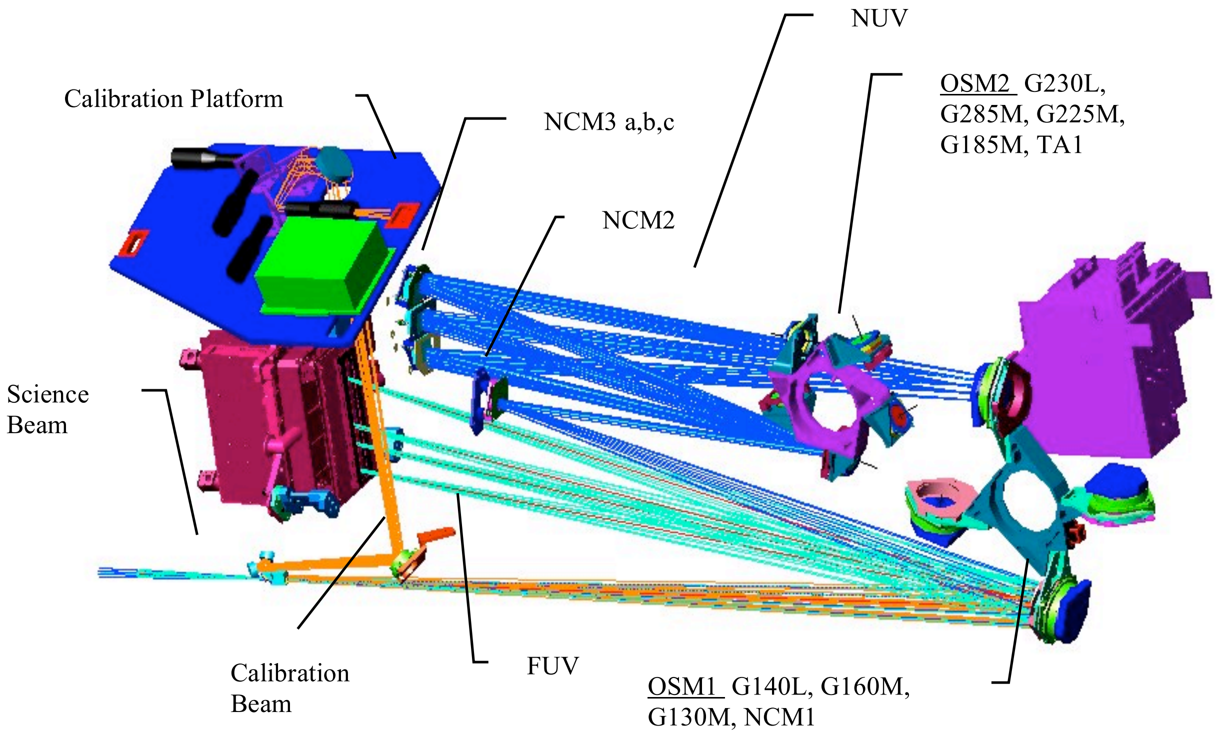

Figure 2.2-2: *Layout of the science and calibration beams in COS. Each beam can be directed toward either detector. The format of the dispersed beams on the detectors is shown in Figs. 1.3-14 and 1.3-15.*

There are three specific categories of tasks that will use data supplied by the calibration subsystem:

Wavelength calibration. The raw data produced by COS will consist of a list or image of detected photon events and the geometrical position at which they occurred on the detector. The reduction of these data will include transforming the count rate into flux, and the pixel coordinates into wavelengths. Wavelengths assigned to data points in the fully reduced and calibrated COS spectra shall have accuracy equivalent to absolute uncertainties of ±15 km s^{-1}, ±150 km s^{-1}, and ±175 km s^{-1} in the modes with resolving powers of R = 20000, 2000, and 1700, respectively (CEI Sec. 4.2.1).

Flat-field calibration. Variations in the detected count rate will be caused by factors such as structure in the spectrum of the target, wavelength dependent differences in the throughput of the telescope and spectrograph, and local irregularities in the sensitivity of the detector. The flat-field calibration process will measure small-scale detector irregularities so that they can be removed from the raw data. The calibration process shall allow the relative response to be corrected with an RMS uncertainty of 3% or less, as measured with data points corresponding to spectral resolution elements in the extracted net spectrum (CEI Sec. 4.3.2). Elimination of small-scale detector irregularities may be accomplished through a combination of flat-fielding and FP-SPLITS (see Sec. 5).

Target acquisition. The COS flight software will include capabilities to recognize the presence of a target and to request small angle maneuvers of the HST calculated to place the target at the optimum location in the center of the aperture. The calibration subsystem will provide a geometrical reference point that will define the relationship between a known location at the aperture plane and the detector pixel coordinates in which the measurements are made. The target acquisition algorithms, supported by the calibration process, shall allow the target to be centered in the science aperture with an accuracy of ±0.3 arc seconds (CEI Sec. 4.3.2).

2.2.1 Safe and Efficient Operations

Stability and repeatability. The brightness of the signal produced by the calibration subsystem must be predictable to operators and users. Preplanned power settings and exposure times must result in data quality that satisfies the needs of the exposure. The subsystem must not produce useless under-exposed data or violations of BOP limits when operated in a configuration predicted to give valid and safe exposures.

Bright Object Protection. It shall be possible to use the calibration subsystem with any allowed spectroscopic mode without violating Bright Object Protection constraints. The purpose of this requirement is to ensure that for every mode of COS there exists at least one configuration of the calibration subsystem capable of providing a calibration signal which is compatible with the BOP limits. Any combination of lamp, power level, optical mode, wavelength, and detector that does violate a BOP limit shall be identified, documented, and its use avoided. This includes both global and local count rate restrictions (CEI Sec. 4.3.5).

Transient brightness. Calibration lamps usually have a momentary spike of brightness when first ignited. Transients may have a duration of several tens of milli-seconds, and can be several times brighter than the steady-state mean. Analysis and testing shall ensure that turn-on spikes do not pose a threat to the detectors. Operational procedures and BOP flight software shall be designed and implemented to ensure the safety of the detectors and to avoid responding to transients as dangerous events if they do not pose a real threat. BOP limits for each COS detector are defined in Section 4.

Telemetry. Engineering data should be available that provides unambiguous information to controllers regarding the state of the subsystem. The status of each lamp, including on/off, current, voltage and temperature should be easily visible (CEI Sec. 5.5.2).

Parallel operations. Use of the calibration subsystem shall be possible as a parallel activity with other HST science instrument operations. It shall be possible to make internal calibration exposures while another SI is observing an external target (CEI Sec. 4.3.4). The external shutter shall be closed to avoid stray light from escaping the COS instrument during calibration exposures.

Multiple power settings. The subsystem will include three power settings for each lamp. The setting used for an observation will depend on the grating being used. The intent of this requirement is to provide signal strengths to accommodate the range of sensitivity of the various COS modes, the range of intrinsic brightness of UV light sources over the COS wavelength range, and the possibility of changing lamp output or instrument sensitivity over the lifetime of the instrument. A minimum power level shall be high enough to ensure that the lamp will operate reliably without flickering or risk of failure to start. A maximum power level shall not exceed the safe operation of the lamp or other subsystem components. Operation of the lamp at the maximum level shall not result in violation of instrument thermal constraints. Use of the maximum level shall not significantly reduce the lifetime of the lamp or any component of the calibration subsystem or the COS instrument. Schematic diagrams for safe usage of the Pt-Ne and deuterium lamps are shown in Figures 2.2-3 and 2.2-4 in the following subsections, including current levels for the aperture location phases of target acquisition (Sec. 5.2). These recommended settings will be tested during ground calibration.

Aperture alignment. If the apertures, optics, and detectors of COS are re-aligned periodically to place the spectrum on fresh regions of the detectors, the calibration subsystem must accommodate this shift. The illumination for the flat-field must cover the new locations of the primary science aperture and the bright object aperture spectra, and the relationship between the wavelength calibration spectrum and both science aperture spectra must be re-established. It is not necessary that the relationship remain identical before and after such a shift, but a procedure must exist to derive a new relationship.

2.2.2 Wavelength Calibration Lamp

COS shall contain two lamps whose spectra contain emission lines suitable for specifying the wavelength scale of any spectroscopic mode (CEI Sec. 4.3.2). The calibration source(s) shall cover the wavelength range of COS, $1150Å < \lambda < 3200Å$ (CEI Table 4-1). Pt-Ne hollow cathode lamps will be used for wavelength calibrations. Each lamp shall be operable from any legal electrical and operational configuration of COS

(CEI Sec. 5.5.3). The count-rate requirements and restrictions are summarized in Table 2.2-1.

Minimum brightness. For any allowed combination of grating, wavelength range, and detector the subsystem shall provide a spectrum containing sufficient spectral information to facilitate cross-correlating the wavecal spectrum against a reference spectrum to determine offsets in the wavelength scale. Experience has shown that 60 second exposures are generally sufficient for this activity. Table 2.2-2 lists the wavelength setting and wavecal exposure times.

Maximum brightness. For any allowed combination of grating, wavelength range and detector the subsystem shall provide a spectrum whose integrated count rate does not exceed the global count rate limit, and in which no individual line exceeds the local count rate limit. Every allowed observing mode must have at least one power setting that produces a signal with acceptable brightness. It must be possible to calibrate any allowed observing mode. Any combination of lamp and power setting that violates bright limits for any mode must be identified and avoided.

Table 2.2-1: Count-rate Limits for COS Wavelength Calibration

Item	**FUV**	**NUV**	**Rationale**
Minimum count rate Minimum of 5 lines in each exposure	0.33 cts/sec/line	0.33 cts/sec/line	count rate integrated over emission line 100 counts in 5 minutes
maximum global count rate (Time-tag)	< 21,000 cts/sec global Time-tag	< 21,000 cts/sec global Time-tag	Maximum time-tag count rate limited by on-board data processing
maximum count rate in one emission line	75 cts/sec/resel	800 cts/sec/resel	Local bright object protection max rate derived from CARD limits: FUV: 1500 cts/sec/resel ÷ 20 NUV: 200 cts/sec/pixel × (2×2) (optimistic resolution)
maximum count rate in one pixel	5 cts/sec/pixel	200 cts/sec/pixel	charge replenishment + uniform image illumination
accumulated counts in emission line image per year	2.2 10^7 cts [300,000 sec exposure = 1000 five min exposures @ 75 cts/sec]	2.4 10^8 cts [300,000 sec exposure 1000 five min exposures @ 800 cts/sec]	Threshold for onset of gain sag: FUV 10^9 cts/mm^2 NUV 10^{10} cts/mm^2

Table 2.2-2: Wavelength Calibration Exposure Times

Grating	Central Wavelength (Angstroms)	Lamp Current Specification	Exposure Time (seconds)
G130M	All	MEDIUM	90
G160M	All	MEDIUM	60
G140L	All	MEDIUM	60
G185M	1786	MEDIUM	60
	1817	MEDIUM	60
	1835	MEDIUM	60
	1850	MEDIUM	60
	1864	MEDIUM	60
	1882	MEDIUM	60
	1890	MEDIUM	60
	1900	MEDIUM	60
	1913	MEDIUM	60
	1921	MEDIUM	60
	1941	MEDIUM	60
	1953	MEDIUM	60
	1971	MEDIUM	60
	1986	MEDIUM	60
	2010	MEDIUM	60
G225M	2186	MEDIUM	60
	2217	MEDIUM	60
	2233	MEDIUM	60
	2250	MEDIUM	60
	2268	MEDIUM	60
	2283	MEDIUM	60
	2306	MEDIUM	60
	2325	MEDIUM	60
	2339	MEDIUM	60
	2357	MEDIUM	60
	2373	MEDIUM	60
	2390	MEDIUM	60
	2410	MEDIUM	60
G285M	2617	MEDIUM	60
	2637	MEDIUM	60
	2657	MEDIUM	60
	2676	MEDIUM	60
	2695	HIGH	60

Grating	Central Wavelength (Angstroms)	Lamp Current Specification	Exposure Time (seconds)
	2709	HIGH	60
	2719	HIGH	60
	2639	HIGH	60
	2850	HIGH	60
	2952	HIGH	60
	2979	HIGH	60
	2996	MEDIUM	60
	3018	MEDIUM	60
	3035	MEDIUM	60
	3057	MEDIUM	60
	3074	MEDIUM	60
	3094	MEDIUM	60
G230L	2635	MEDIUM	60
	3000	MEDIUM	60
	3360	MEDIUM	60

There are two Pt-Ne lamps, each with three current levels. For one lamp the levels are 3, 10, and 14 milli-amps, and for the second lamp the current levels are 6, 10, and 18 milli-amps. This effectively provides six possible count rate levels to use for wavelength calibration exposures. In general, the lowest current levels will be used for the "calibrate aperture phase" of target acquisition and for images with the TA1 mirror. The mid-range current levels will be used for the majority of the spectroscopic calibrations. The maximum levels are available to compensate for degraded count rates over the life of the mission.

Figure 2.2-3 shows a schematic of Pt-Ne lamp current settings versus optic configuration to be used as a guide in assessing safe usage of the wavelength calibration lamps, particularly applicable to the beginning of the mission life.

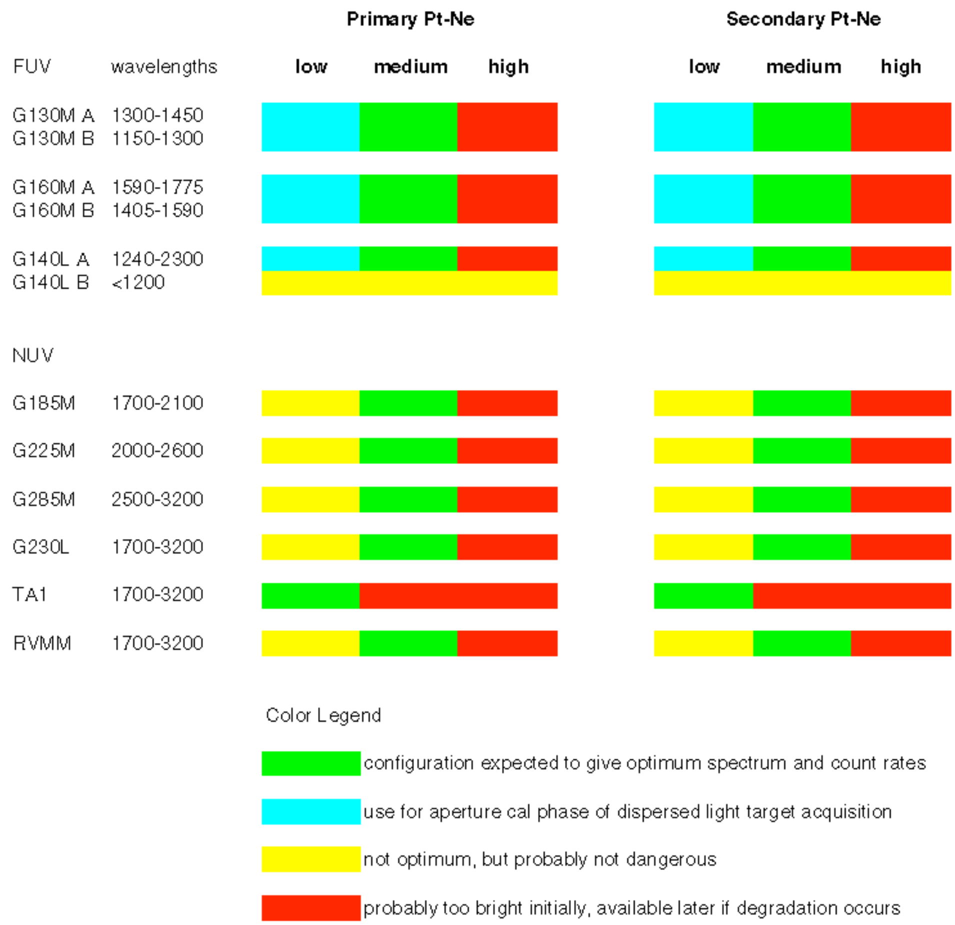

Figure 2.2-3: Color-coded schematic of safe and unsafe usage configurations for the Pt-Ne wavelength calibration lamps with the various COS gratings and mirrors.

Wavelength accuracy. Wavelengths assigned to data points in the fully reduced and calibrated COS spectra shall have accuracy equivalent to absolute uncertainties of ±15 km s^{-1}, ±150 km s^{-1}, and ±175 km s^{-1} in the modes with resolving powers of R = 20000, 2000, and 1700, respectively. In any spectrum exposure there shall be five or more lines suitable for use in the dispersion solution. This is based on the expectation that a cubic polynomial will be used as part of the algorithm. The sources of uncertainty are summarized in Table 2.2-2.

Table 2.2-3: Uncertainties in Wavelength Calibration

Mode	**Total 1σ Uncertainty (km s^{-1})**	**ΔDISP at detector (μm, 1σ)**	**Internal error (pixels, 1σ)**	**External error (arcsec, 1σ)**
G130M	15	34 – 45	3.0 – 4.0	0.09 – 0.12

G160M	15	35 – 43	3.1 – 3.8	0.10 – 0.12
G140L	150	45 – 75	4.0 – 6.6	0.12 – 0.21
G185M	15	43 – 60	1.2 – 1.7	0.03 – 0.04
G225M	15	58 – 80	1.6 – 2.3	0.04 – 0.06
G285M	15	58 – 88	1.6 – 2.6	0.05 – 0.07
G230L	175	50 – 93	1.4 – 2.6	0.03 – 0.07

ΔDISP is the linear distance in the dispersion direction that corresponds to the total error. This total has been allocated equally to internal and external sources, so that when they are summed in quadrature they equal the total. The internal errors are those associated with the wavelength scale, such as the dispersion relationship, aperture offsets, distortions, drifts etc. The magnitude is expressed in detector pixel units here, assuming 6-7 μm pixels for the FUV detector, and 25 μm pixels for the NUV detector. The external error is the part allocated to uncertainty in the location of the target in the aperture, expressed in arcseconds.

Lifetime. The wavelength calibration subsystem shall be designed to provide the required data for the entire lifetime of the COS instrument. The COS shall be designed for a minimum of five years on-orbit operating life and a minimum of ten years calendar life (CEI Sec. 5.1.2). The pre-launch testing and calibration may represent the equivalent of one year of operations. The Design Reference Mission estimates that COS may be prime instrument for ~5,000 orbits, with as many as six wavelength calibration exposures per orbit. The DRM also estimates that approximately 500-1000 individual targets will be observed with COS over its lifetime. Each on-board target acquisition may require at least one exposure of the calibration lamp. The above estimates imply approximately 30,000 wavelength calibration exposures. If each exposure requires one lamp to be on for ~1 minute the requirement is for 30,000 minutes (500 hours) of use. These estimates imply approximately 30,000 turn-on cycles. Further details on lamp lifetime issues can be found in Ball Aerospace & Technologies Corp. SER-SYS-039.

2.2.3 Flat-Field Calibration Lamp

The flat-field calibration process shall allow the relative response to be corrected with an RMS uncertainty of 3% or less, as measured with data points corresponding to spectral resolution elements in the extracted net spectrum (CEI Sec. 4.3.2). The calibration subsystem shall be capable of providing a flat-field normalization over the wavelength range of COS, 1150Å < λ < 3200Å (CEI Table 4-1). The flat-field signal for a given grating mode shall be produced with light whose wavelength is within the nominal band of its detector: FUV modes 1150Å < λ < 1775Å; NUV modes 1700Å < λ < 3200Å. It is not necessary to have a precise match between pixel number and wavelength for each mode, although closer is better. It is likely that a deuterium hollow cathode lamp will be used for flat-field calibration. The calibration subsystem shall provide data from which the flat-field normalization functions can be derived for both the Primary Science Aperture and the Bright Object Aperture. The calibration subsystem shall provide illumination of the pixel regions used by all of the grating modes for each detector. The baseline is to use deuterium hollow cathode lamps for flat-field sources, manufactured by the same vendor that is supplying the Pt-Ne lamps for wavelength calibration.

Dispersion direction. The illumination provided for flat-field calibration shall provide continuous coverage of the detector pixels in the direction of dispersion. The illumination is not required to be uniform, but variations should be smooth enough that structure in the detector response on scales ranging from pixel-to-pixel to several tens of pixels can be determined. The smoothness of the signal at the detector may be achieved by a convolution of the intrinsic spectrum of the source with an optical response function of the calibration subsystem, and by the superposition of calibration exposures taken at two or more instrumental setups (FP-SPLITs, non-standard OSM positions, different gratings). The intrinsic spectrum is not required to be a smooth continuum.

Cross-dispersion direction. The illumination provided for flat-field calibration shall cover at least as many pixels in the cross-dispersion direction as the spectrum of a point source. The calibration spectrum may be wider than the point source spectrum, and the desired goal is to provide a flat-field spectrum that is as wide as a science spectrum of a diffuse source that completely fills the science aperture.

Minimum brightness. The flat-field calibration signal shall be bright enough to produce a minimum of 1000 counts per spectral resolution element in an exposure time of 10^4 seconds for each spectroscopic mode.

Maximum brightness. For any allowed combination of grating, wavelength range, and detector the subsystem shall provide an illumination pattern whose integrated count rate does not exceed the global count rate limit, and in which no bright feature exceeds the local count rate limit. Every allowed observing mode must have at least one lamp with one power setting that produces a signal with acceptable brightness. It must be possible to calibrate any allowed observing mode. Any combination of lamp and power setting that violates bright limits for any mode must be identified and avoided.

The flat-field count-rate requirements and restrictions are summarized in Table 2.2-3.

Table 2.2-4: Count-rate Limits for COS Flat-field Exposures

Item	FUV	NUV	Rationale
minimum count rate	0.0005 cts/pixel/sec	0.025 cts/pixel/sec	1000 cts/spectral resolution element in 10000 seconds
maximum global count rate (Time-tag)	< 21,000 cts/sec total (Time-tag mode)	< 21,000 cts/sec (Time-tag mode)	maximum count rate limited by on-board data processing
maximum count rate in any one pixel	8 cts/pixel sec	200 cts/pixel sec	charge replenishment in pores of MCP
highest average per pixel count rate	0.025 cts/pixel sec (Time-tag mode)	0.34 cts/pixel sec (Time-tag mode)	max global rate uniform illumination with 500μm aperture

There are two deuterium flat-field lamps, each with three current settings. For both lamps the levels are 3, 7, and 17 milli-amps. In general, either the low or medium setting should be used with the FUV gratings G130M and G160M. G130M will be used to flat-field segment A of the FUV detector using the medium setting. G160M will be used to flat-field segment B of the FUV detector using the low setting. For the NUV channel, the total throughput is low and G185M will be used with the high setting to flat-field the three science stripes on the NUV detector. Figure 2.2-4 shows a schematic of deuterium lamp current settings versus optic configuration to be used as a guide in assessing safe usage of the wavelength calibration lamps, particularly applicable to the beginning of the mission life.

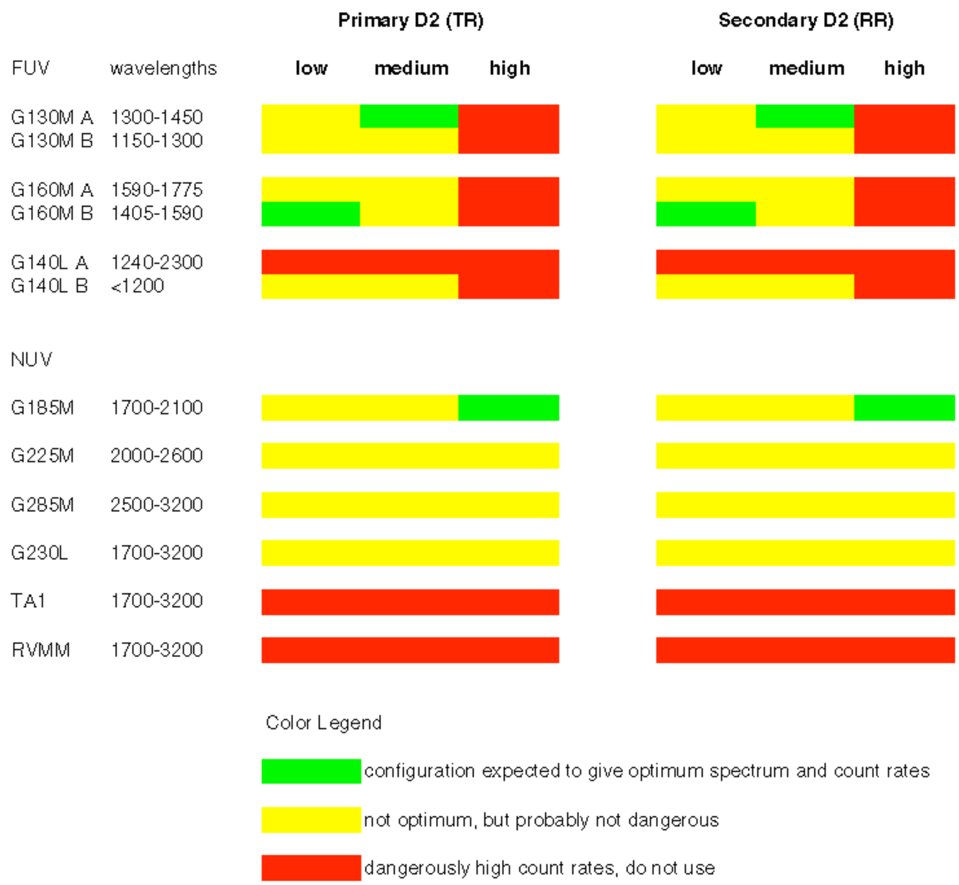

Figure 2.2-4: Color-coded schematic of safe and unsafe usage configurations for the deuterium flat-field calibration lamps with the various COS gratings and mirrors.

Lifetime. The design of the spectrograph, detectors, and calibration subsystem shall support the ability to achieve S/N = 100 per spectral resolution element (CEI Sec. 4.2.5). This is a more stringent requirement than the nominal goal of S/N = 30. Analysis indicates that flat-field information with approximately 1000 counts per pixel will be needed for the FUV modes, and approximately 2500 counts per pixel for the NUV modes. If we plan to produce such data for each spectroscopic mode twice per year for eight years, the total lamp use can be estimated (Table 2.2-5).

Table 2.2-5: Lamp lifetime requirements for flat-field

	FUV		NUV	
	count rate	lifetime hours	count rate	lifetime hours
minimum	0.0005	26640	0.025	1350
max Time-tag	0.025	533	0.34	120
max Accum	0.08	168	4.04	12

The goal of providing flat-fields to support S/N = 100 spectra will not be reached using the on-board subsystem alone if its count rate is near the minimum. It will be feasible if count rates near the maximum can be achieved. The minimum required lifetime would be near 200 hours, with 1000 hours more likely.

2.3 VACUUM SENSING SYSTEM

COS contains a vacuum sensing system which is used to monitor the *in-situ* vacuum pressure of the instrument's optical cavity. Vacuum sensing is implemented by monitoring the voltage and current of a cold-cathode ion pump (Varian model 913-0038). The raw voltage and current data from the ion pump are carried in the RIU direct telemetry and these data can be converted to vacuum pressure via calibration data acquired during the instrument's integration and test effort. The ion pump is mounted on the center of the COS thermal shelf.

The vacuum sensing system is configured to accurately monitor vacuum pressure over a three decade range from 10^{-4} to 10^{-7} Torr. Although the pump can be turned on after the vacuum pressure is less than 0.1 Torr, it is recommended that the pump be turned on only after the vacuum pressure is less than 10^{-4} Torr. Based upon the venting experience with previous HST science instruments, 10^{-4} Torr should be reached within a few days after SI installation into the observatory. Once turned on, the ion pump is used to monitor the instrument's vacuum pressure in order to determine if conditions are appropriate for opening the FUV detector door and then for FUV high voltage (HV) to be operated (see Sec. 4.1).

Although the ion pump itself is single-string, it is serviced by both the A and B sides of the COS electronics. At start-up ($\sim 10^{-4}$ Torr) the ion pump will typically draw several hundred microamps of current and run around 500 volts. As the vacuum improves within COS, the current drawn will decrease and the operating voltage will increase to approximately a few microamps and a few thousand volts at 10^{-6} Torr. The actual values of current and voltage for determining the vacuum level will be calibrated during COS I&T and will be provided in DM-14. Four discrete commands that come from each of the RIUs are used to activate the ion pump. Two of the commands select the source of power for the pump (LVPS1 or LVPS2). Additionally there are Enable and Disable commands to the pump from each RIU. The discrete commands operate relays inside the ion pump box.

The ion pump electronics are self-protecting. The output HV is limited by design to approximately 3 kV into an open circuit. There is an input current limiter to shut the circuitry down if the HV output (or some other internal circuitry) should happen to short out. There is no autonomous means of shutting down the ion gauge by itself. It is possible to damage the pump itself if it is powered at too high a pressure; pump life is a function of pressure. A safe start-up pressure would be less than 0.1 Torr, but the preferred pressure is below 10^{-3} Torr and measurements will only be accurate below 10^{-4} Torr. The pump will take longer to "fire" at extremely low pressures.

It is expected that the ion pump will only be used until that point in time when the vacuum inside COS is of adequate quality that the FUV detector door can be opened and FUV HV operations can commence (see Sec. 4.1.1 for FUV detector vacuum requirements). In the advent of a future servicing mission or for future monitoring of the vacuum conditions within COS, the ion pump can be restarted (although if the pressure is too low, it may not be possible to start the pump). Because the ion pump can contribute significantly to the noise background of the FUV detector, the ion pump should be turned off when the FUV detector door is to be opened and science operations commence.

3. ELECTRONICS AND FLIGHT SOFTWARE

3.1 OVERVIEW

Figure 3.1-1 in Section 3.1.1 shows an isometric drawing of the locations of the main components and subsystems in the COS instrument. Figure 3.1-2 gives an overview of the components of the COS FSW (Flight SoftWare), and shows in a high-level fashion the electronics boxes/boards in which these FSW components reside. Figure 3.1-3 is a true electrical block diagram, showing redundancy and cross-strapping. Figure 3.1-2 addresses FSW and data-flow issues, while Fig. 3.1-3 diagram shows the actual electrical subsystem.

3.1.1 Block Diagrams of the FSW and Electronics

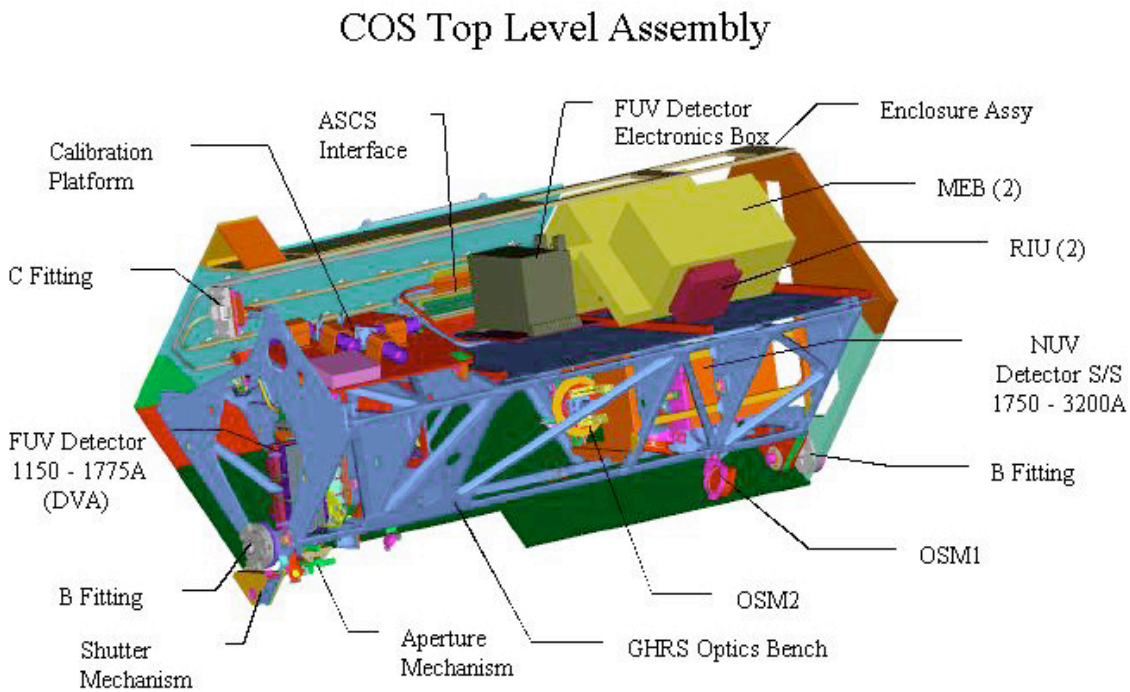

Figure 3.1-1: *Isometric drawing of the main components of the COS instrument, showing the locations of the detector subsystems, mechanisms, calibration subsystem, and MEBs.*

COS FSW Component Overview

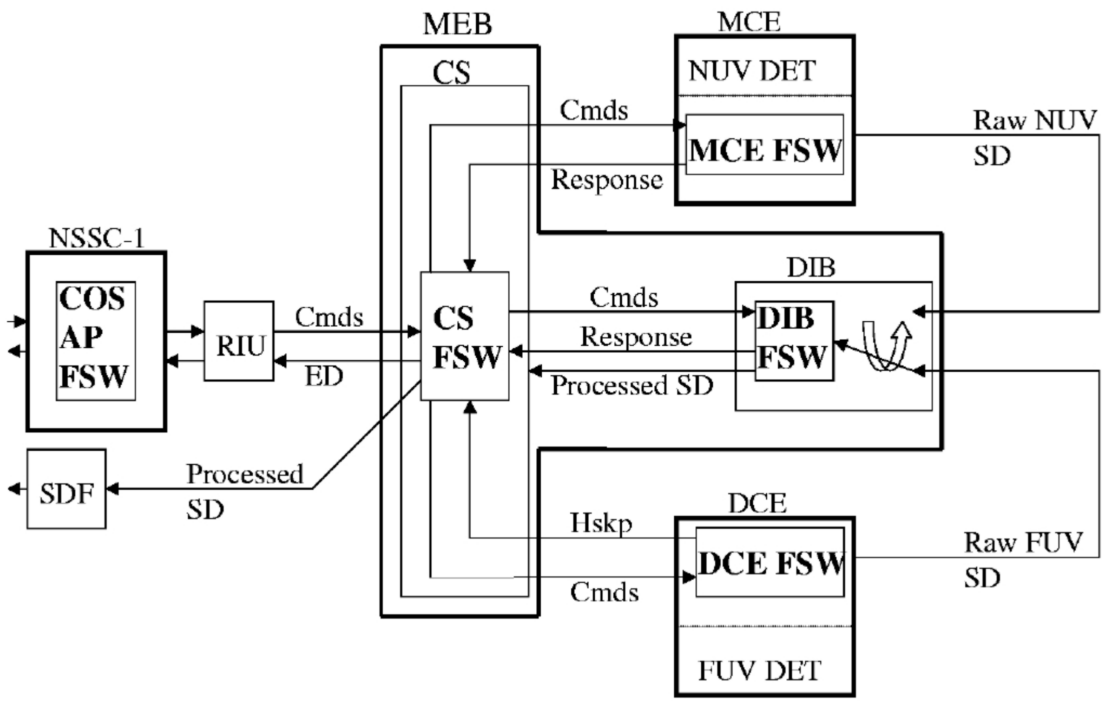

Figure 3.1-2: *Overview of the components of the COS FSW.*

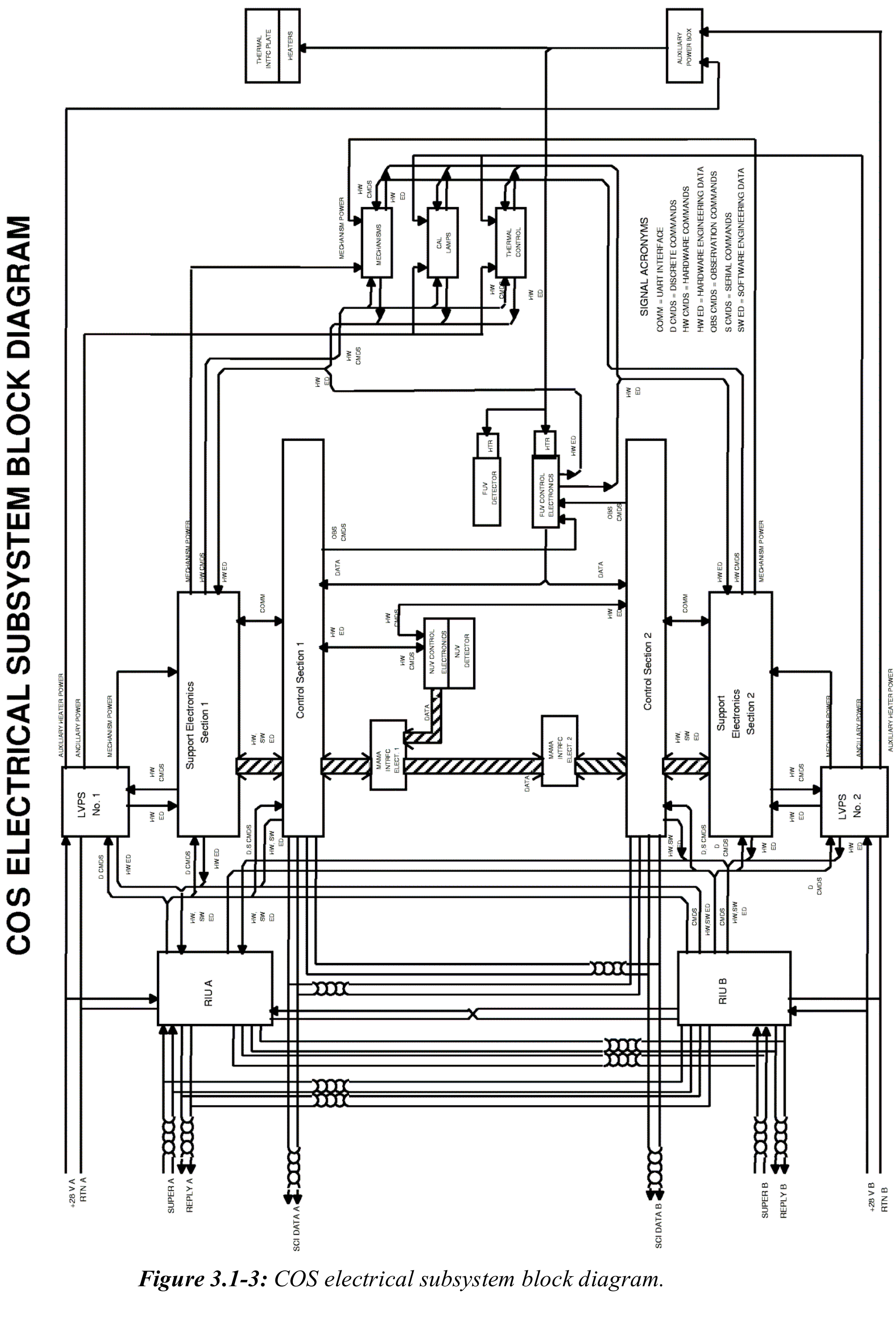

Figure 3.1-3: COS electrical subsystem block diagram.

3.1.2 High Level Description of Functions

There are five components of COS FSW.

3.1.2.1 COS AP (Application Processor) FSW

The COS AP (Application Processor) FSW resides in the NSSC-1. There are three Application Processors. The Macro AP reformats macro commands and command data from the ground system for efficient delivery to the CS (Control Section) FSW. The Safing AP inspects the results of limit-checking of relevant COS engineering data and calls for the execution of the COS Safing Command Sequence if any engineering data items are out of limits for too long. Finally, the CSCOMM AP (Control Section COMMunication) receives information and responds to requests for services from the CS FSW via special engineering data, and passes along the state of the HST Take-Data flag to the CS FSW whenever the state of that flag changes.

3.1.2.2 CS (Control Section) FSW

The CS FSW, the central body of FSW associated with the COS instrument, resides in the Control Section of the MEB (Main Electronics Box) within the COS instrument. The CS FSW receives and executes macro commands from the NSSC-1, retrieves and limit-checks engineering data from around the COS instrument and transmits that engineering data to the NSSC-1 via the RIU (Remote Interface Unit), commands the COS mechanisms, communicates with the MCE (MAMA Control Electronics) FSW, communicates with the DCE (XDL Control Electronics) FSW, communicates with the DIB (Detector Interface Board) FSW, receives both MAMA and XDL processed science data from the DIB FSW and transmits that data to the SDF (Science Data Formatter), manages the science data buffer memory (not shown) within the CS, performs target acquisitions by analyzing MAMA or XDL science data and making requests for HST small angle maneuvers to the CSCOMM AP within the NSSC-1, performs diagnostics exposures and PHD exposures, and performs memory dumps.

3.1.2.3 MCE (MAMA Control Electronics) FSW

The MCE (MAMA Control Electronics) FSW resides in the MCE within the MAMA detector assembly. The MCE FSW receives commands from the CS FSW, provides engineering data responses to the CS FSW, and commands the MAMA count rate electronics and high voltage electronics. The MCE FSW implements the MAMA global count rate algorithm. The MCE FSW executes only atomic commands (i.e., no macros) from the CS FSW, and the ‘intelligence’ for ramping up the MAMA high-voltage resides within the CS FSW.

3.1.2.4 DCE (XDL Detector Control Electronics) FSW

The DCE (XDL Detector Control Electronics) FSW resides within the DCE. The DCE FSW receives commands from the CS FSW, provides housekeeping engineering data asynchronously to the CS FSW, and commands the XDL high-voltage electronics. The DCE FSW commands from the CS FSW, and the ‘intelligence’ for ramping up the XDL high-voltage resides within the DCE FSW.

3.1.3 DIB (Detector Interface Board) FSW

The DIB FSW resides on the Detector Interface Board within the Control Section of the MEB. The DIB FSW receives commands from and provides responses to the CS FSW. The DIB FSW also receives raw detector data from the MAMA and from the XDL, but from only one of those sources for a given exposure. For ACCUM-mode exposures, the DIB FSW computes addresses in CS buffer memory whose contents are incremented during the exposure. For time-tag exposures, the DIB FSW writes event words and coarse-time words into successive CS buffer memory locations.

The electronic switch that routes raw MAMA detector science data or raw XDL detector science data into the DIB FSW is managed by the DIB FSW. There exist macro-commands from the ground system, received by the CS FSW and forwarded by the CS FSW to the DIB FSW, which initiate MAMA exposures or XDL exposures. The DIB FSW sets the switch to the appropriate position based on this information just before the exposure begins.

3.2 SCIENCE DATA BUFFER MANAGEMENT

Valid science data appear 280 ns after a valid photon event is detected by the anode array. The DIB in the MEB can either accumulate the science data over a programmed integration time or the science data can be time-tagged over a programmable acquisition time. In Time-tag mode, the DIB inserts a time word once every 32 ms (if there is an event) into the asynchronous XDL or MAMA science data stream providing a temporal record of the image. The finite buffer space available for the time-tagged science data and the processing overhead required by the DIB to time-tag the data, places a lien on the speed and data capacity for this mode. The speed and architecture of the DIB restricts the DIB data processing rate to ~250,000 events/sec. Actual accumulation mode calibration data measured on the STIS instrument shows the MIE (the STIS analog to the DIB) maintaining linearity up to 278,000 c/s. This image accumulation (ACCUM) mode will be used for brighter targets, calibration stars, and internal test modes. Otherwise, data will be acquired in Time-tag mode, with a maximum count rate of ~21,000 events/sec during “dumping-while-acquiring” (see below). Bright sources can be observed by sub-arraying a portion of the spectrum to limit the count rate sent to the data buffer.

Since it is not possible for the DIB to accept raw MAMA science data and raw XDL science data at the same time, parallel detector operations are not possible on COS. In addition, there is no data compression for COS, further simplifying the CS Buffer Memory Management.

The COS instrument contains a total of 18 MB of CS buffer RAM (Random Access Memory) per side which can be used to store science data images, memory dumps, and diagnostic and PHD data. The 18 MB is enough to store 9 full MAMA ACCUM images, but is not enough to store even 1 full XDL ACCUM image (which would require 64 MB); for this reason, subarrays must always be used for XDL images. Subarrays are used for the MAMA during target-acquisition, and during observations of bright sources (see Sec. 5.3). Science images are stored and dumped in the order in which they are allocated, and the CS FSW allows a maximum of 50 images to be stored at any given time. The types of science data images that are managed by the CS FSW, which may all reside in buffer memory at the same time in any order, include: MAMA images (both ACCUM and Time-tag); XDL images (ACCUM, Time-tag, and PHD); analog, digital and derived diagnostic images; DIB and DCE memory images; and CS memory dump data. All types of science data images are preceded by a header which contains pertinent image information. (See DM-06 for a detailed listing of the header contents.)

The header and required image space are allocated at the start of an operation (i.e., exposure, diagnostic, etc.) for all image types. Headers and image space are automatically deallocated after the science image has been successfully dumped to the SDF. Deallocating image space makes the buffer memory available for reallocation. Additionally, the CS FSW allows the buffer memory pointers to be initialized to an empty state effectively deleting all images currently in memory. There are two buffer memory pointers: the fill pointer which points to the next available buffer memory location which is free to be allocated, and the dump pointer which points to the beginning of the data for the next exposure to be dumped to the SDF.

Science images are allocated a specific amount of CS buffer memory into which all of the science data must fit. Image data are stored in sequential order, which means that as data are gathered by the FSW, they are stored in buffer memory in the next available set of memory locations. CS buffer memory is considered to be a large circular buffer, and all of the data for a given exposure (but see below for Time-tag exposures) must reside in contiguous memory locations of always increasing addresses. For ACCUM exposures, XDL PHD exposures, memory dumps, and diagnostic exposures, a region of buffer memory large enough to contain the image is reserved when the exposure begins.

PHD data from the XDL detector are made available by means of PHD exposures. PHD data are transmitted from the DCE FSW to the CS FSW as part of DCE FSW housekeeping. The CS FSW maintains and updates an accumulating PHD histogram of 256 bins (128 bins per segment), with 32-bits per bin. As with any counter, these bins can overflow if not dumped and cleared, or at least cleared often enough. The CS FSW supports a command to clear these bins in the PHD histogram to zero. In addition, when requested by command from the NSSC-1 to perform a 'PHD exposure', the CS FSW creates a science data header, reserves space in CS buffer memory, and copies the current contents of the PHD histogram into the reserved space in CS buffer memory. That PHD data are then available for dumping to the SDF, just like the data from any other 'exposure' or memory dump or diagnostic. Following the copying of the current PHD histogram to CS buffer memory, the CS FSW clears all the bins to zero in its accumulating PHD histogram and continues to accumulate the histogram from housekeeping data from the DCE FSW. The collection of this histogram is an on-going process, is fed by data from the DCE housekeeping stream, and is independent of the collection and processing of XDL detector data through the DIB.

3.2.1 Buffer Management during Time-Tag Exposures

3.2.1.1 Flight Software Processing

The amount of data generated during Time-tag exposures depends on the photon flux reaching the detector: each photon event requires 4 bytes to store the coordinates of the event plus other information (see event word descriptions in the figures in Sec. 1.3.5) in the science data buffer. The 18-Mbyte COS data buffer (corresponding to 4.7 x 10^6 photon events) is used as a circular buffer for storing Time-tag data. The buffer is required to be empty at the start of a Time-tag exposure. Fill and dump pointers are maintained by the DIB and CS FSW, respectively. The DIB increments the fill pointer as it processes Time-tag events. When the CS receives a command from the ground to dump Time-tag data from the buffer to the SSR, the CS will transfer data beginning at the dump pointer. The amount of data to dump and the time allocated for the dump must be specified in advance using stored commanding. The dump pointer is advanced continuously as data are removed from the buffer during a dump, and is left at the memory location following the last Time-tag event that was dumped.

Buffer dumps are commanded after a Time-tag exposure to dump the expected amount of data. Dumps may also be commanded during the exposure, allowing for exposures that generate more data than the buffer will hold (see below). Since the true count rate is not known in advance, the fill pointer may advance either faster or slower than anticipated when setting up the dumps. If the fill pointer advances faster than expected, the fill pointer may eventually catch up to the dump pointer. At that point, the DIB will stop storing Time-tag data in the buffer, and further events will be lost until the dump pointer begins to advance again after the start of the next commanded dump.

On the other hand, if the fill pointer advances slower than expected, there may be less data in the buffer than the amount the CS has been commanded to dump. In this case, the CS will dump the data up to the location of the fill pointer at the time the dump command was received. The CS will then inform the NSSC-1 of this situation and the NSSC-1 will stop the recorder after padding the remainder of the current line with fill data. This handshaking between the CS and NSSC-1 is a change from the STIS design in order to eliminate unnecessary data volume. It does not change the duration of the dump activity, which is set by stored commanding based on the expected amount of data.

3.2.1.2 Ground System Modeling and Dump Commanding

If there are data in buffer memory from previous exposures, the ground system will command a dump to empty the buffer prior to the start of a Time-tag exposure.

COS proposers using Time-tag mode for either the FUV or NUV detector will be required to estimate the count rate for the purpose of setting up dump commanding. The count rate will be estimated by specifying a time called Buffer-Time (in integer seconds), in which 2.354×10^6 photon events (approximately half the buffer) will have accumulated during the exposure. To ensure that no observed photon events are discarded, the value of Buffer-Time should be based on the maximum count rate expected – i.e., conservatively estimate Buffer-Time to be slightly shorter than expected. Buffer-Time estimates should factor in the COS net throughput efficiency for the desired observing mode, including dead-time characteristics and detector dark count rate.

The time required to dump half the data buffer (9 MBytes of data) to the SSR is ~110 seconds, including ~20 seconds of setup overhead. The ground system will schedule an "interim dump" to start at the end of every Buffer-Time interval during the exposure, provided there is more than ~90 seconds remaining (enough time for the dump to complete) until the end of the exposure. For example, if Buffer-Time is 200 seconds and the integration time is 750 seconds, interim dumps of 9 MBytes each will be scheduled to begin at intervals of 200, 400, and 600 seconds into the exposure. If Buffer-Time is greater than the integration time minus ~90 seconds, no interim dumps will be scheduled. If Buffer-Time is less than 110 seconds, so that data are expected to accumulate faster than it can be dumped (corresponding to a count rate greater than ~21,000 counts/sec), the integration time is required to be no greater than 2 x Buffer-Time. Figure 3.2-1 shows three buffer dumping scenarios: Case 1 has no interim dumps scheduled, Case 2 has one interim dump, and Case 3 has multiple interim dumps scheduled during a long exposure. The minimum specifiable Buffer-Time is 80 seconds, corresponding to a count rate of ~30,000 counts/sec, which is the maximum rate the DIB FSW is required to support in Time-tag mode.

At the end of a Time-tag exposure, the ground system will schedule a "final dump" to dump only the expected amount of data. The amount of data expected in the buffer at the end of the exposure is 9 Mbytes x (T/Buffer-Time), where T is the time from the start of the last interim dump to the end of the exposure, or the full integration time if no interim dumps were scheduled. After completing the final dump, any remaining data will be discarded and the buffer will be re-initialized, leaving it in a clean state for subsequent exposures. This is a change from STIS, which always dumped the entire buffer after an exposure regardless of Buffer-Time. It is motivated by the fact that COS is designed to observe fainter targets than STIS. The majority of COS Time-tag exposures are expected to observe targets so faint that only a small fraction of the buffer will be filled (thereby reducing data volume compared to Accum mode), so that basing the final dump on the expected count rate will significantly reduce its duration. Because any subsequent exposure must wait until that dump completes, and a dump of the entire 18-Mbyte buffer would take over 3 minutes, this change should improve efficiency in situations where multiple COS exposures are taken during an orbit, such as during FP-SPLIT sequences. The cost is that data will be lost in situations where Buffer-Time is overestimated (where the count rate is underestimated). The proposer will be responsible for managing the tradeoff between efficiency and risk of data loss by specifying an appropriately conservative value of Buffer-Time.

Another change from STIS is that an additional interim dump is scheduled during the last Buffer-Time interval in most cases, even though it is not necessary to avoid overflowing the buffer. This change will improve efficiency by reducing the size of any gap between exposures for the final dump, and it also simplifies the modeling of the buffer in the STScI ground system.

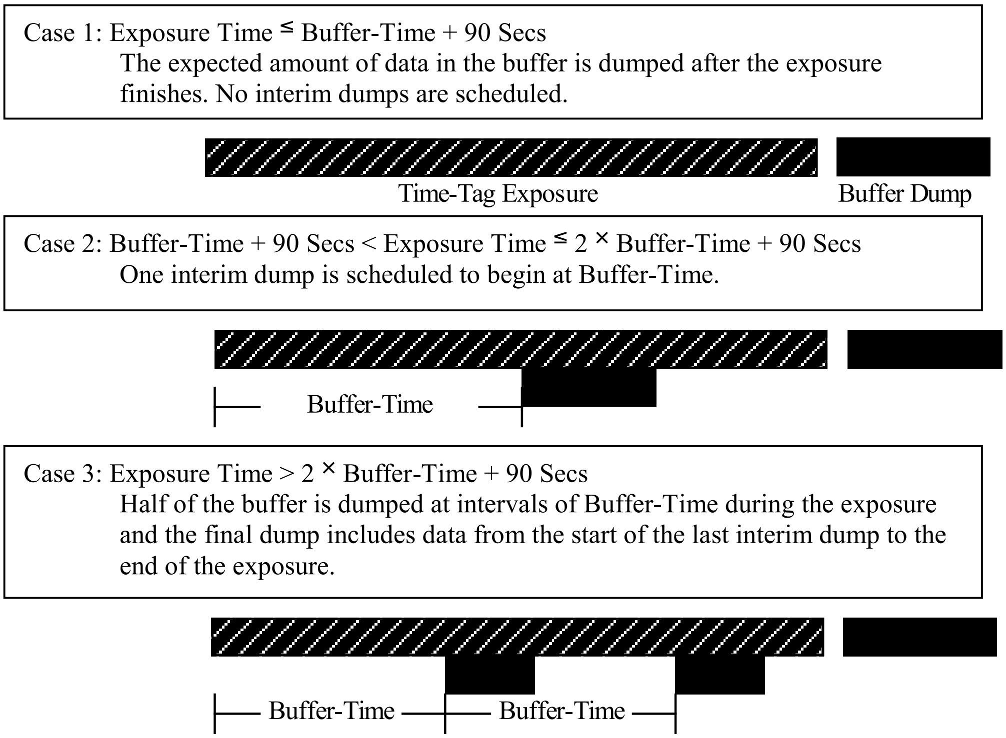

Figure 3.2-1: *Illustration of buffer memory dumping scenarios.*

3.2.2 Science Data Header Format

DM-06 describes the science data header format in detail. The science images from any of the science products will be placed in the science data stream using a Buffered SD (science data) structure. The first 965 word line of each Buffered SD structure will contain an internal header and internal unique data log. Any of the 965 words which are not used are completed with fill data. The remainder of the structure is comprised of image data.

The purpose of the internal header is to allow OPUS to identify the contents of the structure. It will contain the Programmatic Numbers (PROG ID, OBSET ID, and Ground Observation Number) for the science data contained in the structure. After the data is received on the ground this information will allow the data to be associated with the original request for an exposure.

The internal unique data log gives the details required to unpack the image, define its internal structure, calibrate the data, and provide engineering data from the time of the image.

The unpacking information provided is a flight observation number assigned sequentially by the CS FSW (this is not the same as the Ground Observation Number assigned by SOGS), and the number of bytes in the image. This is computed by the CS FSW and includes the number of bytes in the internal header and log and in the actual image.

The image definition is composed of the HST time at the start of the image, image type, detector science data definition, memory dump definition, and diagnostic ED definition.

Definitions for all four types are always included, but the image type specifies which is applicable. The contents of the four definitions are shown below:

- Detector Science Dump - The definition contains the detector identification, detector science data type, subarray definition (number of subarrays, subarray size, subarray starting coordinates), commanded integration time, and actual integration time.
- Memory Dump - The definition contains the memory dump source (CS, DIB, DCE), memory dump starting address, and number of bytes dumped.
- Diagnostic ED Dump - The definition specifies diagnostic mode, ED items collected, collection period, and collection frequency.
- PHD Data Dump – There are no specific items of definition for a PHD Data Dump; 256 bins of 32 bits each are always dumped.

The engineering data snapshot provides a copy of all engineering data items that comprise that part of a major frame collected and reported by the CS FSW, recorded before and after acquiring the image. The telemetry in the ED snapshot is defined in DM-06. The snapshot contains a majority of data available from COS. The data that is most applicable to calibration (such as the XDL count rate) and validation of the image are selected. The CS FSW does no special processing on any of the items in the ED snapshot; the contents of the ED snapshot are simply the values of the selected ED items as the exposure begins and then again as the exposure ends.

3.3 MEMORY DUMPS

COS contains a large amount of onboard memory. It will sometimes be necessary to inspect some of the contents of the onboard memory. Science data dumps can send large volumes of data to the ground efficiently, so this route was selected to dump the contents of the various memories. Macros exist in order to allow the specification of which computer's memory is to be dumped (CS, DIB, or DCE), and to specify the starting memory location and quantity of memory to be dumped.

Memory dump data from the DIB and the DCE are copied from the respective computer and stored in CS buffer memory. CS memory data is dumped directly from the specified CS memory region when a CS memory dump occurs; thus, no CS buffer memory is allocated for CS memory dumps.

3.4 ENGINEERING DIAGNOSTIC DATA

The normal engineering data stream to the RIU is quite slow: 10 bytes per half-second for the entire instrument. In addition to collecting and sending normal engineering data telemetry, COS has the capability to collect normal engineering data including analog engineering data, digital engineering data, and derived engineering data at higher than normal rates and store them in sequential locations in CS buffer memory. This capability exists as a special type of exposure, called a 'diagnostic exposure'. The specification of the desired engineering data parameters, their interrogation rate, and the number of samples to collect are specified by macro command, allowing the requisite amount of CS buffer memory to be allocated as the diagnostic exposure begins. The data are accumulated in CS buffer memory just like data from a science detector exposure. When the diagnostic exposure is completed, the collected data can be dumped to the SDF just like other science exposures.

3.5 DOPPLER CORRECTION

Real-time compensation for Doppler shifting of spectral data is provided for both the XDL detector data and the MAMA detector data, but in ACCUM mode only. Doppler compensation for time-tag exposures is not performed on-board but rather on the ground. For ACCUM exposures, the correction is provided by incremental shifting of the CS buffer memory address within which the accumulating counts are incremented. For ACCUM exposures requiring on-board doppler correction, macro parameters specifying the time for zero doppler correction at the closest point in time prior to the beginning of the exposure, the maximum doppler shift magnitude in pixels, and the orbital period must be provided to the CS FSW in advance of commanding the exposure to begin.

3.6 BRIGHT OBJECT PROTECTION

Detector global rate violations for the XDL detector are detected and managed within the DCE FSW, while global rate violations for the MAMA detector are detected and managed within the MCE FSW. Within the DCE FSW, the XDL detector high voltage is commanded down to safe level. Within the MCE FSW, the MAMA detector high voltage is commanded off.

Local rate violations for both detectors are detected within the DIB FSW and managed within the CS FSW. When commanded to do so, the CS FSW commands the DIB FSW to gather science data from the selected detector, and bin the data in DIB memory. The binned data is subjected to threshold tests within the DIB, and if any of these threshold tests fail, the DIB FSW informs the CS FSW that a local rate violation has occurred. The reaction of the CS FSW is to command the external shutter closed and turn the lamps off. Refer to Secs. 4.1 and 4.2 for additional discussions of BOP for each COS detector.

4. DETECTORS

4.1 FUV XDL DETECTOR

Below is a description and overview of the COS FUV detector and the subcomponents that might be affected by satellite operations. Much of this text is taken from the *FUV Detector Subsystem Interface Control Document (COS-UCB-0001).*

4.1.1 Overview of FUV Detector

One FUV Detector Subsystem will be used in the HST-COS spectrograph. The COS FUV detector subsystem derives its heritage from the detectors developed by EAG for the FUSE project. The FUV detector subsystem is a photon-counting detector that converts light focussed on its photosensitive front surface into a stream of digitized photon coordinates. The digitized events are transmitted to the Detector Interface Board (DIB) within the COS Main Electronics Box (MEB) for processing.

The FUV detector subsystem consists of two major components, the Detector Vacuum Assembly (DVA) and the Detector Electronics Box (DEB), interconnected by ~ 4’ long power, data, signal, and high voltage lines. The DVA performs the conversion of light to analog electronic impulses and is located on the optics bench. The DEB converts the 5 analog signals from the DVA into digitized coordinates and is located on the thermal shelf within the COS enclosure. The DEB also manages the power, commanding, monitoring, and communications with the COS MEB. Figure 4.1-1 shows a functional block diagram of the FUV Detector Subsystem and figure 4.1-2 shows the telemetry and commanding flow between the MEB and DEB.

The FUV detector subsystem is optimized for the COS bandpass of 1150 to 1775Å. The active front surface of the detector is curved to match the design focal surface radius of curvature of 826 mm. To achieve the length required to capture the entire projected COS spectrum, two detector segments are placed side by side with a small gap between them. To mitigate risk of single-point-failure, the two detector segments are independently operable: loss of one segment does not compromise the independent operation of the other. Each detector segment has an active area of 85 x 10 mm digitized to ~14160 x ~400 pixels as shown in Figure 4.1-3.

Precautionary note: The FUV detector is an open face MCP detector. As such, it can be hazardous to the health and safety of the detector to expose the face of the detector to vacuum levels in excess of 10^{-4} Torr. For this reason, the detector is equipped with a door atop the DVA. The door shall be opened only when the DVA is in a vacuum tank with a pressure of $<10^{-5}$ Torr (for ground and instrument I&T processing) or after COS has been installed in the observatory and the vacuum reading from the onboard ion gauge indicates the pressure inside the enclosure is $<10^{-4}$ Torr. The lower pressure for ground operations is required to insure that the detector ion pumps can safely pump down and maintain the vacuum in the vacuum housing assembly. When installed into the observatory the detector ion pumps are inert, thus the concern no longer exists. Additionally, safe operation of the FUV detector's high voltage (HV) systems requires the proper ambient environment. In a vacuum environment, it is only safe to activate the FUV detector's HV after a vacuum of 10^{-5} Torr or better has been achieved.

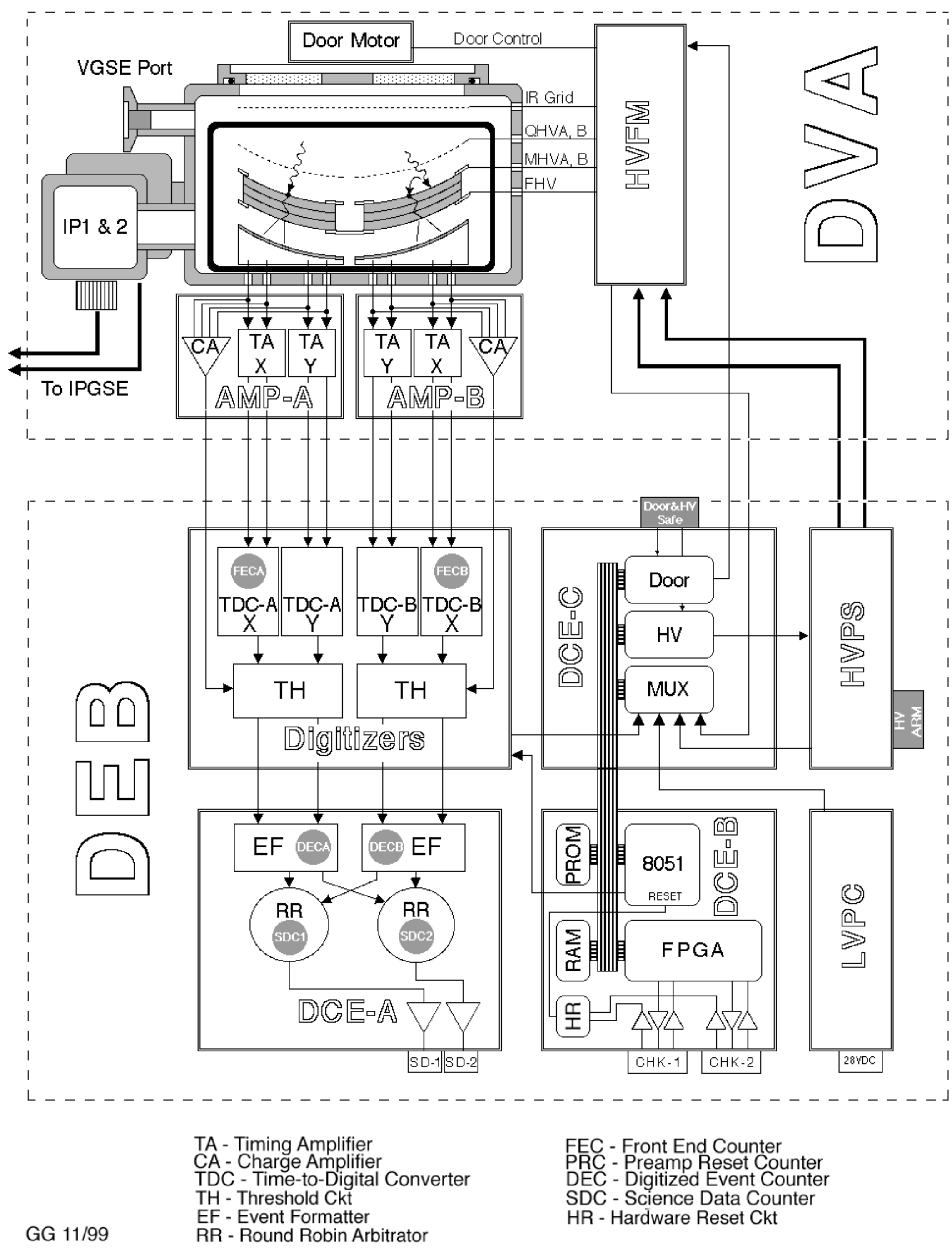

Figure 4.1-1: *FUV Detector System layout.*

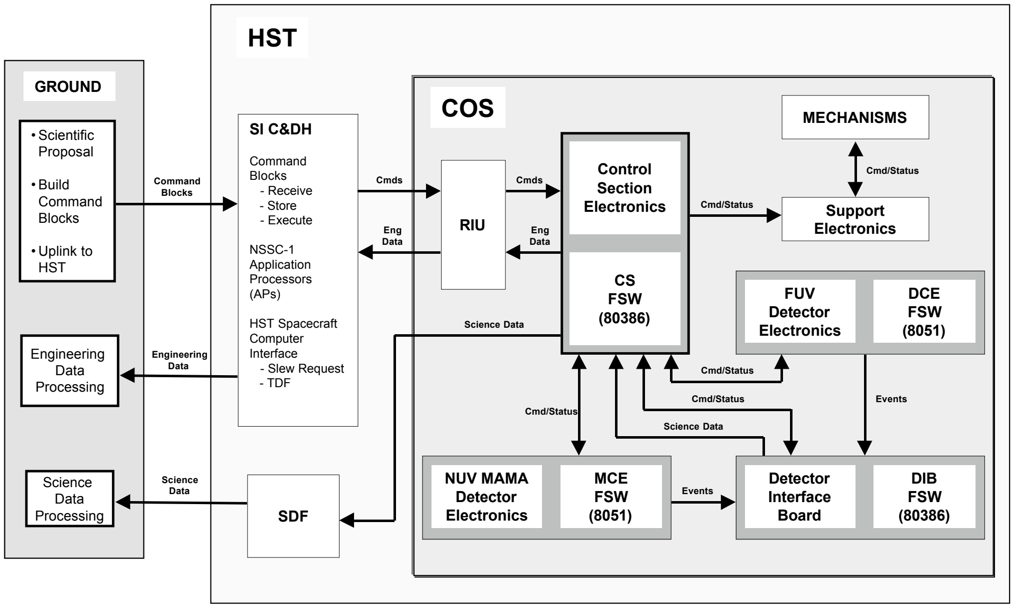

***Figure 4.1-2**: FUV Detector System to MEB Functional Block Diagram.*

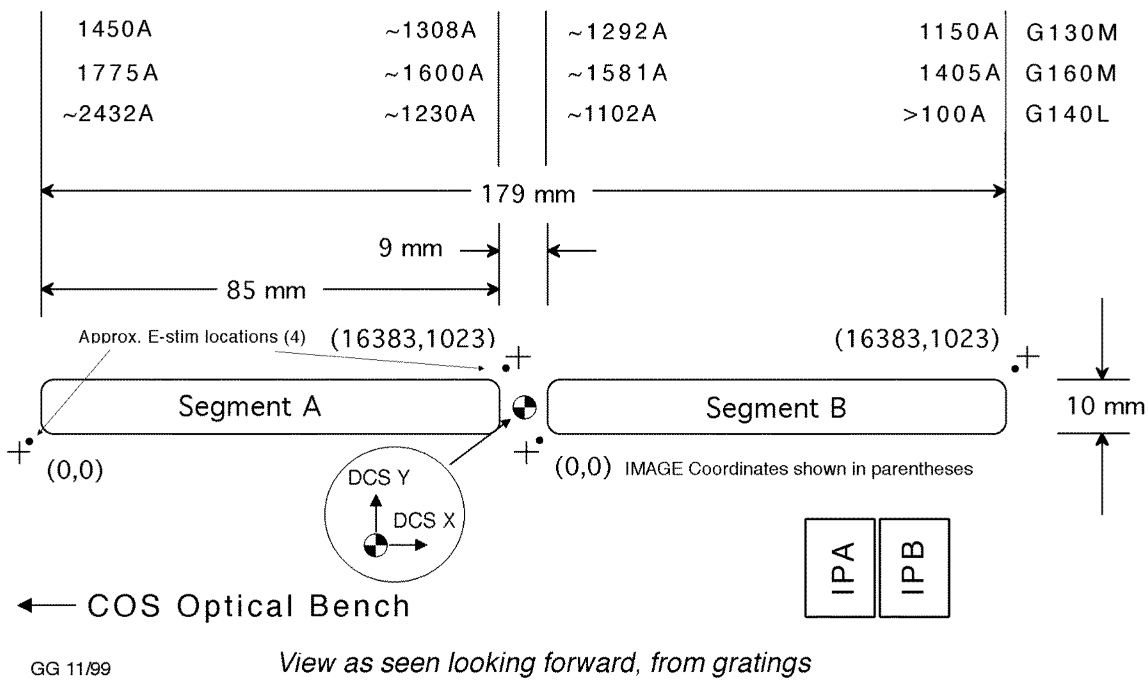

***Figure 4.1-3:** FUV Detector Active Area Layout.*

4.1.2 Detector Subsystem Components

This section provides an overview and description of the subcomponents within the FUV Detector Subsystem important to COS Operations.

4.1.2.1 Detector Vacuum Assembly (DVA)

The DVA contains the photosensitive microchannel plates (MCPs) inside the Detector Body assembly, as well as the high voltage hardware, high vacuum, and electronics required to run them. The DVA produces 5 analog signals for each detected event that are passed to the DEB, i.e., 2 timing signals per axis per segment and 1 charge signal per segment.

4.1.2.1.1 Detector Body Assembly

The detector body assembly houses the microchannel plates which perform the conversion of light to electronic impulses (see Figure 4.1-4).

4.1.2.1.2 Brazed Detector Body

The Brazed Detector Body clamps the two stacks of MCPs in place on the design focal cylinder. The detector body provides the high voltage electrodes for the top and bottom of both MCP stacks.

4.1.2.1.3 Photocathode Material

The photocathode material enhances the photosensitivity of the microchannel plates in the wavelength range of interest. The baseline photocathode material for COS is CsI. Approximately 10,000 Å of photocathode material is evaporated onto the top surface of the top microchannel plate. Photons strike the photocathode material, producing photoelectrons that can be multiplied by the MCPs.

4.1.2.1.4 Microchannel Plates

The MCPs provide the electron multiplication necessary to produce sufficient charge to centroid a photon event. Two stacks of three curved plates each will be used for COS, biased at a voltage of –2.5 to –7kV. Photoelectrons generated within a microchannel initiate electron cascades within the MCP stack. An electron cascade typically produces a gain of 10 million, resulting in measurable charge clouds of 2-3 picocoulombs.

4.1.2.1.5 Quantum Detection Efficiency Grid

Photoelectrons produced at the front surface of the MCP would normally be lost, being accelerated away from the detector by the high negative potential of the front MCP. These "web" photoelectrons can be collected by placing a Quantum Detection Efficiency (QDE) Grid above the MCPs, biased at a potential more negative than the detector surface. This method increases detector efficiency by 20 - 40%, depending on the illumination wavelength.

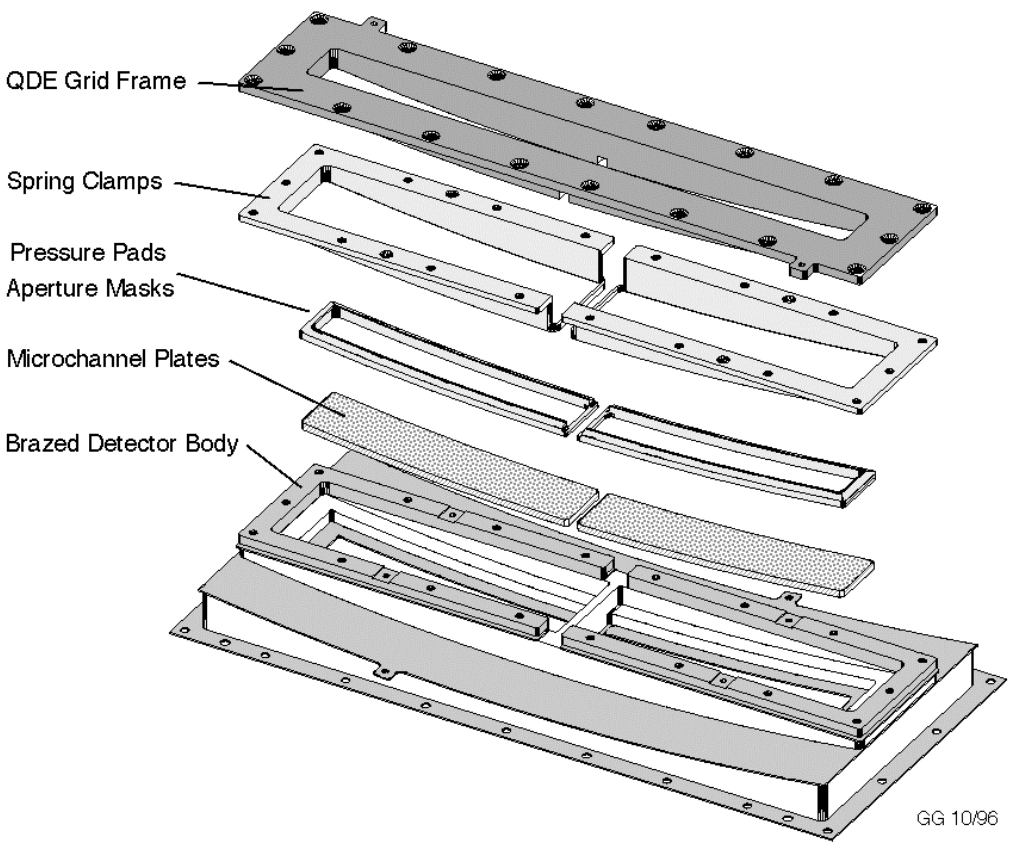

Figure 4.1-4: *Detector Body Assembly.*

4.1.2.1.6 Delay Line Anodes

The delay line anodes locate the photon event by centroiding the charge cloud produced by the MCP stack in both the dispersion and cross dispersion axes. The charge cloud is several millimeters in diameter when it lands on the delay line anode. There are two anodes in the detector body assembly, one anode per detector segment. Each anode has unique traces for the dispersion and cross dispersion axes. The charge cloud lands on, and is divided between two pairs of conductive delay line traces. The event position in either the dispersion or cross-dispersion axis is determined by the difference in arrival times between the two ends of the delay line .

4.1.2.1.7 Detector Door Mechanism

The detector door mechanism provides a means of maintaining high vacuum from final assembly through launch. The door is essentially a gate valve that seals the detector aperture of approximately 200 x 20 mm. UV transmissive windows are mounted in the door frame, above each detector segment, to permit ultraviolet stimulation of small portions of the detector while the door is closed. During thermal vacuum testing, the door will be opened and closed; however, once in orbit, the door is activated once and remains open for the duration of the mission.

The door is driven by a brushed DC gear-motor and gearbox. The door may also be opened by a redundant spring release mechanism activated by a wax actuator. The wax actuator has redundant heater windings. The spring release mechanism can be reset with an operating door motor. The door mechanism mounts to the top of the vacuum housing.

4.1.2.1.8 Ion Repeller Grid

The ion repeller grid reduces the detector background count rate by preventing low energy thermal ions from entering the DVA. It is mounted across the detector aperture on the inside of the vacuum housing, and is biased at +15V. The ion repeller grid voltage is provided by the low voltage power supply (LVPS) in the DEB and comes on when the LVPS is powered.

4.1.2.1.9 High Voltage Filter Module (HVFM)

The HVFM takes raw high voltage from the high voltage power supply (HVPS) in the DEB and produces the five HV levels required by the MCP stack. These are the field high voltage (FHV), the microchannel plate high voltages (MHVA and MHVB), and the QE enhancement grid high voltages (QHVA and QHVB). The HVFM also filters the MHVA and MHVB to suppress noise and high voltage oscillation.

1) *FHV (Field High Voltage)*, common to both segments, for focussing the electron charge cloud from the MCPs onto the delay line anodes (–400 to –500V).

2) *MHVA, MHVB (MCP High Voltages)*, one for each detector segment (–2.5 to –7kV).

3) *QHVA, QHVB (QDE enhancement grid voltages*), biased –1.5 KV above MHVA, B . These voltages are fixed by hardware relative to MHVA, B.

4.1.2.2 Detector Electronics Box (DEB)

This sub-section describes the components of the FUV Detector Electronics Box (DEB).

4.1.2.2.1 Detector Control Electronics (DCE)

The DCE manages all of the communications, commanding, housekeeping, and autonomous operation of the detector system. Its functions are divided among three boards: DCE-A, B, and C.

- *DCE-A* filters the event stream and combines two streams into one. The event stream drives a RS422 3-wire interface referred to as Science Data. No Science Data appear in housekeeping.
- *DCE-B* is the command/housekeeping interface board and provides software control of the other boards. The board includes PROM for storing executable code, RAM from which code executes and data are stored, an 8051 microcontroller that executes the code, and RS422 hardware to support command/housekeeping.
- *DCE-C* provides door control, high voltage (HV) control, and analog-to-digital conversion for sensors.

4.1.2.2.2 Time to Digital Converters (TDCs) and Stim Pulses

The TDCs process the amplified anode timing signals to calculate photon position coordinates. These digitized events are then sent to the MEB.

Each TDC contains a circuit which produces two alternating, periodic, negative polarity, tailed pulses which are capacitively coupled to both ends of the delay line anode (see Figure 4.1-5). When active these electronic stims (e-stims or stim pulses) emulate counts located at the edges of the anode, beyond the illuminated regions of the detector (see Figure 4.1-2). The e-stims are useful for several reasons. They provide a means to test the functionality of the conversion and encoding electronics without applying high voltage to the detector. Because their "physical" locations are known they can be used to set the proper digitizer scalings and offsets. Finally, e-stims can be used at low rates during long scientific integrations to track temporal image shift and stretch, allowing a first-order removal of these distortions. They can also be used as a first-order check of the detector dead-time correction.

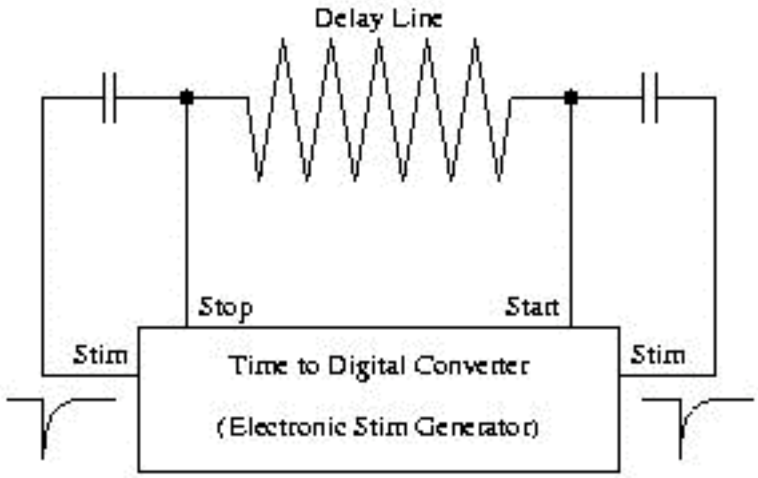

Figure 4.1-5: *Stim Diagram.*

A multirate e-stim pulse system will allow rates of 0 (off), 2, 30, and 2000 Hz. These rates are commandable and are intended to suit specific observational needs; for example, the high rates would be used for shorter exposures (see also Sec. 5.3.4).

4.1.2.2.3 Low Voltage Power Converter (LVPC)

The LVPC converts the nominal +25 volt input from the spacecraft power bus into numerous low-noise and ground-isolated voltage outputs used by the various components of the FUV detector subsystem. +/- 17V for the HVPS and HVFM, +30V for the HVPS, +7 and +/-17V for the amplifier units and TDCs, and +7 and +/-17V for the DCE are all provided as secondary outputs. All outputs are post-regulated at the point of use. A current-limited two-fault tolerant +30V switched output is also provided, to service the various auxiliary functions required by the FUV detector subsystem. These functions include reversible motor drive for the detector door and redundant actuator power.

4.1.2.2.4 High Voltage Power Supply (HVPS)

The HVPS produces one commandable high voltage output for each of the two detector segments (2-5kV). These two high voltages connect to the High Voltage Filter Module on the Detector Vacuum Assembly.

4.1.3 Normal Detector Operations

The FUV detector produces science data in the form of event dispersion (IMAGE-X) and cross-dispersion (IMAGE-Y) positions and pulse height. Events will be detected and processed when the electronics are powered and the high voltage is on and set high enough that the event pulse height exceeds the charge threshold. The operational configuration of the FUV detector is to then send these events in digital form (14 bit IMAGE-X, 10 bit IMAGE-Y, 5 bit PH, 1 bit segment ID) to the detector interface board (DIB) within the MEB. "Accumulation" and "time-tagged" modes are determined by how the MEB handles the FUV detector's events. Once on at nominal HV, no commands to the FUV detector are required to start or to stop data flow. The MEB will control the exposure by how it handles the collection of the data sent by the FUV detector.

The following seven FUV detector states are defined (see Figure 4.1-6):

- **FUV Hold** (**FUVHold**): the FUV subsystem is off.
- **FUV Boot (FUVBoot)**: the state after a power-on (or other) reset. The **Boot** state loads a code image whose functionality is restricted to allowing an upload of the software image from the MEB to RAM.
- **FUV Operate (FUVOper)**: the FSW code image is loaded and running, and all system presets are loaded.
- **FUV HV LOW (FUVHVLow)**: the FUV detector is operating with HV to both segments at a low value.
- **FUV HV Nominal (FUVHVNom)**: the FUV detector is operating with HV to both segments on at a nominal detector setting.
- **FUV HV Segment A (FUVHVsgA)** : the nominal HV is on for segment A only.
- **FUV HV Segment B (FUVHVsgB)**: the nominal HV is on for segment B only.

The operating state of the FUV detector can be changed by the following commands from the MEB, or autonomously from the DCE itself. Italics differentiate MEB scripts from DCE commands in this list and in Figure 4.1-6.

A. ***LDCERSET, LDCECRST*, POR**. These reset commands reset the DCE, a diagnostic is issued, and the operating state is changed to **Boot**. The reset process requires a maximum of 12 seconds.

B. ***LDCE2OPR***. An MEB script that loads the code image to RAM and initializes the FUV detector subsystem.

C. ***LDCHVPWR***. An MEB script turns on HV power supply. With the HV power supply on the voltage is –2500V.

D. ***LDCHVRMP***: This command transitions the DCE HV for both segments A and B from their current setting to one of four pre-programmed states. The four states are FUVHVLow, FUVHVNom, FUVHVsgA, and FUVHVsgB.

E. **CRP**. Count Rate Protection shutdown (see section 4.1.4 for further details)

F. **WDR**. Watchdog Reset (see section 4.1.4 for further details)

G. **HVI**. An over-current condition is detected in either the HV current (HVIA, B) or AUX current (AUXI).

Segments A and B may be controlled independently, though normally both segments will be operated together. After a POR (power-on-reset), the FUV begins in the **FUVBoot** state. To bring up high voltage to observing levels, the proper sequence of commands must be sent from the MEB to reach the **FUVHVNom** state. On arrival at each HV state, the appropriate status bit is set.

HV presets need to be loaded during the transition from **FUVBoot** to **FUVOper**. This consists of setting the nominal HV presets (HVI limits, HV levels for **FUVHVNom** and **FUVHVLow** states, HV ramp parameters). These presets would normally be loaded along with initialization of all FUV system settings.

FUVHVLow puts the HV to a minimal value as defined in Table 4.1-1. To go to the final operating voltage (**FUVHVNom**) will require additional ground command (via the MEB) to the DCE to ramp the high voltage from the **FUVHVLow** value to the final value. On command, the DCE FSW will increase HV settings for each segment in single bit increments (1 bit =15.69 volts) from **FUVHVLow** towards their nominal operating value (Note: HV for each segment is controlled via two 8 bit words. **FUVHVLow** and **FUVHVsgA**,**B** represent different values of these 8 bit words.). The time between increments is commandable. A bit in Housekeeping indicates that the DCE is in the process of ramping HV. Ramping up HV is intended to slowly and uniformly warm-up the MCPs components. It is not necessary to ramp the HV back down.

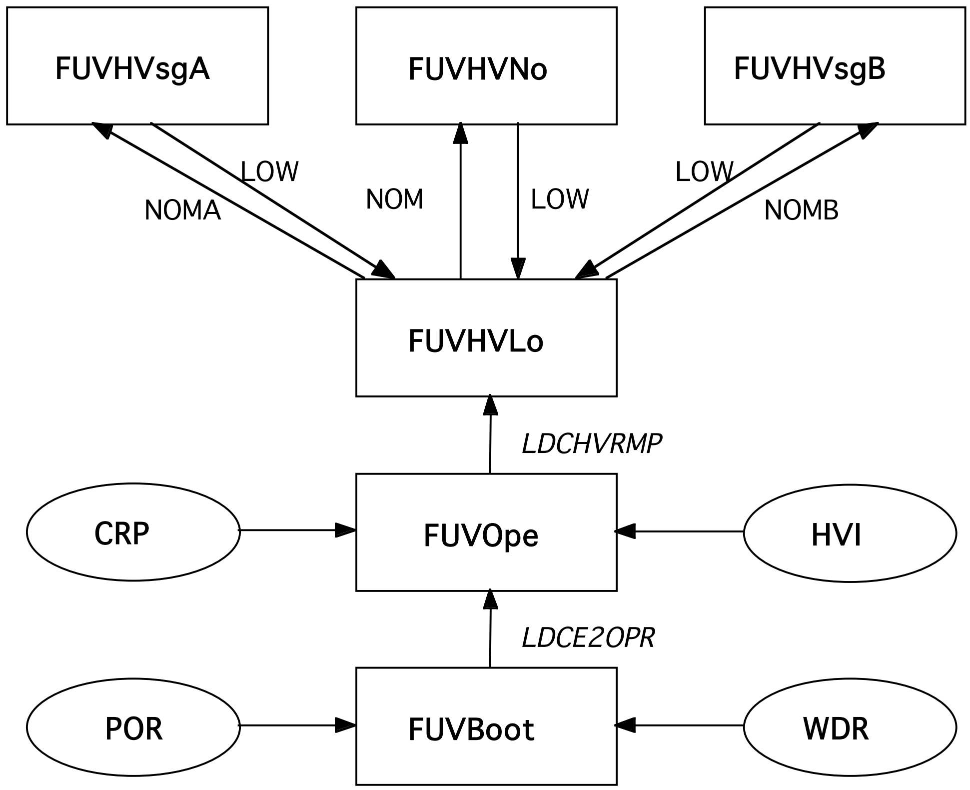

Figure 4.1-6: *COS/DEB Operating States and Transitions.*

Figure 4.1-6 depicts the operating states and transitions of the FUV detector. Not all state transitions are shown (see DM-05), and the scripts indicated in italics contain multiple commands.

4.1.3.1 Operating Parameters

In Table 4.1-1 are the FUV detector command and parameters that will be used during normal operations.

4.1.3.2 Housekeeping Data

The DCE will generate 512 32-bit words per second across the Housekeeping Data link on receipt of a command from the MEB. The data transferred includes internal state information, event counters, internal voltage readings, temperatures, and pulse height histogram increments. A separate memory dump packet of 512 words is sent when commanded.

Table 4.1-1 FUV Detector DCE Command & Parameter List

DCE Command	Parameters	Parameter Range	Nominal Value			
LFGBWK	SETTING	0 – 255 COUNTS	101	96	100	96
	SEGMENT	0 = A, 1 = B	0	0	1	1
	DIR	0 = DISP, 1 = XDISP	0	1	0	1
LFGEWK	SETTING	0 – 255 COUNTS	98	96	100	96
	SEGMENT	0 = A, 1 = B	0	0	1	1
	DIR	0 = DISP, 1 = XDISP	0	1	0	1
LFGSHF	SETTING	0 – 255 COUNTS	237	179	132	141
	SEGMENT	0 = A, 1 = B	0	0	1	1
	DIR	0 = DISP, 1 = XDISP	0	1	0	1
LFGSTR	SETTING	0 – 255 COUNTS	35	128	65	58
	SEGMENT	0 = A, 1 = B	0	0	1	1
	DIR	0 = DISP, 1 = XDISP	0	1	0	1
LFGTT	SETTING	0 – 255 COUNTS	200	208	208	208
	SEGMENT	0 = A, 1 = B	0	0	1	1
	DIR	0 = DISP, 1 = XDISP	0	1	0	1
LFGUQT	SETTING	0 – 255 COUNTS	255		255	
	SEGMENT	0 = A, 1 = B	0		1	
LFGLQT	SETTING	0 – 255 COUNTS	11		11	
	SEGMENT	0 = A, 1 = B	0		1	
LFGSTIM	SETTING	0, 1, 2, or 3	OD		OD	
	SEGMENT	0 = A, 1 = B	0		1	
LFHVENA	HIVOLT	0 = DISABLE 1 = ENABLE	OD			
LFHQPWR	QE GRID POWER	0 = OFF, 1 = ON	OD			
LFHVPWR	POWER	0 = OFF, 1 = ON	OD			
LFHSTATE	STATE	1 = NOMA 2 = NOMB 3 = NOMAB 4 = LOW	OD			
LFHRAMPT	RAMPRATE	0.1 – 6553.5 SECONDS	OD (Nom. = 1)			
LFHVLOW	VOLTAGE	-6500 - -2500 VOLTS	-4096		-4096	
	SEGMENT	0 = A, 1 = B	0		1	
LFHVMAX	VOLTAGE	-6500.95 – -2500VOLTS	-5300		-5250	
	SEGMENT	0 = A, 1 = B	0		1	
LFHVNOM	VOLTAGE	-6500.95 – -2500VOLTS	-5300		-5250	
	SEGMENT	0 = A, 1 = B	0		1	
LFHVSET	VOLTAGE	-6500.95 to -2500VOLTS	OD		OD	

DCE Command	Parameters	Parameter Range	Nominal Value	
	SEGMENT	0 = A, 1 = B	0	1
LFHVILIM	HV I LIMIT	MICROAMPS 0 = DISABLE	150	
LFRILIM	AUX POWER I LIMIT	MILLIAMPS 0 = DISABLE	235 Nom/OD	
LFPCRP	INTERVAL	0 = DISABLE 1 – 255 SECONDS	10	10
	SEGMENT	0 = A, 1 = B	0	1
	COUNT RATE	0 – 65535 COUNT/SEC	60000	

Notes: The values in this table are initial values as of 2/12/04 and will be updated after COS is installed and operational in HST. "OD" stands for Operationally Determined, where values for these parameters are determined based on the operational configuration of the COS instrument.

4.1.4 Autonomous Operations

4.1.4.1 Power-on Reset (POR)

After a power-on reset, all internal memory will be initialized and the DCE will be left in the **FUVBoot** state.

4.1.4.2 Watchdog Reset (WDR)

The DCE includes a watchdog reset circuit built into the 8051 microcontroller. The circuit is disabled by default when the DCE is initialized (**FUVBoot**), but may be commanded on. Once enabled, if the DCE FSW fails to service the watchdog within ten seconds, the circuit will trigger and the DCE FSW will be forced to the **FUVBoot** state. It is possible for some other event (such as an SEU or on command) to force the DCE into the **FUVBoot** state.

4.1.4.3 Other Resets

Other kinds of resets may be detected, including reset circuitry test, watchdog test, and resets of unknown origin. After a reset, the DCE FSW puts the hardware in a state with HV off. Non-power-on resets avoid initializing all memory to avoid losing data that could reveal the source of the reset. DCE FSW reports diagnostics in Housekeeping to indicate that a reset happened and may provide clues to understanding the source of a reset. After any other kind of reset the DCE FSW will be forced to the **FUVBoot** state.

4.1.4.4 HV Overcurrent Protection

The current limit protection task checks the HV and Aux current readings for over-limit conditions. It reads the current values, records the information as data samples, and determines if an over-limit condition occurred.

This task runs as fast as possible to monitor the power current levels. It reads the analog-to-digital converter (ADC) for HV current and Aux current. It saves the samples in RAM so that they can be downloaded for analysis if necessary. This task is capable of reporting HV glitches without turning off the HV. It is also capable of recognizing a sustained over-limit condition. If the current level remains out of limits, the task powers off the HV and reports the over-limit event in housekeeping.

If a single over-limit event is detected, this task reports a diagnostic. Subsequent over-limit samples are counted but no diagnostic is posted until the consecutive out-of-limits count is reached. The out-of-limits count is a patchable constant. If a power current value within limits is read, the consecutive out-of-limits counter is reset to zero. When the consecutive out-of-limits count is exceeded, this task turns off power to the HV supply. After a limit violation has occurred, there is no autonomous method for turning HV back on.

Default parameters for the Current Limit Protection Task are loaded during power-on reset initialization. The parameters can then be modified via DCE commands.

4.1.4.5 Count Rate Protection

The DCE FSW creates a Global Rate Monitor by routinely comparing the number of photon events counted by the Fast Event Counter (FEC) during a commandable interval against a commandable rate limit. When the count rate exceeds the limit over a given interval, then the DCE FSW autonomously changes state to **FUVHVLow**. The DCE will remain in the **FUVHVLow** state until commanded to another state. This rate is usually chosen conservatively to be just above the maximum source count rate allowed. The FEC in the FUV detector is a non-paralyzable counter and is therefore ideal for use as a rate monitor. The Global Rate monitor not only protects against over-illumination, but also the SAA, low-level coronal breakdown, field emission, etc. It also acts as a backup to the HV current monitor. So even though the detector could handle high global rates for longer than 1 second without much gain degradation, the 1-second response time must be maintained to protect the detector for unforeseen failure mechanisms.

The count rate at which HV is set to **FUVHVLow** should be set conservatively to be above the maximum allowable count rate for the detector. Rates much higher than the set point (currently set at 20,000 cts/sec per segment for ground testing) indicate a problem, either internal to the detector or due to an operational error (e.g., failure to turn HV down for SAA) and the detector HV is set to **FUVHVLow**.

The Global Rate monitor algorithm in the DCE monitors the Fast Event Counter (FEC) which is the counter on the front end of the TDC electronics that counts every event detected (whether "valid" or not) without respect to x,y position on the detector. This counter is read out every second.

The shutdown algorithm can be summarized in the following way: Two parameters are used in the algorithm, trigger count C and samples N. At detector turn-on the flight software sets up rolling buffer of N elements. Each second the flight software populates an element of the rolling buffer with the FEC value for that segment and computes the average of all the values in the rolling buffer. If the average count rate exceeds C, then the detector HV is set to **FUVHVLow**. In other terms, the count rate protection algorithm compares a boxcar average against a preset value.

4.1.4.6 Other Autonomous Operations

In this section are grouped other significant autonomous detector operations. These operations differ from those described above in that they do not result in a change of detector state, as defined by Figure 4.1-6.

4.1.4.6.1 Autonomous Door Operations

Door motion may be initiated on command only. Autonomous behaviors regarding the detector door involve only stopping the door motion, disabling the actuator, and resetting internal timers. All events detected by the DCE FSW result in the execution of a general door safing routine that always leaves the door motor and actuator powered off. There are 5 events that will autonomously affect the door.

1) Endswitch. At the limit of its range of travel, the door will trigger endswitches that disable the motor and stop door motion in the direction of travel toward the switch. Endswitches may be overridden on command.
2) Latch just opened. If the DCE FSW detects the door latch just opened, the cause is presumed to be the wax actuator’s successful opening of the door, so the actuator is disabled .
3) Latch just closed. If the DCE FSW detects the door latch just closed, the cause is presumed to be the door motor being driven to re-engage the door assembly, so the motor is disabled.
4) Door timeout. The motor driven door takes about 3 minutes to open/close; the actuator requires about 2 minutes to disengage the door latch and spring open the door. Many door-related commands initiate a 3 minute, 30-second timeout after which the door safing routine disables all door motion.

5) Auxiliary (Door) overcurrent detected. A possible source of the overcurrent is the door being driven against its endstop. Door overcurrent detection results in the immediate calling of the door safing routine.

4.1.4.6.2 Background memory checking

DCE FSW executes a background routine to compute a Cyclic Redundancy Check (CRC) value on various regions of internal memory that are not expected to be modified during routine operations. Computed CRC values for each region are compared against previous computations to detect a change to memory. The purpose of this background activity is to detect Single Event Upsets (SEUs) and multi-bit errors in memory.

Detected changes are reported in the Housekeeping data stream as diagnostic codes. The DCE FSW does not take autonomous action other than reporting a possible CRC change. CRC-changed diagnostics will be suppressed while commanding an upload to DCE memory.

4.1.5 Bright Object Protection

There are five levels of bright object protection (BOP) for the FUV detector which are active in hardware, software, and operations. It is important to note that windowless MCP detectors are rather robust to many damage mechanisms. UCB has never seen a detector fail catastrophically from over illumination or over-pressure if simple HV shutdown precautions are in place that monitor HV current and global count rate. More likely to happen is detector degradation in either or both gain or background rate. Very short periods of high illumination usually leave no permanent effects. If adsorbed gas is released, it quickly disperses into the instrument cavity away from the MCPs. High local rates can cause the local gain to sag, decreasing extracted charge and slowing the local degradation. However, if not stopped, over illumination will cause permanent gain degradation and possibly a temporary background rate increase. Count rate protection addresses this threat to the FUV detector.

The levels of bright objection protection are as follows:

1) HV Overcurrent Protection - The most basic defense mechanism of the FUV detector is the HV overcurrent shutdown procedure, which runs in the DCE software, and is described for the FUV detector in Sec. 4.1.4.4. This autonomous operation will protect the detector from HV breakdown due to an over-light condition.

2) Global Rate Monitoring – As discussed in Section 4.1.4.5, the FUV detector DCE flight software monitors the global event rate for each of the two detector segments. If the total count rate on either segment exceeds a commandable threshold, the HV to that segment will go to FUVHVLow. The CS flight software will also close the external shutter and turn off the lamps in response to this event.

3) Local Rate Monitoring – It is possible permanently damage a localized region of the MCPs without exceeding the maximum global count rate. For example, this could occur while observing an object with a few strong emission lines. Bright local illumination will cause local gain degradation, not catastrophic failure of the detector. The BOP limit is 75 events/s per resolution element and is derived from the CARD limit of 1500 events/second per resolution element. The local rate BOP algorithm operates in the MEB FSW (see Sec. 3.6). To perform a BOP check, the FSW takes photon data from the FUV detector and creates a one-dimensional array by collapsing the Y position (cross-dispersion) and binning only in X (wavelength). Each segment is binned into 4096 pixels by dropping the two LSBs, which results in a bin the size of half of a resolution element in wavelength. When this histogram is divided by the exposure time, any individual element count rate should not exceed the BOP limit given above. Exposure times are chosen to be long enough to avoid triggers caused by statistical fluctuations yet short enough to provide protection from degradation. The CS flight software response to a local rate check failure is to close the external shutter and turn off the calibration lamps.

4) TDF Monitoring – The fourth level of protection is provided by monitoring the Take Data Flag (TDF) during an exposure. If the TDF flag is dropped (due to loss of lock, for example), the CS flight software will command the external shutter closed.

5) Target Screening – Emission line objects such as dMe stars will be the sources most likely to cause a BOP trigger. Continuum sources (early stars, white dwarfs) will trigger the global rate monitor before they trigger the BOP. There are approximately 100,000 sources in the sky that can cause a 1% local QE loss in an exposure of 10,000 seconds. Since there is a shutter on COS and most objects that will be too bright are known, careful planning should prevent bright objects from illuminating the detector. BOP minimizes the risk associated with planning and incomplete knowledge of the characteristics of the source in the field of view of the aperture.

Most of the targets capable of causing a violation of the FUV detector BOP limits are known. Thus, care in scheduling should make invocation of BOP an extremely rare event, confined predominantly to bright and highly variable objects such as flare stars. Based on effective area parameters given in the COS proposal, a dMe star brighter than approximately 10^{th} magnitude would cause a violation of the CARD limits; however, this magnitude estimate will need to be revisited as orbital operations progress. After a BOP event occurs, there is nothing to prevent further commanding from re-opening the shutter or turning the lamps back on. However, the STScI command instructions will always perform a local rate check on the active detector immediately after opening the shutter or turning on a lamp.

4.1.6 Thermal Runaway of Microchannel Plate Detectors

Thermal runaway is a condition experienced by microchannel plate (MCP) detectors, which can, if left unchecked, lead to complete destruction of the microchannel plates. The condition is brought about by two characteristics of microchannel plates, the low thermal conductivity of the MCP glass and the inverse relationship between the resistance of the glass and temperature.

Starting with a MCP detector at room temperature, consider the top plate as isothermal with the edges in contact with the MCP housing. When the high voltage is turned on there is uniform current flow through the MCP as the resistance is uniform across the MCP. However, because the microchannel plate is resistive, power is dissipated in the microchannel plate, thus warming the microchannel plate. Now the problem becomes one of heat flow. As the MCP warms heat begins to flow out through the MCP to body interface. The heat flow is not very efficient given the poor thermal conductivity of the MCP glass, so a temperature differential forms with the geometric center of the MCP being the warmest.

This thermal gradient leads to a resistive gradient, due to the inverse dependence on the resistance to temperature, with the center of the microchannel plate having the lowest resistance. This situation is, therefore, subject to a feedback loop, which causes the thermal runaway.

The feedback loops goes as follows. As the resistance drops the current flow, and thus the power dissipated in the microchannel plate, increases. As the power dissipated increases the resistance correspondingly drops, which leads to an increase in power and so on until the temperature at the center of the microchannel plates becomes so high that the glass actually melts and the detector is destroyed. Obviously the sensitivity of this feedback mechanism is completely dependent upon the exact nature of the MCP resistance versus temperature.

The conditions that lead to thermal runaway can be avoided through prudent start up procedures that minimize the likelihood of a thermal gradient, sufficient to initiate thermal runaway, from forming across the microchannel plate surface. Prudence is defined as allowing sufficient time during HV ramp up for the microchannel plates and detector body to thermalize, thus minimizing the potential of a strong thermal gradient across the microchannel plates.

Modeling this situation is likely to be a straightforward thermal model to develop, however, the details of the physical properties of the specific MCP glass, MCP to body interface, and physical properties of the MCP body are not well known, so the accuracy of the model will always be suspect. At this time only experience and caution can be used as guides for determining the actual start up times needed to safely turn the detector on.

4.1.7 Detector Pulse Height Diagnostic Data

The pulse height distribution (PHD) is probably the most potent diagnostic for overall health of a microchannel plate detector. It measures the gain of the MCP electron amplification. The distribution of the pulse heights of photon events is peaked at the average gain of the MCPs with a width determined by the MCP characteristics. Background events, both internal and cosmic ray induced, tend to have a falling exponential distribution in pulse height with most events at very low pulse heights. On board charge threshold discriminators are used to preferentially filter out very large and small pulses to improve the signal to background characteristics of the detector.

For COS there are two ways for a PHD to get to the ground. A PHD can be accumulated on board over a fixed time interval and telemetered to ground as a PHD exposure consisting of 256 pulse height bins (128 for each detector segment), each 32 bits deep. Alternatively, in the time-tagged mode, the individual event pulse heights can be accumulated into a histogram on the ground into a PHD. In this case the PHD can be investigated as a function of the position on the detector and event time. An observer can use the pulse height distribution to maximize the signal to noise ratio of the observation, if in time-tagged mode, by using software pulse height discriminators on each event to remove background events unfiltered by the hardware discriminators in orbit.

In imaging mode, where the individual event pulse heights are not available, the PHD exposure might be investigated to show that the detector is operating correctly and that the photon events are not being incorrectly discriminated against. It can also hint at the source of background though it cannot be used to improve the S/N ratio, as is the case of the time tagged mode. Both modes of the PHD should therefore be available to the observer. The FUV detector PHD should be routinely monitored by the COS operations team to check for gain drift, gain uniformity and background stability, all of which are early indicators of detector degradation.

4.1.7.1 <u>Ground processing of pulse height data in time tag science data</u>

The pulse height of each event should be included in any delivery of photon event data to the observer, along with DCS-X, DCS-Y, and time. Software tools should also be available to filter on pulse height when creating spectral images or spectral light curves, as well a creating simple pulse height histograms for a given exposure. It is not generally necessary to deliver a pulse height histogram as a standard processing product.

4.1.7.2 Ground processing of pulse height histograms

Pulse height exposures will be taken after ACCUM exposures. As the observer cannot verify the quality of the PHD from the raw data set as in time tagged mode, the pulse height histogram should be delivered to the observer as part of the standard processing products.

The FUV detector pulse height spectrum should be inspected on a regular basis to monitor for gain degradation. This process could be automated by fitting a gaussian function to the pulse height peak and reporting peak location and width, as long as the signal is dominated by photon events. It is expected that the peak position will decrease as a function of total fluence until the X-DISP position on the detector is moved to a new area.

4.2 NUV MAMA DETECTOR

4.2.1 Detector Overview

The COS Multi-Anode Microchannel Array (MAMA) Near Ultraviolet (NUV) detector employs a semi-transparent proximity focused Cs_2Te photocathode on a re-entrant MgF_2 window, which allows single photon counting operation in the 1150Å < λ < 3200Å spectral region. The 25.6 x 25.6 mm active area contains 1024 by 1024 pixels on 25 μm centers. The NUV MAMA detector subsystem consists of; 1) a sealed detector tube that is processed at BATC, 2) charge amplifier-discriminator assembly, 3) low and high voltage power supplies, 4) MAMA Control Electronics (MCE), and 5) event decoder. Commanding of this detector subsystem is achieved through either the primary or redundant Main Electronics Boxes (MEBs). Detector telemetry and science data is sent to the active MEB and processed by the flight software as defined in Section 3. The fully qualified NUV MAMA detector subsystem for the COS instrument is the flight spare detector from the HST Space Telescope Imaging Spectrograph (STIS).

Figure 4.2-1 shows the operation of the MAMA detector system. Photons from the spectrograph are imaged through a stepped MgF_2 window onto the Cs_2Te photocathode with a diode mode QE of 17% at 250 nm. The window is stepped since the photocathode must protrude into the tube body to within 0.25 mm of the MCP. At this spacing and with a photocathode to MCP gap potential of 800 volts, the spatial resolution at 250 nm is 35 μm FWHM. A photoelectron emitted by the photocathode has a 68% probability of being collected by the MCP. This collection efficiency is defined by the MCP open area ratio and the electric field generated by the MCP pores. The MCP multiplies the detected photoelectron to generate a space charge saturated pulse containing ~7×10^5 electrons. This charge cloud subtends and is divided by multiple anodes on the coded anode array. A charge pulse from an illuminated anode is converted to a logic level pulse by the charge amplifier-discriminator assembly if the anode charge exceeds the programmable discriminator threshold. The event decoder samples these signals within a 40 ns window, which allows for amplifier walk time variations. A small fraction of the events striking the anode array fail to meet the valid event criteria of the decoder, resulting in an anode array efficiency of 94%. The detection quantum efficiency is the product of the MCP collection efficiency, the anode array efficiency and the diode mode QE. The 20 (significant non-zero) bits of science data, made available to the Detector Interface Board (DIB) FSW, consist of 10 bits of row addresses and 10 bits of column address. The MAMA high-resolution mode provided with the STIS instrument is not supported by COS.

For more information on the MAMA scientific performance requirements refer to the COS Critical End-Item Specification CDRL No. CM-02 and to NUV MAMA Subsystem Performance SER COS-NUV-001.

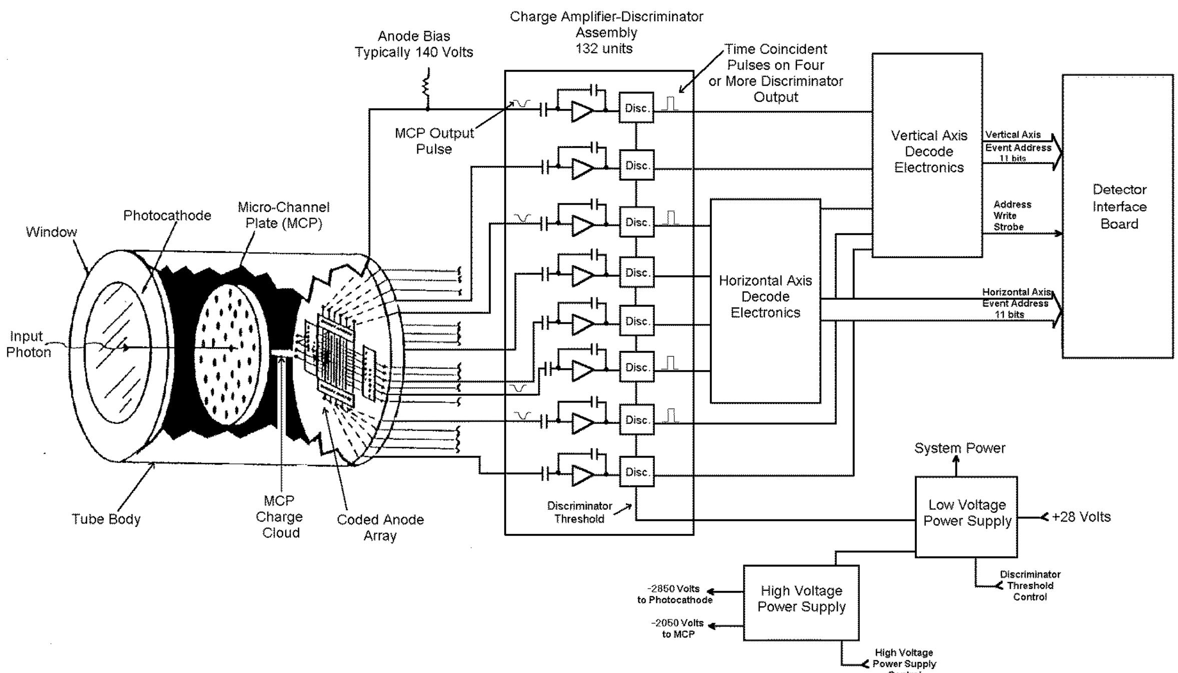

Figure 4.2-1: *NUV MAMA Detector Subsystem Operation. The 11th bit in the "Vertical" and "Horizontal" axes in the figure has a value of zero.*

4.2.2 Detector Subsystem Components

This section describes the function of the various components in the NUV MAMA detector subsystem.

4.2.2.1 MAMA Detector Tube

The MAMA detector tube is comprised of a Microchannel Plate (MCP), coded anode array structure, multi-layer ceramic header, re-entrant MgF_2 window with a proximity focused photocathode and a ceramic-kovar tube body. A schematic of the tube body is shown in Figure 4.2-2.

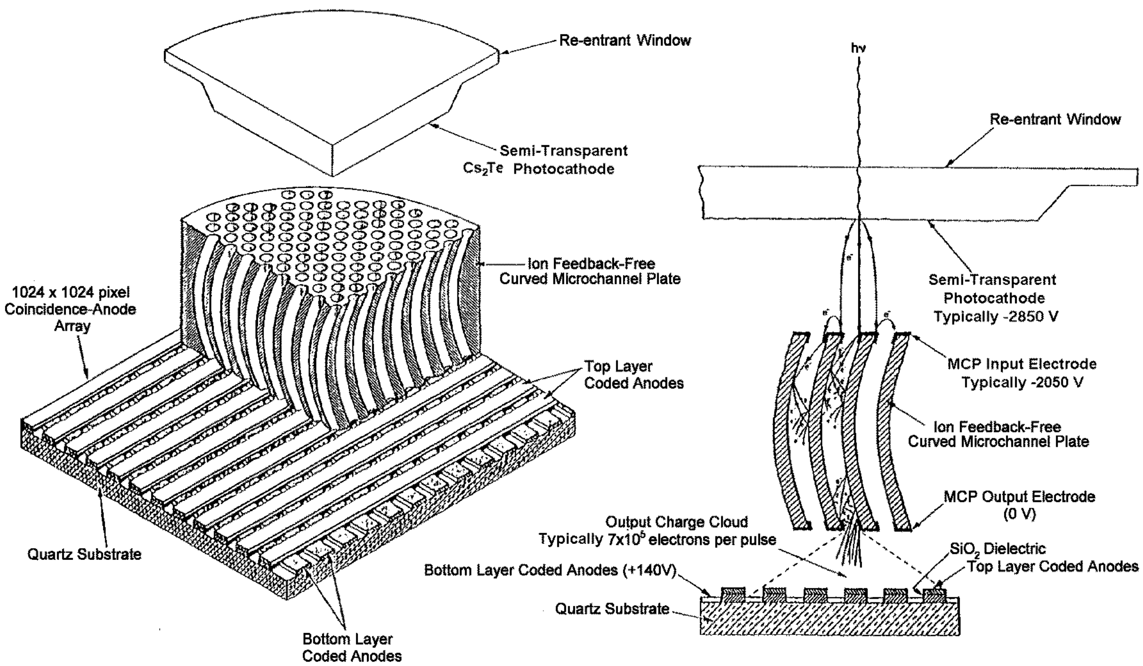

Figure 4.2-2: *Cut-away View of NUV MAMA Detector Tube.*

4.2.2.1.1 Microchannel Plate

A single curved MCP manufactured by Litton Electro-Optical Systems is used to multiply photoelectrons generated by the photocathode into a charge pulse containing

~7x10^5 electrons. The channel curvature suppresses ion feedback to the proximity focused photocathode and greatly improves the detector efficiency over a chevron MCP configuration. The curved MCP or C-plate has the following characteristics:

- Input bias angle: ~12^o
- Pore diameter: 12 μm
- Pitch: 15 μm
- L/D: ~120/1
- Resistance: ~40 Mega-ohms at 2 KV
- Open area ratio: >65%
- Channel offset due to curvature: >10 channels
- Operating voltage: -2050 volts

4.2.2.1.2 Coded Anode Array and Multi-layer Ceramic Header

The MAMA tube coded anode array consists of 4 anode types, W, X, Y and Z. The W and X anodes define the cross-dispersion direction pixel locations and reside on the bottom layer of the MAMA anode array. The W anodes consist of 15 groups of 34 anodes on 50 μm centers, labeled W0 ... W33, while the X anodes consist of 16 groups of 32 anodes on 50 μm centers, labeled X0 ... X31. The Y and Z anodes, which reside on the top layer of the MAMA anode array, are orthogonal to the W, X anodes, define the dispersion direction pixel locations and are in the same configuration as the bottom layer anodes. The Y anodes consist of 15 groups of 34 anodes labeled Y0 ... Y33, while the Z anodes consist of 16 groups of 32 anodes labeled Z0 ... Z31. Anodes on the bottom layer (W and X) are separated from the top layer anodes (Y and Z) by 3 μm of SiO. The individual anode groups are connected together through vias and fan-outs on the array substrate. This region is called the decode region. Decode regions for each anode group type are located around the perimeter of the array. Events from the MCP that strike this decode region will produce events detected by the decoder but do not produce imaging events.

Figure 4.2-3 shows the configuration of the bottom layer anodes. By interlacing the 66 W and X anodes, with a period difference of two, 1088 unique anode combinations are possible. Therefore it requires 132 amplifiers connected to the 66 top and bottom layer anodes to map a 1024 by 1024, 25 micron pixel region of the MCP. The anode array is biased at +140 volts, where the bottom layer anodes are biased ~4 volts more positive than the top layer anodes. The anode array is attached to a multi-layer ceramic header and gold ribbon is used to make connection between the array and header bond pads. Three gold pads ~0.10 mm tall are affixed to the header assembly and act as the mechanical mounting and electrical return for the MCP. The header also contains the mounting studs for the MCP hold down assembly.

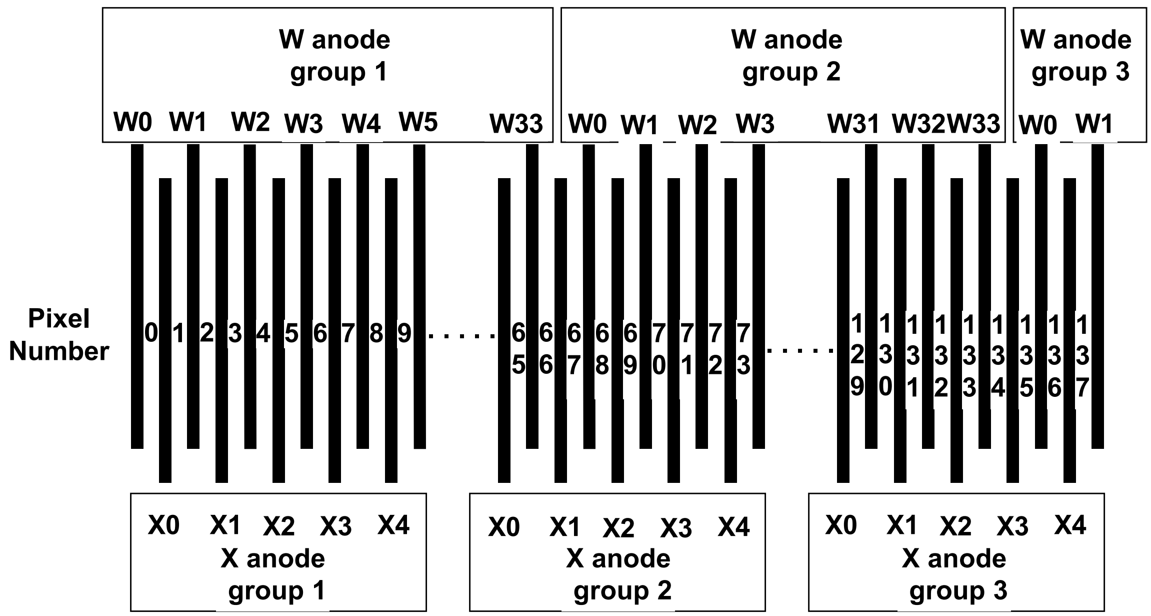

Figure 4.2-3: *Bottom layer anode configuration.*

4.2.2.1.3 MgF_2 Window and Photocathode

A semi-transparent Cs_2Te photocathode is deposited onto a stepped (also known as re-entrant) MgF_2 window during tube processing at BATC. Electrons produced by the photocathode are focused onto the MCP by applying 800 volts across the 0.23 mm photocathode to MCP gap. As the final tube processing step, the MgF_2 window is sealed onto the tube body using Indium solder. The nature of the stepped window requires that an optically opaque mask be installed to prevent light from striking the metallized re-entrant bevel.

4.2.2.1.4 Ceramic-Kovar Tube Body

The tube body is in the wafer configuration, where two annular alumina ceramic insulators are brazed between three kovar electrodes. A window seal ring contains a profiled vacuum processed indium-tin alloy and also makes the electrical connection to the photocathode. The middle electrode is connected to the MCP input. A large double convoluted kovar flange at the rear of the tube is welded to the header-anode assembly. This weld flange is internally connected to the MCP return for EMI considerations.

4.2.2.2 Detector Electronics

The detector electronics consist of the charge amplifier-discriminator assembly, low voltage power supply (LVPS), high voltage power supply (HVPS), decoder and MCE. A block diagram of the MAMA detector subsystem is shown in Figure 4.2-4.

4.2.2.2.1 Charge Amplifier-Discriminator Assembly

Custom application specific integrated circuit (ASIC) charge amplifiers and discriminators were fabricated for the STIS effort to obtain a 1 GHz unity bandwidth, <10 c/s false event rate at a discriminator threshold of 20,000 electrons and 50 ns pulse pair resolution. Ten amplifier-discriminator pairs are packaged on a single board so that the 132 required amplifiers are contained on fourteen boards. The discriminator threshold voltage is commandable from 10^4 to 10^5 electrons. As a diagnostic aid, the 132 discriminator outputs can be individually disabled and enabled.

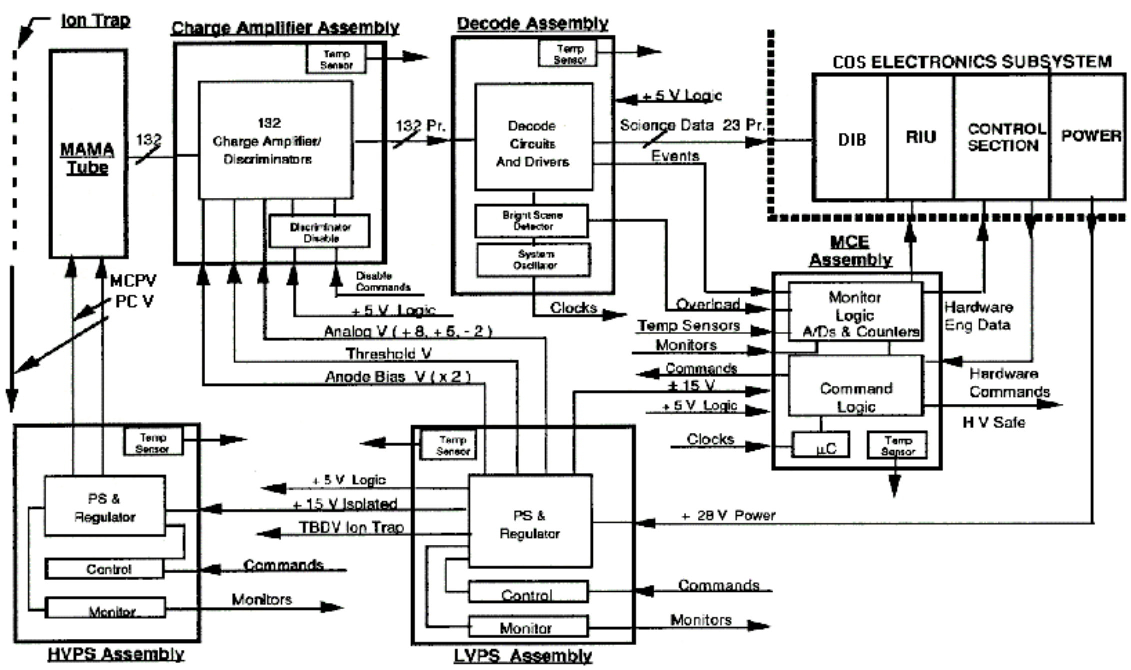

Figure 4.2-4: *COS NUV MAMA Detector Subsystem Block Diagram.*

4.2.2.2.2 LVPS

The low voltage power supply converts the +28 volts spacecraft power and generates the following voltages:

Table 4.2-1: LVPS voltages.

Voltage	Destination
+ 5V analog	Discriminator
+ 5V digital	Decoder, MCE, discriminator
+ 8V analog	Charge amplifier
+15V analog	MCE, HVPS
-15 V analog	MCE
- 2V analog	Discriminator
.2 to 2.8V analog	Commandable discriminator threshold
140V analog	Bottom layer anode array bias
136V analog	Top layer anode array bias

4.2.2.2.3 HVPS

A commandable high voltage power supply provides the detector tube voltages. The HVPS consists of a MCP power supply that is referenced to ground and a PC power supply that is referenced to the MCP output. The HVPS has the following characteristics:

- MCP output voltage span: 0 to -2550 volts
- PC output voltage span (with respect to the MCP output):
- +20 to –1000 volts
- PC and MCP output voltage command/telemetry resolution: 0.6 volts
- MCP current monitor: 0 to 200 μa; .05 μa resolution
- MCP output ripple: <50 mV
- Maximum MCP output current: 250 μa

4.2.2.2.4 Decoder

The decoder board consists of two ASICs in a master-slave configuration, where the master decodes the top layer anode events (Y, Z) and the slave decodes the bottom layer anode events (W, X). A valid event (VE) or write strobe is generated when valid addresses are coincidentally generated by the master and slave decoders. Any W, X, Y or

Z event will initiate the decoding sequence. The decoder dead time or decoder processing time is ~280 ns for masked decode illumination. Masked decode illumination refers to optically filling only the active area of the anode array thereby avoiding the decoding of invalid events that land on the array fan-out electrodes. Each decoder processes two fold to six fold events, where events encompassing 2 to 6 contiguous anodes per axis, occurring with the 40 ns input gate time, will produce a valid event. The distribution of anode events can be measured by selecting the fold type for each decoder and observing the VE rate. This monitoring technique is a very accurate diagnostic of the detector health since it is directly related to the MCP gain and pulse height distribution. In addition to the VE rate, the decoder generates W, X, Y, Z ,OR (W+X+Y+Z) and EV (W·X·Y·Z) rates to the variable integration counters on the MCE board.

4.2.2.2.5 MAMA Control Electronics (MCE)

The MCE responds to commands generated by the control section (CS). These CS commands are telemetry requests and contain subsystem commands. A complete description of the MCE control electronics hardware can be found in STIS-SER-MAMA-074. In order to prevent SEU resets, as seen on-orbit with the STIS MAMA detectors, the minimum input pulse width to the opto-isolators required to generate a reset will be increased from <20 ns to 100 μs. Radiation induced resets generate a 20-50 ns pulse that reset all the logic gates but fails to meet the minimum reset pulse width of 4.7 μs for the 80HC51 microcontroller.

An especially critical function of the MCE is the screening of high voltage commands. To enable the HVPS, the MCE must receive a high voltage enable command and a high voltage on command. This is done by the FSW. High voltage limit checking for the MCP takes place within the MCE as well. A command from the CS is sent that sets the upper limit for the MCP high voltage. Any MCP high voltage commands that are larger than this limit are ignored.

4.2.3 Operational Modes and Transition Sequences

This section provides an overview of the modes and transition sequencing required to activate and use the MAMA detector. A detailed list of commands to perform these operations will be provided in the COS DM-05 document. COS instrument protection is provided by the CS limit checking flight software and the NSSC-1 COS Safing Applications Processor (AP).

4.2.3.1 MAMA Mode: HOLD

In the HOLD mode, power to the MAMA detector subsystem is disabled. The MCE will not accept commands and telemetry data is limited to LVPS power levels and temperature data. A resistive (strip) heater, mounted on the external surface of the subsystem electronics box, is available to maintain the detector temperature at a software selectable point. The heater is triggered by a thermister, that is read by the RIU, at 0°C. This selectable setpoint can be changed by the NSSC-1. The MAMA subsystem survival temperatures range from -15°C to 50°C (as specified on the STIS instrument).

4.2.3.2 MAMA Mode: LVON

In this mode the MAMA power relay is closed enabling MAMA Low Voltage (+28 VDC). The +28 VDC powers the MAMA low voltage power supply, which in turn powers the MCE, charge-amplifier discriminators and event decoder. At power-on, the MCE begins executing its embedded software enabling its functions for subsequent commanding. In the initial power-on state, the discriminator threshold voltage (THV) are set to the maximum value (+2.80 V) with the decoder event fold selects disabled. The MAMA detector subsystem requires no warm-up time prior to operation. Detector operations in the LVON mode are limited to collecting non-imaging noise counts from the charge amplifier-discriminators in aliveness check mode.

4.2.3.3 MAMA Mode: HVON

The MAMA high voltage power supply (HVPS) is commandable by the Control Section (CS) through the MCE. Two unique commands are required to enable the HVPS. The HV enable command must be sent first prior to issuing the HV ON command. When the HV enable/ HV ON command sequence is sent, the inverters in the HVPS are enabled, which results in ~-30 volts to appear at the MCP. The photocathode (PC) voltage tracks the MCP voltage and is more positive than the MCP by ~20 volts for PC voltage command zero.

Nominally the MCP voltage is ramped to its full voltage in 50-volt steps with five second waits between each step. At the completion of the MCP voltage ramp, the PC voltage ramp occurs with the same voltage step size and wait time. The nominal values for the MCP voltage and the PC voltage for the COS NUV MAMA are –2050 volts and –2850 volts, respectively. Thermal loads that affect image stability are of opto-mechanical concern and are not related to any MCP to anode movement within the MAMA detector tube. In the fully operational mode, with the high voltage ON, the MAMA detector subsystem consumes 22 watts. The thermal effects of this heat source on the optical bench and surrounding components are the primary image stability drivers.

Table 4.2-2 summarizes the nominal NUV MAMA parameter values when the NUV detector is in HVON. A complete listing of all nominal NUV macro input parameters is given in DM-05.

Table 4.2-2: NUV MAMA Parameter Values

DESCRIPTION	UNITS	VALUE
CHARGE AMP THRESHOLD VOLTAGE	volts	0.48
FINAL MCP VOLTAGE	volts	-2050.0
FINAL PC VOLTAGE	volts	-800.0
NOMINAL GLOBAL EVENTS TYPE	-	ORCOUNTS
GLOBAL EVENT COUNT LIMIT	counts	77000
GLOBAL EVENT INTEGRATION PERIOD	Milliseconds	100

4.2.3.4 MAMA Mode: HVSAA

The baseline NUV MAMA HV state during SAA passage is HVSAA. The opto-isolator relay problem that is limiting STIS MAMA usage will be corrected on COS. However, the background count rates due to fluorescence of impurities in the MgF_2 window on the COS MAMA are predicted to exceed the Global Count Rate limit (predicted count rate of ~3×10^6 cts/s during SAA passage; possibly higher during intense solar activity). Therefore, during SAA crossing (or more commonly, whenever the NUV channel is not being used for science observations) the voltage to the MAMA will be back-biased to inhibit events from cascading down the microchannel plates and extracting charge.

In HVSAA configuration the voltage difference between the photocathode and the MCPs is reversed from the HVON sate, inhibiting the flow of electrons from the photocathode to the MCPs, thereby substantially attenuating the count rate induced by window fluorescence. (Charged particles that induce cascades directly in the MCPs are not affected.) This back-biased voltage state for the NUV MAMA will be used in a manner similar to the HVLOW state of the FUV XDL detector. Science data should not be obtained during SAA passage, nor should the HV be ramped during SAA passage. When the MAMA has been in the back-biased configuration, the voltages should be re-set to their nominal HVON values prior to commencing science observations.

The HVSAA state is commanded using the macros LMCPM and LPCVM. The voltage ramps in 50-volt steps, with a 5 second wait time between steps. The final PC and MCP voltages in the HVSAA state are +20 (command zero) and –1750, respectively. It takes approximately 2 minutes to transition from the HVSAA state to the HVON state.

4.2.3.5 First Time On-orbit Turn-on

The first time turn-on of the NUV MAMA detector is performed the same way as the anomalous recovery turn-on (see Sec. 4.2.3.6 below).

4.2.3.6 Anomalous Recovery Turn-on

An anomalous recovery is performed whenever there has been an overlight on the NUV detector that is suspected of causing damage to the tube. Severe overlight can cause a gas cloud to form in the pores of the microchannel plate, and if high voltage is applied, can cause arcing and severe damage to the detector. The anomalous turn-on is performed via stored commanding and takes at least four days to complete. Each step is performed on a separate day, and the resulting data are analyzed to determine if it is safe to proceed.

The first step is to turn MAMA LV on, clear the internal InhibitCmdMCExHVOff flag, clean up after a possible MCE reset, set amp threshold to 0.28, collect telemetry, then turn MAMA LV off.

The second step is to turn MAMA LV on, clear the internal InhibitCmdMCExHVOff flag, clean up after a possible MCE reset, then, during a MAMA Time-tag dark exposure, partially ramp up HV. This provides count data for analysis. Then, a NUV dark ACCUM exposure is commanded and all global event types are cycled through. Finally, MAMA HV and LV are turned off.

The third step is to turn MAMA LV on, clear the internal InhibitCmdMCExHVOff flag, clean up after a possible MCE reset, then, during a MAMA Time-tag dark exposure, completely ramp up HV. Then, a NUV dark ACCUM exposure is commanded and all global event types are cycled through. Then, restore the nominal software global monitor.

If everything looks good, execute an internal exposure with the software global monitor at a special setting then execute a MAMA fold test, and finally turn MAMA HV off. If all of the above commanding reveals no problems, the detector can resume normal operations.

4.2.3.7 Precautions

The following precautions should be adhered to prevent damaging the COS NUV MAMA detector subsystem.

- For vacuum operation: The low voltage can be turned on at $5x10^{-5}$ torr. For initial operation after pump down, the high voltage can be safely turned on at pressures $<10^{-5}$ torr after twelve hours of low voltage operation.
- The maximum input local count rate shall not exceed 200 counts per pixel per sec, which is equivalent to a 10% loss in DQE due to the MCP pore recharge time. A 1% permanent loss in the detector sensitivity may occur after exposure to 200 counts per pixel per sec for >200 hours.
- The global input rate shall not exceed 10^6 counts per second. This number has been selected to assure that the decoder deadtime correction is not more than 25% based on global software monitor considerations.
- The MCP voltage shall not be more negative than –2250 volts.

4.2.3.8 Bright Object Protection

In common with most photon counting detectors it is possible to damage the COS MAMA detector by subjecting it to excessive light levels. In addition to the possibility of over-illuminating by observing an excessively bright source there is the possibility of inadvertently over-illuminating the detectors during internal lamp observations. The COS provides both hardware and software protection to mitigate over-illumination of the MAMA detector to ensure its safety. As an added measure of protection, the STScI will adopt stringent target screening policies and procedures to minimize instances of over-illumination. The COS instrument provides five levels of Bright Object Protection:

1) The highest level of protection is the Bright Scene Detection which is performed by the detector electronics. When a pre-set threshold of 17000 counts/0.138 milli-seconds is exceeded, the high voltage supplied to the MAMA detector is turned off. This threshold is not commandable and the resulting action of turning off the high voltage is not patchable. The CS flight software will also close the external shutter and turn off the lamps in response to this event.
2) The second level of protection is the Software Global Monitor (Sec. 3.1.2.3) which monitors the MAMA global count rate (ORCOUNTS), and if the count rate exceeds the 77000 counts/0.1 second threshold, the high voltage is turned off. When the MAMA's high voltage is being ramped up, the Z counter (see Secs. 4.2.2.1 and 4.2.2.2) is monitored instead due to erratic ORCOUNT rates observed during MAMA high voltage ramp-ups. Note that the action taken by the first two levels of protection is disruptive and requires corrective actions to turn the

MAMA high voltage back on in order to resume the timeline. The CS flight software will also close the external shutter and turn off the lamps in response to this event.

3) The third level of protection is the Local Count Rate Checking which takes a short exposure and checks for groups of pixels with excessive count rates. The CS FSW will respond to notification that the local rate monitor threshold has been exceeded by closing the external shutter and turning off the calibration lamps. The value of the local rate monitor threshold is commandable on-orbit.

4) The fourth level of protection is provided by monitoring the Take Data Flag (TDF) during an exposure sequence. If the TDF flag is dropped (due to loss of lock for example), the CS FSW will command the external shutter closed and turn off the calibration lamps. Note that levels 3 & 4 provide bright object protection using the external shutter which maintains the current timeline since the high voltage to the MAMA can be maintained.

5) The fifth and final level of protection is provided at the STScI by screening the targets and surrounding field of views for objects deemed too bright for COS. After a BOP event occurs, there is nothing to prevent further commanding from re-opening the shutter or turning the lamps back on. However, the STScI command instructions will always perform a local rate check on the active detector immediately after opening the shutter or turning on a lamp.

5. OBSERVING STRATEGIES

5.1 ON-ORBIT ALIGNMENTS AND CALIBRATIONS

On-orbit alignments fall into two categories – activities that will need to be done once after the installation of COS into HST, and those that will be performed occasionally to maintain optimum performance of the instrument.

Normal operation of the COS mechanisms will be done using “absolute moves.” The mechanism motions commanded during initial on-orbit alignment procedures will be a combination of absolute and relative moves.

5.1.1 Initial Alignment aboard HST

The activities described in this section are part of the initial COS commissioning and are intended to result in the correct positioning of the OSM1 optics with respect to the HST secondary mirror, followed by the correct positioning of the aperture with respect to the light path. This section identifies the calibrations that will be conducted, but not the details of the measurements. The order in which the calibrations are executed is not necessarily reflected in the order of the presentation. The alignment algorithms follow simple flows depending upon which channel is being aligned. The baseline plan is to align the NUV channel first, followed by the FUV channel. This plan is based on the assumption that the NUV detector will be turned on earlier in SMOV-V, as it can operate at a higher pressure ($P<1X10^{-5}$ Torr for the NUV detector versus $P<5X10^{-6}$ Torr for the FUV detector).

Scenarios under which OSM1 will be moved in single step or small increments include on-orbit focussing of the FUV and NUV channels (described here) and FP-SPLIT observations (see Sec. 5.3.8). The focussing of the COS FUV and NUV channels will require precision adjustments in rotation and z focus position of the OSM1 mechanism. The spectra with the best resolution across the appropriate detector will identify the optimum combinations of focus and tilt for OSM1. This focussing will be conducted during SMOV-V and may be repeated over the lifetime of the instrument as required to maintain peak performance. At this time, we assume that each optic on OSM1 has a unique z focus position for optimum performance.

Under the assumptions stated above, a brief summary of the flow of alignment activities is: (a) start by configuring all of the mechanisms (OSM1, OSM2, ApM) for each optic in their *ground-based* optimized positions; (b) get light into the instrument by raster scanning a point source to center the target in the aperture; (c) modify the HST pointing and OSM1 rotation and z focus to their *on-orbit* optimized positions; and (d) modify the ApM position so that the target, which might have been moved in order to optimize spectral resolution, is again well-centered in the aperture and throughput is maximized.

5.1.1.1 NUV Initial Alignment

Confirm OSM1 qnd OSM2 Position Using Internal Pt-Ne Lamp

The ground-based calibration program will include many observations of the internal calibration lamps for each NUV spectroscopic mode. The preferred position of OSM1 to relay the light to the NUV side, and the positions of OSM2 for each mode will be tabulated. Early in SMOV, observations of internal lamps will either confirm that these are still the optimum positions or result in updated positions. New OSM2 mechanism positions will be derived only if changing a grating rotation position will bring the central wavelength of the spectrum closer to the center of the detector format.

Calibrate V2, V3 Coordinates of PSA

The purpose of this activity is to calibrate the location of the PSA in HST coordinates so that subsequent SMOV activities may be conducted. This initial calibration is temporary and will be updated during the grating to secondary alignment.

The location of the PSA aperture in HST coordinates will be predicted based on ground-based metrology of the instrument. With the OSM1 and OSM2 mechanisms configured for NUV observations with one of the NUV optics, an astronomical target will be raster scanned in a pattern centered on the expected aperture location (e.g., a 5×5 grid search) and the count rate of the NUV detector will be recorded for each position. The data will be analyzed on the ground to determine the center of the aperture in HST coordinates for future observations.

Refine OSM1 "Δz " Position for Optimum NUV Resolution

Mirror NCM1 is located on mechanism OSM1 and relays light to the NUV optics. Its position in the z direction needs to have an accuracy of ±0.224mm in order to produce the best spectral and spatial resolution. To align NCM1, a point source of suitable intensity will be placed in the center of the aperture and a TA1 image will be acquired. The center of the image will be compared to ground test results. HST pointing will then be adjusted so that the image falls at the same detector position as it did during ground testing. Following the HST pointing adjustment, the aperture should be repositioned by a similar adjustment to center the aperture on the target to insure maximum transmission through the aperture.

Following that procedure, the OSM1 z focus position will be scanned ±110 steps and an image recorded at each position. The image size for each z position will be analyzed on the ground and the position with the smallest image (i.e., best focus) will be the optimum z location for the OSM1 mechanism with the NCM1 optic. Following this, a point source whose spectrum includes many very narrow absorption lines will be observed with each of the NUV gratings at varying z positions to verify the NUV spectral performance.

In the event that this procedure fails to produce performance characteristics comparable to ground test results, it may be necessary to conduct a series of scans versus image location at the aperture (V2, V3). This type of multi-parameter search for best focus will only occur in the unlikely event that a gross misalignment of the instrument occurred during launch.

Final Alignment of the Aperture Mechanism

The PSA location in HST coordinates will be determined by raster scanning an astronomical target across the PSA location and recording the count rate of the NUV detector for each position. The data will be analyzed on the ground to determine the location of the center of the aperture in HST coordinates for future observations. The aperture will then be moved to the correct location. This step may find that the aperture is already correctly located, as it was repositioned earlier in the alignment flow. However, recalculating the aperture center in HST coordinates is a sound verification step worth repeating. Please note that the purpose here is to align the aperture to the light path, which has been adjusted to optimize COS performance; not the other way round. The NUV alignment flow is summarized in Fig. 5.1-1.

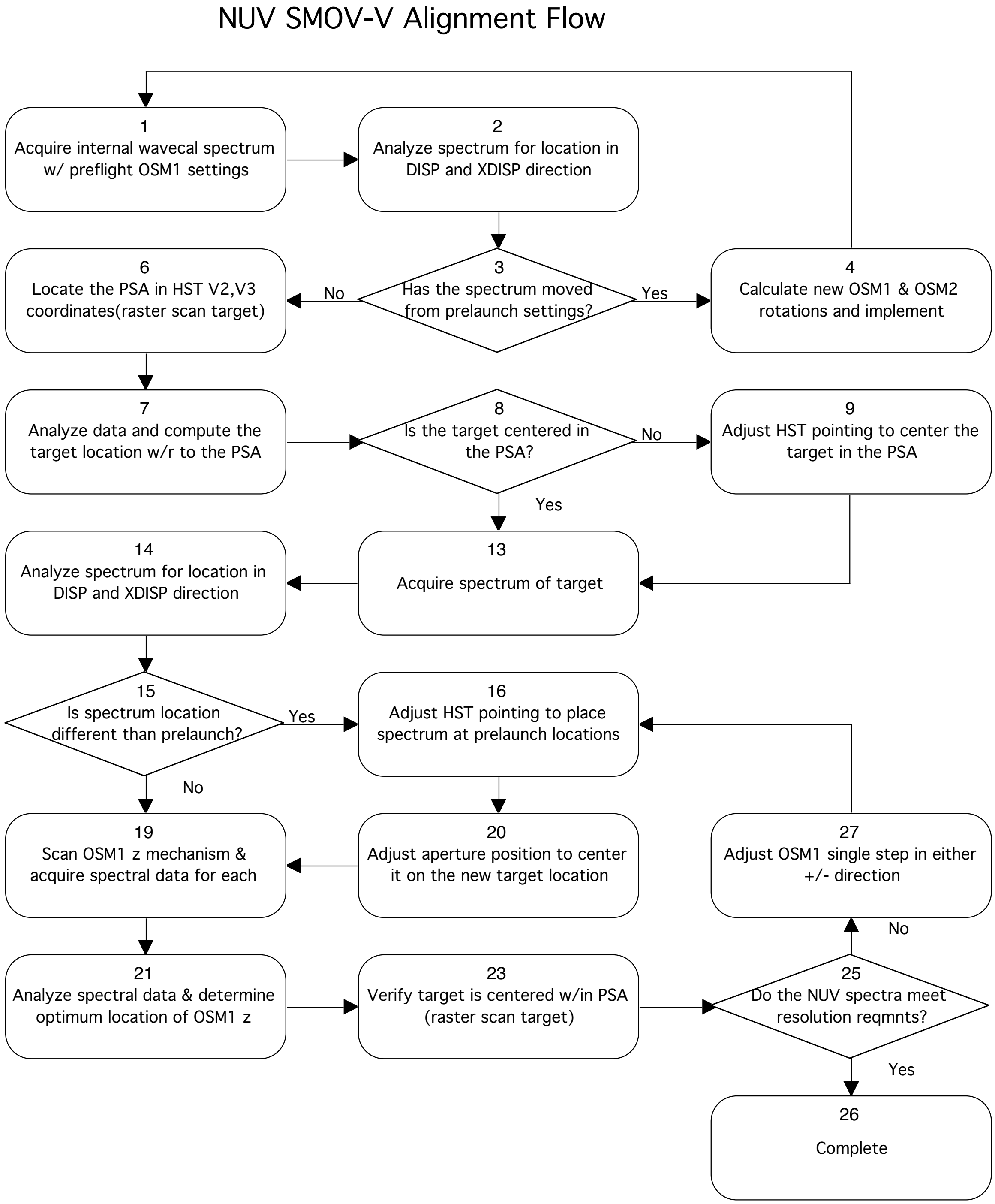

Figure 5.1-1: *Flow chart showing the complete alignment algorithm for the NUV channel.*

5.1.1.2 FUV Initial Alignment

The alignment of the FUV channel follows a similar methodology to the NUV channel alignment. The internal FUV alignment is verified and adjusted based on wavelength calibration spectra. Then HST is pointed so that the spectrum falls onto the correct position on the detector. The OSM1 z focus position for each grating is then adjusted to optimize the distance between the grating and HST OTA secondary. Finally, the aperture location is adjusted to center it on the image formed at the aperture location.

5.1.1.2.1 Confirm OSM1 Positions Using Internal Pt-Ne lamps

The ground-based calibration program will include many observations of the internal calibration lamps for each FUV spectroscopic mode. The preferred position of OSM1 for each mode will be tabulated. Early in SMOV, observations of internal lamps will either confirm that these are still the optimum positions, or will result in updated positions. The criteria for accepting the existing position for any one grating will be that the specified central wavelength cannot be brought closer to the desired position with one or more steps of the mechanism. The spectra obtained at the existing mechanism positions will be analyzed on the ground. Any revisions to the optimum position will be uploaded to the CS FSW for future use.

The motions introduced here would be rotations about the axis of the mechanism, which is parallel to the "x" coordinate in the mechanical design. This motion is referred to as θX in COS engineering literature.

This step correctly positions the grating with respect to the detector and, therefore, uniquely defines direction cosines of the input beam with respect to the grating provided the gratings have not moved anomalously during ascent.

5.1.1.2.2 Calibrate V2,V3 Coordinates of PSA

In the likely event that the NUV channel is aligned prior to the FUV channel, this activity will not have to be conducted. However, should the FUV channel be aligned first this activity will follow the exact flow as described for the NUV channel except that the FUV detector will be used to monitor the count rate through the aperture.

5.1.1.2.3 Refine Target Position for Optimum FUV Performance

The next step is to identify the location of the *target* in the V2,V3 direction that correctly positions the diffracted spectrum on the detector. The criteria will be that the wavelength offset between the calibration aperture and the science aperture should be minimized and the distance from the science spectrum to the wavelength calibration spectrum in the cross-dispersion direction should agree with pre-launch measurements. At this point in the alignment process, the HST secondary and FUV grating are oriented correctly, but the distance between the two optics is not necessarily optimum.

This step may not be necessary, because the NUV channel was aligned first. However, it will be verified during the alignment of the FUV channel.

5.1.1.2.4 Refine OSM1 "Δz" Position for Optimum FUV Resolution

The FUV gratings must be aligned to the HST secondary mirror with an accuracy of ±0.010mm along the V1 axis to provide the required image quality at the detector. We cannot guarantee that the gratings will be located with this precision upon installation of COS into the focal plane structure. OSM1 includes a linear adjustment motion with a range of 14mm and a granularity of 0.007mm. Observations will be made of a point source, whose spectrum includes many very narrow absorption lines, at multiple z positions of the OSM1 mechanism. The spectra will be analyzed on the ground for each of the 3 FUV optics on OSM1 and new z locations for each optic will be calculated. This information can then be uploaded to the CS FSW for future use.

5.1.1.2.5 Verify Alignment of the Aperture Mechanism

The final location of the PSA aperture in HST coordinates will be found by raster scanning an astronomical target pattern centered on the aperture location and the count rate of the FUV detector will be recorded for each position. The data will be analyzed on the ground to determine the center of the aperture in HST coordinates for future observations.

The FUV alignment flow is summarized in Fig. 5.1-2.

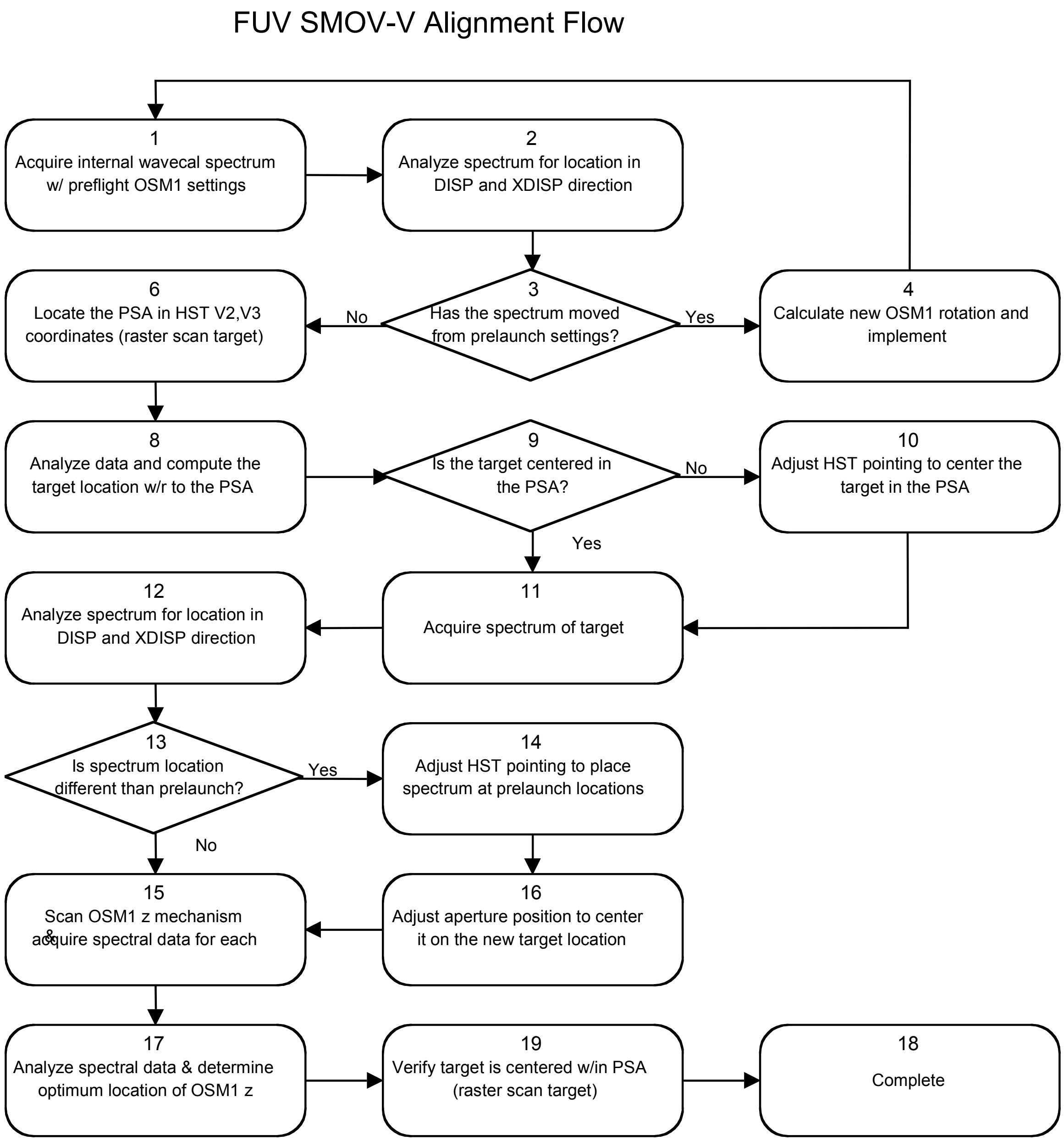

Figure 5.1-2: *Flow chart showing the complete algorithm for aligning the FUV channel.*

5.1.2 HST Secondary Mirror Adjustments

The most critical alignment for COS is the relationship between the optics on OSM1 and the HST secondary mirror. If the position of the secondary mirror is changed after the alignments described in Section 5.1.1, say to optimize the focus for another instrument that is not perfectly confocal, the COS alignments can be adjusted to allow COS to remain in use. The primary motion should be an adjustment of the "z" coordinate of OSM1. The mechanism has a range of 14mm, which should be enough to accommodate any foreseen adjustment of the HST SM.

5.2 TARGET ACQUISITION PROCEDURES

Elements of the discussion in this section are excerpted from Ball SER-FSW-001 ("Target Acquisition Concepts for COS") and the CU TER's COS-11-0014 ("Recommended TA FSW and Operations Changes, based upon the TAACOS: Phase I Reports for the FUV and NUV Channels"), COS-11-0016 ("TAACOS FUV Phase I Report"), COS-11-0024 ("TAACOS: NUV Phase I Report"), and COS-11-0027 ("TAACOS: Target Acquisition with the TA1 Mirror"). Refer to those documents for details, which are treated incompletely here for the sake of brevity. Some details have been revised during the preparation of this document. In cases of conflict this document should take precedence.

COS has two autonomous modes of target acquisition: dispersed light target acquisition with either the FUV or NUV detector, and imaging target acquisition with the TA1 mirror and NUV detector. They use only hardware and software capabilities within COS.

5.2.1 COS Autonomous Target Acquisition

The autonomous target acquisition modes are designed to center the HST aberrated point spread function (PSF) of a UV point in a COS science aperture, as shown in Fig. 5.2-1. In practice, they should be suited to most COS science targets:

1) A UV point source in an uncrowded field (i.e., no other UV-bright target within ~10 arcseconds) whose flux is within the acceptable range for one or more of the COS spectroscopic and imaging modes.
2) A UV point source at a fixed offset from the UV science target that can be acquired by COS, and that is within the range of small angle maneuvers that HST can perform.
3) A small but resolved target that does not entirely fill the aperture.

4) An extended object that is larger than the aperture, but which has a region of enhanced brightness for the target.

5) Extended diffuse objects with no preferred precise target position (no target acquisition required).

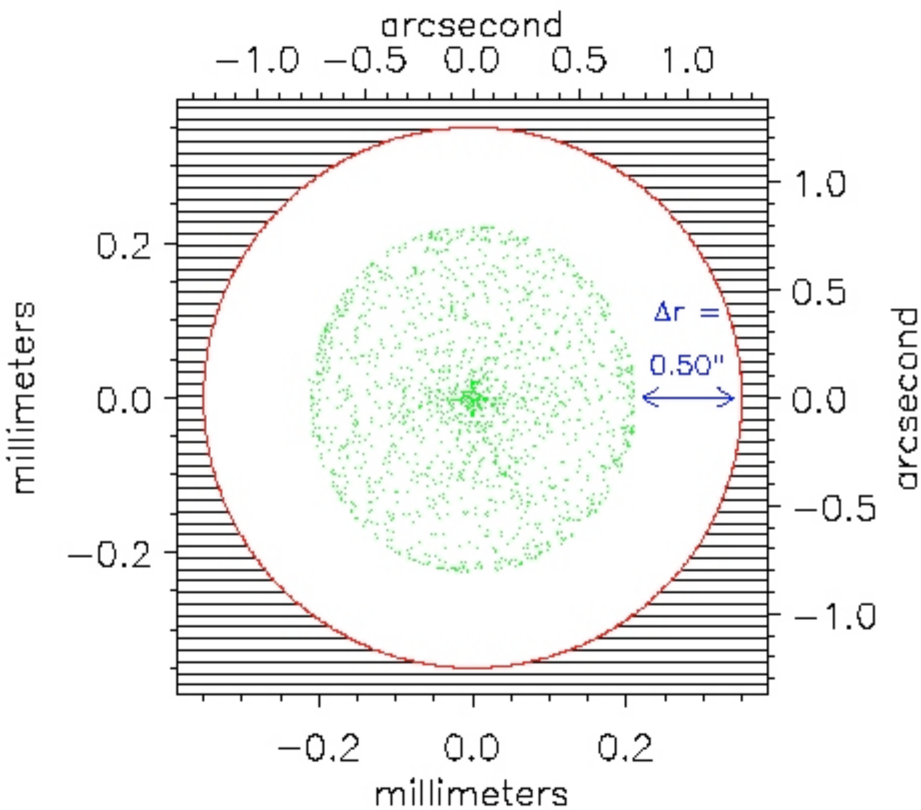

Figure 5.2-1*: The HST PSF as compared to the COS PSA. The aberrated, out of focus, HST PSF (in green) is approximately circular with a radius of ~0.2 mm at the COS aperture plate. The COS PSA is circular with a radius of 0.35 mm, which corresponds to 1.25" on the sky. The HST PSF is smaller in radius than the COS PSA by 0.136 mm or ~0.5".*

The first event in the acquisition process is for HST to slew to a position based upon the coordinates provided by the proposer and STScI selected guide stars. The COS external shutter will be closed during all such slews, as a normal precaution in the BOP plan. Experience with GHRS, FOS, and STIS acquisitions shows that, using the HST Guide Star Catalog I (GSC I), the initial pointing places the target within ±1 arcsecond of the center of the aperture 60% to 75% of the time, and within ±2.5 arcseconds essentially 100% of the time. The initial pointing precision is expected to improve with GSC II, which will be in use by the time COS is installed.

After the initial slew and acquisition of guide stars the sequence of events unique to the COS autonomous target acquisition (TA) process will begin. The Phase I Configuration and Phase 2 Target Search phases are applicable to all COS TA modes, then the discussion is broken out into subsections applicable to dispersed light TA, followed by imaging TA. The motivation for the sequence of events that occur in either dispersed light or imaging TA is similar, though the implementation differs. Sub-arrays that are necessary for dispersed light or imaging TA are discussed in Section 5.2.2.

Four observing modes are provided for target acquisition:

ACQ mode (target search)
ACQ/PEAKXD mode (cross-dispersion peakup)
ACQ/PEAKD mode (dispersion peakup)
ACQ/IMAGE mode (TA1 imaging acquisition)

Observers may specify any combination of these modes in any order, and some of the steps (notably the target search) may be repeated. ACQ/PEAKXD and ACQ/PEAKD modes require dispersed light and will be used in conjunction with one or more of the COS gratings (G130M, G160M, G140L; G185M, G225M, G285M, G230L). (Although there is nothing in the target acquisition FSW that would prevent one from using the NUV TA1 mirror with the ACQ/PEAKXD and ACQ/PEAKD modes, doing so would merely duplicate the functionality of the ACQ/IMAGE mode. Therefore, proposers should not be allowed to specify the TA1 mirror as the spectral element during the ACQ/PEAKXD and ACQ/PEAKD modes.) ACQ/IMAGE mode uses undispersed light and requires the use of the NUV mirror (TA1, TA1-RVMM). At the end of the ACQ/IMAGE procedure, a "confirmation image" will automatically be taken in ACCUM mode and downlinked to the ground to facilitate diagnosis of target acquisition problems. ACQ mode (target search) may be done in either dispersed or undispersed light, depending on whether a grating or the NUV mirror is selected as the spectral element. The FUV detector STIM pulses should be turned off (rate set to 0 Hz) during any target acquisition mode using the FUV detector.

The peakup and image acquisition modes are designed to center a target within a science aperture that already contains appreciable flux from the target. Acquisitions for which the initial pointing uncertainty is greater than 1.7 arcseconds should begin with a target search to locate the target in the aperture. If the target can already be placed in the aperture with high confidence, this step may be skipped. Centering the target in the aperture can be accomplished either by repeating the target search, carrying out the two peakup steps (normally an ACQ/PEAKXD followed by an ACQ/PEAKD sequence of exposures), or performing an ACQ/IMAGE exposure. The strategy selected will depend on factors such as the brightness of the source, the morphology of the source (i.e., point source vs. diffuse), the initial pointing uncertainty, and the detector and spectral elements to be used for the subsequent science.

Phase 1 *Configuration*

The initial setup (not necessarily in this order) includes initializing the flight software for the acquisition, ensuring that the external shutter is closed, turning on the detector and letting it warm up (if applicable), moving the mechanisms to their required positions, and whatever else may be included in a standard preparation. This phase does not require any unique COS target acquisition flight software capabilities.

Phase 2 *Target Search (ACQ mode)*

HST initially slews to the nominal target position, regardless of whether a target search is executed or whether the target search is even-ordered or odd-ordered. For even-ordered search patterns, the target acquisition FSW will compute the small slew necessary to move HST from the nominal target position to the first dwell point of the spiral, such that the nominal target position is the geometric center of the completed spiral. The target search may be performed in dispersed or undispersed light.

Since we cannot be 100% certain that the initial pointing of the HST will place the target in the aperture, a search can be performed to move the target into the aperture. This phase can be used for targets intended to be observed with either the Primary Science Aperture or the Bright Object Aperture. The PSA and BOA are separated in the cross-dispersion direction by 3.7 mm = 13.2 arcseconds. In addition to screening target regions to verify no bright source would fall into the aperture not being used, the size of the search pattern for the BOA must not exceed ~10 arcseconds in the direction of the PSA in order to minimize the chance that light from a bright target could spill into the un-attenuated primary aperture. This condition is satisfied if the maximum offset between dwell points in the cross-dispersion direction is ≤ 2 arcseconds.

The external shutter will remain open for the target search phase. It shall remain open during the small angle maneuvers between dwell points. The same exposure time should be used at all dwell points. BOP checks are performed at each dwell point of the target search and peakup phases.

2a. The search consists of moving the telescope through a square spiral pattern of 2 – 5 dwell points on a side. The dwell points of a spiral search will therefore cover an area on the sky of $\{[\Delta DW \times (n-1)] + (2 \times 1.25)\}^2$ arcseconds^2, where ΔDW is the offset in arcseconds between dwell point centers, n is the number of dwell points on a side of the spiral search, and 1.25 arcseconds is the radius of the aperture. (In reality, the area covered is a few arcseconds larger on a side because the aberrated wings of a target centered outside the aperture can still be detected.) Simulations show that dwell point offsets larger than 2 arcsecs will introduce target acquisition errors due to unsampled areas within the search pattern. Therefore the square area on the sky covered should be less than $[2 \times (n-1)] + 2.5$ arcseconds on a side. TAACOS simulations indicate the optimum dwell point offset is $\Delta DW_{optimum} = 1.767$ arcsecs, the largest dwell point offset which leaves no interior sky positions unsampled.

The choice of the number of dwell points on a side (2, 3, 4, or 5) should be left to the observer and generally should be made based upon their assessment of the quality of the target coordinates. TAACOS simulations suggest that performing a 2×2 spiral search on a typical (faint) COS target should be avoided for *dispersed light* target searches with the NUV channel.

The flight software algorithm for commanding the search pattern will be adapted from STIS. Note that including even numbered spiral searches requires an offset from the nominal target coordinates to the first dwell point.

If the BOP check fails, the flight software will close the external shutter and the TA software will exit. This response to BOP violation will ensure the safety of the detector and will preserve the current timeline. The shutter will be re-opened by a command inserted by the ground system at the start of the next phase of target acquisition or, if subsequent phases are not performed, at the start of the next science exposure.

2b. After completing the search pattern, the series of flux measurements are analyzed and the preferred position is computed. The flight software will compute a flux-weighted centroid of all of the positions whose flux exceeds a patchable threshold. This will be the default algorithm. An alternative, "return to brightest point" procedure will also be available.

2c. Request a slew to point the telescope at the preferred position, starting at its current pointing at the last dwell point in the spiral. After the slew, the target will be in the aperture, but not necessarily well centered. Note that when the centroid algorithm is used, the pointing of the HST after this phase will probably not be one of the dwell points visited during the search.

The total flux detected at each dwell point should be retained for downlink. It is not necessary to save the entire spectrum or image from each point. The location of the computed centroid and the parameters of the requested slew should be downlinked.

This centroid process may place the target in the aperture with precision that is sufficient for many science observations. If additional precision is needed, two autonomous peakup steps are available for dispersed light (ACQ/PEAKXD and

ACQ/PEAKD) or the autonomous imaging target acquisition sequence is available for undispersed light (ACQ/IMAGE). A spiral search could also be repeated with the same or fewer dwell points. The precision of the centroid algorithm and the need for additional target search or peakup steps will be determined during SMOV. Note that while the target search phase places the target within the science aperture, the location of the target or aperture on the detector is not known until the science data are downlinked and analyzed, or the "Calibrate Aperture Location" phase is executed as part of a subsequent ACQ/PEAKXD or ACQ/IMAGE sequence.

5.2.1.1 Dispersed Light Target Acquisition

Phase 3 Calibrate aperture location in detector pixel coordinates (ACQ/PEAKXD mode)

The goal of target acquisition is to move the HST to place the target at a preferred position within the aperture. Light which enters COS from a fixed location at the aperture plane will not always fall on precisely the same pixels, due to variations in the mechanical position of the grating, and variations in the conversion of photoelectron events to digitized pixel values. Phase 3 of target acquisition is an attempt to compensate for these small variations by measuring the pixel location of light from a fixed calibration aperture, whose offset from the center of the science aperture is known. The external shutter should remain closed for this phase.

3a. Turn on one of the spectral calibration (PtNe) lamps and record its spectrum through the WCA in Time-tag mode for a prescribed length of time to achieve an appropriate S/N. Use only the counts that arise from pixels within a sub-array that encloses the spectral calibration image (see Tables 5.2-1 and 5.2-3). (In the nominal configuration for this phase, the flat-field aperture is behind a mask and any light that might enter the FCA should not be able to reach the detector.)

3b. Determine the position of this comparison spectrum in the direction perpendicular to dispersion, in units of detector pixels. The simplest algorithm is to find the mean position of the events in the cross-dispersion direction. Computer simulations (TAACOS) indicate this method is sufficient for both the FUV and NUV detectors. The comparison spectrum has an offset from the optimum location of the target spectrum. The offset may be different for each grating because the cross-dispersion image profile of the calibration spectrum may differ slightly for each grating. The offsets for each grating will be calibrated during ground and SMOV testing.

It is not necessary to save and downlink the full image data from this phase. The measured comparison spectrum mean position and the total counts should be downlinked.

Phase 4 Peakup in cross-dispersion direction (ACQ/PEAKXD mode)

The next step is to move the telescope to improve the centering of the target in the direction perpendicular to dispersion.

4a. Record the target spectrum in Time-tag mode for a prescribed period of time by accumulating counts within the sub-array (see Table 5.2-2 and Table 5.2-5) for the grating and detector in use.

4b. Compute the location of the spectrum in the cross-dispersion direction. TAACOS simulations suggest that calculating the mean position of the events should suffice for the FUV channel. But for the NUV channel, a median algorithm should be used, due to the higher detector background rate. Here, too, the units are detector pixels.

4c. From the measured comparison spectrum and the tabulated offset, calculate the location on the detector where the target spectrum will be when the target is properly centered in the aperture. The size and location of the science target sub-array are established during the observation planning process and are not changed here. The sub-array size and location will be designed to avoid bright airglow lines in the FUV spectrum (see Sec. 5.2.2.). The sub-array will be large enough to capture the target spectrum with the target anywhere in the science aperture, and with the largest likely range of locations on the detector.

4d. Calculate the telescope slew needed to move the target so that its spectrum aligns with the preferred location. The preferred position will be the location of the calibration spectrum found in step 2b modified by the fixed offset stored in a table of calibration data.

4e. Request the slew. The directions of all slews commanded by target acquisition are specified in the detector (X,Y) coordinates. The magnitude is in units of 2^{-27} radians. The angle between the COS detector coordinates and the HST (V2,V3) directions will be measured during pre-launch testing, determined accurately during SMOV, and rotation matrices for each detector will be included in a ground calibration database, parts of which may be loaded into and used by the NSSC-1.

The data downlinked from phase 4 should include both the measured cross-dispersion mean of the science spectrum and the desired cross-dispersion coordinate computed by the flight software.

Phase 5 Peakup in dispersion direction (ACQ/PEAKD mode)

For this phase, we try to maximize the flux through the aperture, rather than define a location of the spectrum on the detector. We assume that the flux is maximum when the target is at the center. The external shutter must be open for this phase, and shall remain open during the small angle maneuvers described below.

5a. This peakup consists of a linear scan of the telescope in a direction that displaces the spectrum parallel to its dispersion. The total flux in the spectrum within the sub-arrays (see Tables 5.2-2 and 5.2-4) is measured at each dwell point. The same exposure time is used at each dwell point. Each flux measurement should be BOP checked. The response to a failed BOP check is the same as that described in step 3a.

The calculation of the linear scan will be adopted from the STIS flight software. The scan will be defined by a set of parameters such as the number of dwell points and their spacing. It will be possible to alter these parameters, especially during testing and calibration. Sensible default values will be defined, and general observers will not routinely choose these parameters. The order in which to visit the dwell points is not specifiable by any macro parameters or patchable constants, but is built into the logic of the target acquisition of the flight software (exactly as is done for STIS).

5b. The default algorithm will be the flux-weighted centroid. A “return to brightest” option will also be available. During normal science operations, one preferred algorithm will be identified and used as the default by the flight software. General observers will not specify which algorithm to use.

5c. Request the slew needed to move the target to the preferred point from its current pointing at one end of the linear scan. At the end of the peakup phase the target should be well centered in the aperture.

The data to be downlinked include the fluxes measured at each dwell point, the computed flux-weighted centroid or brightest dwell point, and the parameters of the slew requested by the flight software.

Post-peakup offset

This step allows a small adjustment of the pointing to be made by the ground system following the autonomous peakup. The FUV and NUV channels may have a slightly different optimum target location, due to possible differences in the alignment of the optics on the mechanisms. It is not absolutely necessary to do the acquisition and the spectrum observation with the same grating, or even the same channel. This is a small adjustment to the location of the object currently centered in the aperture. It is not an offset to a separate nearby target.

5.2.1.2 Imaging Target Acquisition with the TA1 Mirror

COS will be capable of performing autonomous imaging target acquisition using the TA1 mirror on OSM2 and the NUV detector. Experience with STIS suggests that this may be the fastest and most accurate method of centering a point source in the COS science aperture. (We note that if COS is operated with only one detector on at a time, it almost certainly would not be faster to use the NUV imaging TA mode and then switch to the FUV channel for science observations, instead of performing dispersed light target acquisition using the FUV detector.) Imaging TA with the TA1 mirror is limited to targets for which the initial HST slew can position the target within 1.7" of the center of the science aperture – i.e., the target coordinates must be good enough so that the target can be placed somewhere within the science aperture. If the target coordinates are not good enough to place the target in the aperture with high confidence, then a target search must be performed, either with the TA1 mirror or a grating, prior to executing the imaging target acquisition sequence.

Assuming the target coordinates are good enough to place the target within the aperture with the initial HST slew, the Phase 1 Configuration will place the NCM1 mirror on OSM1 to its proper position for illuminating the NUV channel; then OSM2 will place the TA1 mirror to its proper position, where either the primary TA1 image or the TA1-Rear-View-Mirror-Mode (TA1-RVMM) – that uses the front surface reflection off the TA1 order sorter filter – is accessed. After the Phase I Configuration is complete, the TA1 imaging TA mode uses the following sequence. The procedure is depicted in Figure 5.2-2 below.

Phase 3 *Calibrate Aperture Location (LTAIMCAL of ACQ/IMAGE)*

Due to possible mechanism mis-alignments, it is necessary to flash the wavelength calibration lamp, with OSM2 rotated to the TA1 mirror, to determine the position on the detector corresponding to the wavelength calibration image. The extraction sub-array for this TA phase is provided in Section 5.2.2. Once the location of the wavelength calibration image is determined, a known offset is applied (via patchable constants) to calculate the detector location corresponding to the center of the science aperture. If the flux of the target is high enough such that the TA1-RVMM is used to image the science target, then the wavelength calibration image should also be obtained with the TA1-RVMM.

3a. Turn on one of the spectral calibration (PtNe) lamps and record its spectrum through the WCA in Time-tag mode for a prescribed length of time to achieve an appropriate S/N. Use only the counts that arise from pixels within a sub-array that encloses the spectral calibration image (see Table 5.2-6). The external shutter should be closed during this phase.

3b. Determine the position of the wavelength calibration image in both X and Y pixel positions on the NUV detector using a median algorithm. TAACOS simulations show that using the median algorithm to determine the X and Y centroids of the wavelength calibration image should produce approximately ± 0.01" errors in the predicted location of the center of the science aperture.

It is not necessary to save and downlink the wavelength calibration image. The measured X and Y centroids and total counts should be downlinked.

Phase 4 Science Image Centering (LTAIMAGE of ACQ/IMAGE)

After measuring the X and Y centroids of the wavelength calibration lamp image and knowing the X and Y pixel offsets to the detector position of the center of the science aperture being used (where the offsets to the PSA and BOA will be the same since the current plan is to move the BOA to the same position as the PSA for bright objects), a short exposure of the science target is then obtained, the X and Y centroids measured, and an HST small angle maneuver is executed to place the target at the center of the science aperture. Note that for targets with flux greater than ~1.3×10^{-14} ergs/cm^2/s/Å, to avoid BOP rate violation it is necessary to attenuate the TA1 image either by observing with the TA1-RVMM or the BOA science aperture, or both (see Section 5.3.9 for a discussion of exposure times *versus* science target flux).

4a. Following a BOP check exposure, record the science target image in ACCUM mode within the appropriate sub-array (see Table 5.2-7).

4b. Compute the pixel positions of a 170p×170p (or 4" × 4") "small box" that is centered on the detector at the expected location of the science aperture center, based on the offsets calculated in the previous phase. Compute the X and Y pixel centroids of the science target within the "small box" using a STIS-based Moving Box Plus Flux Centroid (MBPFC) algorithm. The MBPFC algorithm moves a 9×9 pixel box across all possible box locations within the "small box" to find the position containing the maximum counts. At this maximum count position, the flux-weighted X and Y centroids of the science target are calculated within the 9×9 pixel box.

4c. Calculate the telescope slew needed to move the target so that it is centered at the preferred location.

4d. Request the slew.

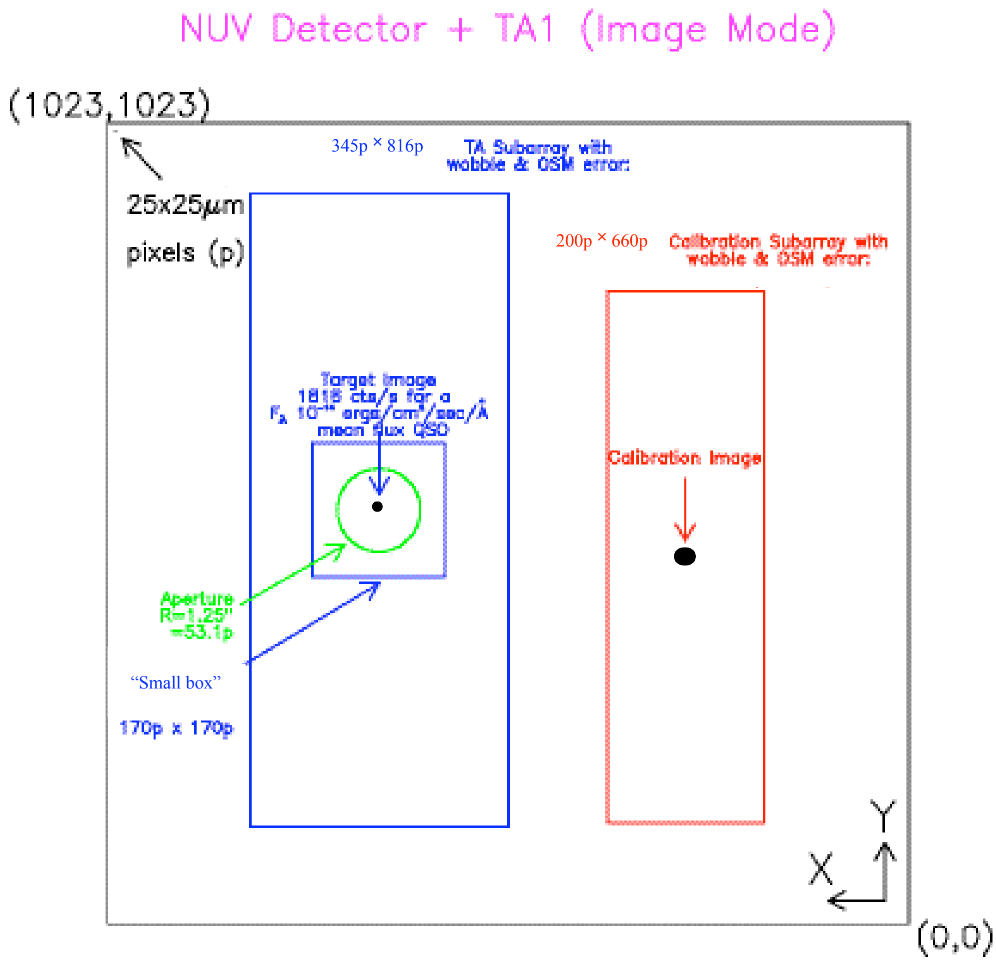

Figure 5.2-2: *TA1 imaging target acquisition sub-array summary. The wavelength calibration image is recorded within the large red sub-array (defined in Table 5.2-6). The science target image is recorded in the large blue sub-array (defined in Table 5.2-7). Based on the measured position of the calibration image and known X and Y offsets to the center of the science aperture, a "small box" is defined within which the science target position is measured using the MBPFC method. A slew is then requested to move the target to the center of the science aperture.*

The ACCUM image from this phase should be downlinked, along with the total counts, the computed X and Y centroids of the science target, the X and Y pixel locations of the preferred target position, and the X and Y offsets commanded in the slew. A subsequent exposure can then be commanded and downlinked to verify that the target ended up in the preferred location.

Note: The TA1-RVMM imaging mode actually produces two images: a primary image from the first surface of the order-sorter filter, and a secondary image from the second surface of the filter. Thus, the downlinked TA1-RVMM images will contain "double sources." Ground testing shows that the secondary image will contain ~1/2 the flux of the primary image. Due to the slight wedge-shape of the order-sorter filter, the secondary image projects ~20 pixels in the –Y (dispersion) direction (MAMA detector coordinates) from the primary image. Simulations show that the MBPFC algorithm properly computes the centroid of the primary image for an isolated point source. However, for extended sources or for crowded fields, the presence of the secondary image may compromise the accuracy of the MBPFC algorithm.

5.2.2 Sub-arrays for Target Acquisition

Dispersed light target acquisition (TA) exposures are obtained in Time-tag mode. Imaging target acquisition exposures using the TA1 mirror or TA1-rear-view-mirror mode (TA1-RVMM) are in ACCUM mode. The sub-arrays specified below are optimized for isolated UV point sources. There is no need for Doppler correction during target acquisition. The science sub-arrays are the same for either the Primary Science Aperture (PSA) or Bright Object Aperture (BOA). Wavelength calibration spectra or lamp images taken through the Wavelength Calibration Aperture (WCA) use different sub-arrays. The sub-arrays specified assume there are no hot spots or dead spots on the detector. If such features develop and need to be excluded from target acquisition, additional sub-arrays may need to be specified.

5.2.2.1 FUV TA Sub-arrays

Target acquisition with the COS FUV detector is in dispersed light only. The pixel coordinates specified are relevant to the initial FUV detector region used for science observations, and will need to be adjusted appropriately when fresh detector regions are used for detector lifetime purposes. The specified FUV sub-arrays assume FUV pixels that have spatial extents of 1 X (dispersion) pixel = 6 microns, and 1 Y (cross-dispersion) pixel = 24 microns. In general, the X (dispersion) dimension of the FUV sub-arrays, which are positioned to avoid geocoronal airglow lines, are not a power of 2.

The FUV sub-arrays on each segment for each grating will be used to isolate the most useful portions of the input spectrum for target acquisition. For G130M, the sub-arrays exclude the strongest geocoronal airglow lines, which could bias the target acquisition calculations. For G140L, the sub-arrays exclude large portions of the detector which are not illuminated by the science spectrum as well as geocoronal airglow lines. The bright FUV airglow lines that are to be avoided during target acquisition are Lyman α 1216Å, O I 1304Å, and O I 1356Å. The airglow lines will appear as bright, comparatively diffuse blobs because the airglow represents uniform emission that fills the aperture.

The FUV XDL stim pulses should not be included in the flux measurements for each dwell point in target acquisition, and, therefore, the stim pulses are not included in any TA sub-arrays. (It is recommended that the stim pulses be turned off during target acquisition exposures by setting the rate to 0 Hz.)

The FUV TA sub-arrays for the different phases of target acquisition follow.

Phase 3 – Calibrate aperture location

The wavelength calibration spectrum TA extraction sub-arrays are shown in Table 5.2-1.

Table 5.2-1: Phase 3 FUV Wave Cal TA Extraction Sub-arrays

Aperture/Grating	Central λ (Å)	Sub-array Sizes (pixels)	Pixel Coordinates of FUV Sub-array Vertices (segment specified)
WCA/G130M	1291	(14200 × 32) (14300 × 32)	Segment A, Sub-array 1: (1100,572),(1100,604),(15300,604),(15300,572) Segment B, Sub-array 1: (1300,631),(1300,663),(15600,663),(15600,631)
WCA/G130M	1300	(14200 × 32) (14300 × 32)	Segment A, Sub-array 1: (1100,572),(1100,604),(15300,604),(15300,572) Segment B, Sub-array 1: (1300,631),(1300,663),(15600,663),(15600,631)
WCA/G130M	**1309**	(14200 × 32) (14300 × 32)	Segment A, Sub-array 1: (1100,572),(1100,604),(15300,604),(15300,572) Segment B, Sub-array 1: (1300,631),(1300,663),(15600,663),(15600,631)
WCA/G130M	1318	(14200 × 32) (14300 × 32)	Segment A, Sub-array 1: (1100,572),(1100,604),(15300,604),(15300,572) Segment B, Sub-array 1: (1300,631),(1300,663),(15600,663),(15600,631)
WCA/G130M	1327	(14200 × 32) (14300 × 32)	Segment A, Sub-array 1: (1100,566),(1100,598),(15300,598),(15300,566) Segment B, Sub-array 1: (1300,624),(1300,656),(15600,656),(15600,624)
WCA/G160M	1577	(14200 × 32) (14300 × 32)	Segment A, Sub-array 1: (1100,566),(1100,598),(15300,598),(15300,566) Segment B, Sub-array 1: (1300,624),(1300,656),(15600,656),(15600,624)
WCA/G160M	1589		Segment A, Sub-array 1:

Aperture/Grating	Central λ (Å)	Sub-array Sizes (pixels)	Pixel Coordinates of FUV Sub-array Vertices (segment specified)
		(14200 × 32) (14300 × 32)	(1100,566),(1100,598),(15300,598),(15300,566) Segment B, Sub-array 1: (1300,624),(1300,656),(15600,656),(15600,624)
WCA/G160M	**1600**	(14200 × 32) (14300 × 32)	Segment A, Sub-array 1: (1100,566),(1100,598),(15300,598),(15300,566) Segment B, Sub-array 1: (1300,624),(1300,656),(15600,656),(15600,624)
WCA/G160M	1611	(14200 × 32) (14300 × 32)	Segment A, Sub-array 1: (1100,566),(1100,598),(15300,598),(15300,566) Segment B, Sub-array 1: (1300,624),(1300,656),(15600,656),(15600,624)
WCA/G160M	1623	(14200 × 32) (14300 × 32)	Segment A, Sub-array 1: (1100,566),(1100,598),(15300,598),(15300,566) Segment B, Sub-array 1: (1300,624),(1300,656),(15600,656),(15600,624)
WCA/G140L	1105	(14200 × 32)	Segment A, Sub-array 1: (1100,579),(1100,611),(15300,611),(15300,579) Segment B: (no sub-array, high-voltage to low)
WCA/G140L	**1230**	(14200 × 32)	Segment A, Sub-array 1: (1100,579),(1100,611),(15300,611),(15300,579) Segment B: (no sub-array)

Phases 2, 4, and 5 – Target Search (LTASRCH) and Peak-ups (LTAPKD, PTAPKXD)

The FUV science object TA extraction sub-arrays are given in Table 5.2-2.

Table 5.2-2: Phases 2, 4, 5 FUV Object TA Extraction Sub-arrays

Aperture/Grating	Central λ (Å)	Sub-array Sizes (pixels)	Pixel Coordinates of FUV Sub-array Vertices (segment specified)
PSA or BOA/G130M	1291	(7451 × 64) (6670 × 64) (5710 × 64) (8411 × 64)	Segment A, Sub-array 1: (958,452),(958,516),(8408,516),(8408,452) Segment A, Sub-array 2: (8756,452),(8756,516),(15425,516),(15425,452) Segment B, Sub-array 1: (958,512),(958,576),(6667,576),(6667,512) Segment B, Sub-array 2: (7015,512),(7015,576),(15425,576),(15425,512)
PSA or BOA /G130M	1300	(8433 × 64) (5688 × 64) (6692 × 64) (7429 × 64)	Segment A, Sub-array 1: (958,452),(958,516),(9390,516),(9390,452) Segment A, Sub-array 2: (9738,452),(9738,516),(15425,516),(15425,452) Segment B, Sub-array 1: (958,512),(958,576),(7649, 576),(7649,512) Segment B, Sub-array 2: (7997,512),(7997, 576),(15425, 576),(15425,512)
PSA or BOA **/G130M**	**1309**	(9415 × 64) (4706 × 64) (7674 × 64) (6447 × 64)	Segment A, Sub-array 1: (958,452),(958,516),(10372, 516),(10372,452) Segment A, Sub-array 2: (10720,452),(10720,516),(15425,516),(15425,452) Segment B, Sub-array 1: (958,512),(958,576),(8631, 576),(8631,512) Segment B, Sub-array 2: (8979,512),(8979, 576),(15425, 576),(15425,512)
PSA or BOA /G130M	1318	(10397 × 64) (3724 × 64) (7674 × 64) (5465 × 64)	Segment A, Sub-array 1: (958,452),(958,516),(11354, 516),(11354,452) Segment A, Sub-array 2: (11702,452),(11702,516),(15425,516),(15425,452) Segment B, Sub-array 1: (1940,512),(1940,576),(9613,576),(9613,512) Segment B, Sub-array 2: (9961,512),(9961,576),(15425,576),(15425,512)
PSA or BOA /G130M	1327	(11379 × 64) (2742 × 64)	Segment A, Sub-array 1: (958,452),(958,516),(12336,516),(12336,452) Segment A, Sub-array 2: (12684,452),(12684,516),(15425,516),(15425,452)

		(7674 × 64) (4483 × 64)	Segment B, Sub-array 1: (2922,512),(2922,576),(10595,576),(10595,512) Segment B, Sub-array 2: (10943,512),(10943,576),(15425,576),(15425,512)
PSA or BOA /G160M	1577	(14468 × 64) (14468 × 64)	Segment A, Sub-array 1: (958,446),(958,510),(15425,510),(15425,446) Segment B, Sub-array 1: (958,505),(958,569),(15425,569),(15425,505)
PSA or BOA /G160M	1589	(14468 × 64) (14468 × 64)	Segment A, Sub-array 1: (958,446),(958,510),(15425,510),(15425,446) Segment B, Sub-array 1: (958,505),(958,569),(15425,569),(15425,505)
PSA or BOA **/G160M**	**1600**	(14468 × 64) (14468 × 64)	Segment A, Sub-array 1: (958,446),(958,510),(15425,510),(15425,446) Segment B, Sub-array 1: (958,505),(958,569),(15425,569),(15425,505)
PSA or BOA /G160M	1611	(14468 × 64) (14468 × 64)	Segment A, Sub-array 1: (958,446),(958,510),(15425,510),(15425,446) Segment B, Sub-array 1: (958,505),(958,569),(15425,569),(15425,505)
PSA or BOA /G160M	1623	(14468 × 64) (14468 × 64)	Segment A, Sub-array 1: (958,446),(958,510),(15425,510),(15425,446) Segment B, Sub-array 1: (958,505),(958,569),(15425,569),(15425,505)
PSA or BOA /G140L	1105	(11409 × 64) (534 × 64)	Segment A, Sub-array 1: (958,459),(958,523),(12366,523),(12366,459) Segment A, Sub-array 2: (13392,459),(13392,523),(13925,523),(13925,459) Segment B: (no sub-array, high-voltage to low)
PSA or BOA **/G140L**	**1230**	(12698 × 64) (961 × 64)	Segment A, Sub-array 1: (958,459),(958,523),(13655,523),(13655,459) Segment A, Sub-array 2: (14465,459),(14465,523),(15425,523),(15425,459) Segment B: (no sub-array)

5.2.2.2 NUV TA Sub-arrays

The sub-arrays specified below are for dispersed light target acquisition with the NUV detector. The NUV MAMA pixel sizes are 25 microns in X (cross-dispersion) and Y (dispersion). The spectral stripes run along the Y pixel direction on the NUV MAMA detector.

In general, the NUV sub-arrays to be used for target acquisition will depend on the spectral *stripe* being used, rather than by the wavelength setting. However, for G230L, the optimum stripe to use does depend on the wavelength being observed, and may be stripe A or B. (See Table 1.3-2 for the spectral coverage in each stripe for different G230L settings.) In order to avoid light from one stripe leaking into the sub-array of an adjacent stripe, the science spectral stripe sub-arrays generally will not be a power of 2 in cross-dispersion dimension. There are no appreciably bright airglow lines in the NUV portion of the spectrum.

The proposer will be responsible for specifying the NUV spectral stripe, hence TA extraction sub-array, to be used for the calibrate aperture and cross-dispersion peak-up phases. The default for all modes is to use stripe B (the middle stripe). The FSW uses a single cross-dispersion offset constant between the science stripe and the spectral calibration stripe. This offset constant will be set to that appropriate for stripe B; if stripe A or C is used, the target will be slightly misplaced in the cross-dispersion direction. While this misplacement will not appreciably affect the flux transmitted through the aperture or the wavelength calibration in the dispersion direction, the proposer should be made aware of it.

Phase 3 – Calibrate aperture location

The wavelength calibration spectrum TA extraction sub-arrays are shown in Table 5.2-3.

Table 5.2-3: Phase 3 NUV Wave Cal TA Extraction Sub-arrays

Aperture/Grating	Central λ (Å)	Sub-array Sizes (pixels)	Pixel Coordinates of NUV Sub-array Vertices (spectral stripe specified)
WCA/G185M	1700-2100	64 × 1024	Stripe A: (435,0),(435,1023),(499,1023),(499,0) **Stripe B: (341,0),(341,1023),(405,1023),(405,0)** Stripe C: (210,0),(210,1023),(274,1023),(274,0)
WCA/G225M	2100-2500	64 × 1024	Stripe A: (455,0),(455,1023),(519,1023),(519,0) **Stripe B: (352,0),(352,1023),(416,1023),(416,0)** Stripe C: (212,0),(212,1023),(276,1023),(276,0)
WCA/G285M	2500-3200	64 × 1024	Stripe A: (427,0),(427,1023),(491,1023),(491,0) **Stripe B: (331,0),(331,1023),(395,1023),(395,0)** Stripe C: (201,0),(201,1023),(265,1023),(265,0)
WCA/G230L	1700-3200	64 × 1024	Stripe A: (454,0),(454,1023),(518,1023),(518,0) **Stripe B: (352,0),(352,1023),(416,1023),(416,0)** Stripe C: (not used with G230L)

Phases 2 and 5 – Target Search (LTASRCH) and Dispersion Peakup (LTAPKD)

The total counts from all three stripes (G185M, G225M, G285M) can be used to maximize the photon counting statistics. For G230L, stripes A and B can be combined. Even if a particular setting (e.g., for G230L between 2000-2500 Å on stripe A) produces few or no counts on one of the stripes, we can foresee no problem using a large sub-array during these phases. The science TA extraction sub-arrays for the NUV detector for Phases 3 and 5 are specified in Table 5.2-4.

Table 5.2-4: Phases 2 and 5 NUV Object TA Extraction Sub-arrays

Aperture/Grating	Central λ (Å)	Sub-array Sizes (pixels)	Pixel Coordinates of NUV Sub-array Vertices (spectral stripe specified)
PSA or BOA/G185M	1700-2100	335 × 1024	Stripes A,B,C: (568,0),(568,1023),(903,1023),(903,0)
PSA or BOA/G225M	2100-2500	335 × 1024	Stripes A,B,C: (568,0),(568,1023),(903,1023),(903,0)
PSA or BOA/G285M	2500-3200	335 × 1024	Stripes A,B,C: (568,0),(568,1023),(903,1023),(903,0)
PSA or BOA/G230L	1700-3200	224 × 1024	Stripes A,B: (700,0),(700,1023),(924,1023),(924,0) Stripe C: (not used with G230L)
PSA or BOA/TA1	1700-3200	345 × 816	(561,123),(561,938),(904,938),(904,123)
PSA or BOA/TA1-RVMM	1700-3200	345 × 816	(397,123),(397,938),(742,938),(742,123)

Phase 4 – Cross-dispersion Peakup (LTAPKXD)

The nominal centers of the science stripes are at X = 794, 680, and 566 for stripes A, B, and C, respectively. The proposer can choose which stripe with which to do the cross-dispersion peak-up, though this stripe should be the same one selected for the wavelength calibration stripe in Phase 2.

The pixel differences between the science and calibration stripes are +396, +393, and +391 pixels for stripes A, B, and C, respectively. Because the FSW only carries a single constant for the offset, the value of +393 pixels will be used and the COS Handbook should encourage proposers to use stripe B for cross-dispersion peak-up. If an alternate stripe is selected, the peak-up will be offset by +/- 2-3 pixels depending on which stripe (A or C) is selected. This 2-3 pixel offset corresponds to < +/- 0.09", so there should be little effect on the transmitted flux. Note that stripe C should not be used with G230L, because no first-order light is imaged onto stripe C with this grating. The science TA extraction sub-arrays for the NUV detector for Phase 4 are specified in Table 5.2-5.

Table 5.2-5: Phase 4 NUV Object TA Extraction Sub-arrays

Aperture/Grating	Central λ (Å)	Sub-array Sizes (pixels)	Pixel Coordinates of NUV Sub-array Vertices (spectral stripe specified)
PSA or BOA/G185M	1700-2100	51 × 1024	Stripe A: (832,0),(832,1023),(883,1023),(883,0) **Stripe B: (736,0),(736,1023),(787,1023),(787,0)** Stripe C: (604,0),(604,1023),(655,1023),(655,0)
PSA or BOA/G225M	2100-2500	51 × 1024	Stripe A: (846,0),(846,1023),(897,1023),(897,0) **Stripe B: (741,0),(741,1023),(792,1023),(792,0)** Stripe C: (600,0),(600,1023),(651,1023),(651,0)
PSA or BOA/G285M	2500-3200	51 × 1024	Stripe A: (820,0),(820,1023),(871,1023),(871,0) **Stripe B: (724,0),(724,1023),(775,1023),(775,0)** Stripe C: (591,0),(591,1023),(642,1023),(642,0)
PSA or BOA/G230L	1700-3200	51 × 1024	Stripe A: (844,0),(844,1023),(895,1023),(895,0) **Stripe B: (741,0),(741,1023),(792,1023),(792,0)** Stripe C: (not used with G230L)

5.2.2.3 <u>NUV TA1 Imaging TA Sub-arrays</u>

The sub-arrays specified below are for imaging target acquisition with the TA1 mirror and NUV detector. The sub-arrays in Table 5.2-6 are to be used for the "Calibrate Aperture Location" phase (LTAIMCAL) of the TA1 imaging target acquisition sequence.

One sub-array is designated for the primary TA1 imaging mode, and the other is for the TA1-rear-view-mirror mode (TA1-RVMM). The primary TA1 calibration image will nominally be centered +55 pixels from the middle of calibration stripe B. The TA1-RVMM image will be centered –55 pixels from the middle of stripe B. The sub-array size for each mode, which captures the spot produced by the wavelength calibration lamp, accounts for mechanism wobble, +/- 1 rotation (dispersion direction) step drift in the rotary mechanisms for both OSM1 (+/- 240 pixels) and OSM2 (+/- 49 pixels), plus some buffer in case the spot should appear near an extreme.

Table 5.2-6: TA1 Wave Cal TA Sub-arrays

Aperture/Mirror	λ Coverage (Å)	Sub-array Sizes (pixels)	Pixel Coordinates of NUV TA1 Sub-array Vertices
WCA/TA1	1700-3200	200 × 660	(280,141),(280,800),(480,800),(480,141)
WCA/TA1-RVMM	1700-3200	200 × 660	(118,141),(118,800),(318,800),(318,141)

Table 5.2-7 gives the sub-arrays needed for isolating the science target on the NUV detector during a target search with the TA1 mirror (ACQ) or during TA1 imaging target acquisition (LTAIMAGE of ACQ/IMAGE). One sub-array is designated for the primary TA1 imaging mode, and the other is for the TA1-RVMM. The primary TA1 science image will nominally be centered +55 pixels from the middle of science stripe B. The TA1-RVMM image will be centered –55 pixels from the middle of stripe B. The size of these science target sub-array allows for mechanism wobble, +/- 1 rotation step drift in the rotary mechanisms for both OSM1 and OSM2, the field of view at the aperture (+/- 2 arcsecs = +/- 80 pixels), plus some buffer in case the target should appear near an extreme.

Table 5.2-7: TA1 Science TA Sub-arrays for ACQ and ACQ/IMAGE

Aperture/Mirror	λ Coverage (Å)	Sub-array Sizes (pixels)	Pixel Coordinates of NUV TA1 Sub-array Vertices
PSA or BOA/TA1	1700-3200	345 × 816	(561,123),(561,938),(904,938),(904,123)
PSA or BOA/TA1-RVMM	1700-3200	345 × 816	(397,123),(397,938),(742,938),(742,123)

5.2.3 Camera Assisted Acquisitions

Some targets may be difficult or impossible to acquire using the procedures described above. In these cases obtaining an image of the field days or weeks prior to the COS observations may improve the chances of success. The following situations might benefit from an "early acquisition image":

1) One particular object in a crowded field of comparable objects, when two or more could be difficult to distinguish. Examples include stars in trapezium or R136 type systems, and knots within a complex group of nebulosity or ejecta.
2) A bright target that would violate Bright Object Protection concerns if its light entered the COS Primary Science Aperture.
3) A target whose coordinates are uncertain by more than about two arcseconds.

The strategy for these situations will be to obtain an image of the field including the target ahead of time, identify the target and measure its coordinates in that image with respect to the guide stars. It may be sufficient to measure the location of the target with respect to a reference pixel in the image that was the intended destination, and use that offset to adjust the pointing. If the guide stars used for the image and for the later COS observation were from the same guide star plate, the uncertainty in the target coordinates should be ~1 arc second or less. It should thus be possible to place the target within either the PSA or the BOA on the initial pointing. If coordinates have been specified with respect to the actual guide stars for the COS observation, the spiral search phase may be skipped, and even the peakups may be considered optional.

There will be two ways to obtain the early-acq image; using a CCD instrument or using the COS NUV image mode. Either ACS, STIS, or WFC3 may be used to obtain the image. If COS is used, the spiral search pattern will be executed, and the image obtained with the NUV mirror and MAMA detector will be down-linked at each dwell point. The individual frames can be assembled (by the proposer) into a mosaic with a larger field of view on the ground.

We do not expect to use an acquisition mode involving autonomous acquisition with a CCD followed by an offset to the COS aperture. This would usually require a guide star handoff, which is not routinely supported.

5.3 SCIENCE OBSERVATIONS

5.3.1 Time-tag Mode

The preferred mode of data acquisition for the COS FUV and NUV channels will be Time-tag photon event lists. In Time-tag mode, the DIB inserts a time word once every 32 ms (if there is an event) into the asynchronous XDL or MAMA science data stream, providing a temporal record of the image. Because COS is optimized for observing faint sources with low count rates, memory usage and data storage are minimized using Time-tag data acquisition. There are 18 Mbytes of on-board buffer memory. Each Time-tag event contains 4 bytes. It has been shown that, given the choice, observers generally prefer Accum mode for STIS MAMA data acquisition. However, if most data are taken in Accum mode with COS (especially on the FUV detector), the data volume estimates in the COS Design Reference Mission – which assumed Time-tag data acquisition for most observations – will be significantly under-predicted. Therefore, it has been suggested that Time-tag be the preferred mode, and Accum acquisition be an "available" mode, requiring special permission of the Contact Scientist at STScI to be used.

5.3.1.1 Doppler Correction for Time-tag Science Observations

The flight software does not make any adjustments for the Doppler shift of the spectrum when observing in Time-tag mode. The Doppler correction will be applied during ground processing of the data. HST orbital data will need to be referenced, and a Doppler correction algorithm will need to be incorporated into the CALCOS pipeline.

5.3.1.2 Sub-arrays for Time-tag Exposures

Time-tag exposures will be enclosed in sub-arrays that include the entire detector. On the FUV detector, two sub-arrays are used, one for each detector segment. (Note that the FUV sub-arrays include active detector area as well as the surrounding inactive area where the stim pulses are located.) Should the science need arise, STScI could implement additional sub-array choices for the FUV and NUV detectors, since the capability exists to do so. The sub-arrays needed during target acquisition are discussed in Sec. 5.2.2.

Table 5.3-1 lists the sub-arrays available for Time-tag exposures.

Table 5.3-1: Sub-arrays for Time-tag Exposures

Aperture Used	**Sub-array Size (pixels)**	**Pixel Coordinates of Sub-array Vertices**
FUV XDL:		**(for each FUV segment)**
Whole segment	16384 × 1024	(0,0),(0,1023),(16383,1023),(16383,0)
NUV MAMA:		

Whole detector	1024 × 1024	(0,0),(0,1023),(1023,1023),(1023,0)

5.3.1.3 Pulse-Height Distribution Data for Time-tag Mode Observations

The FUV detector returns five bits of pulse-height information with every photon event. These 5 bits are included in the downlinked telemetry when in Time-tag mode. Ground-based software will create a pulse-height histogram for analysis. An observer can maximize signal-to-noise of their observations using ground software by filtering out suspected background events based on the PHD. Further details about the PHD histograms are discussed in Sections 3.2 and 4.1.7.

5.3.2 Accum Mode

Accum mode will be used primarily for brighter targets, where the high count rate would fill COS on-board buffer memory if the data were taken in Time-tag mode. Data included in Accum mode images are captured in sub-arrays on the FUV detector. No sub-arrays are necessary for NUV science data.

5.3.2.1 Doppler Correction for Accum Mode Science Observations

The flight software will adjust for the Doppler shift of the spectrum, due to the orbital motion of the spacecraft when observing in Accum mode. The Doppler correction is updated whenever the HST orbital motion shifts the spectrum across a pixel boundary. Before the exposure begins, the DIB FSW uses the maximum Doppler correction, the time of zero Doppler shift, and the HST orbital period to compute the contents of a table, which it then uses during the course of the coming exposure. The table contains, among other things, the length of time until the next Doppler correction update and the value of the next Doppler correction. During the exposure, a timer in the DIB is used to generate an interrupt to the DIB FSW whenever it is time to update the Doppler correction, based on the contents of the table. At each update, the timer is reset to generate the next interrupt when the next Doppler update needs to occur. The dispersion of the relevant grating (see Tables 1.3-1, 1.3-3) is used on the ground to compute the maximum Doppler correction in integer pixels. Doppler corrections apply to science exposures on both the FUV and NUV detectors. Proposers will be advised that Accum exposures longer than 900 seconds may blur the FUV spectra by 1-2 pixels (~1/6 to 1/3 of a resolution element) due to wavelength dependent deviations from the mean Doppler correction. Table 5.3-2 shows the maximum number of integer pixels that the spectrum could be shifted for the Doppler correction. These values are based on a maximum HST Doppler correction of approximately +/- 7.4 km/s ($= 2\pi R / t$, where $R \approx 6800$ km orbital radius from the center of the Earth, and $t \approx 96$ min = 5760 sec is the orbital period of HST).

Table 5.3-2: Maximum Doppler Shifts and BFACTORs

Grating	$\lambda_{central}$ (Å)	Dispersion * (Å/pixel)	BFACTOR (=$\lambda_{central}$/Disp) (pixels)	Max shift (integer pixels)
G130M	1300	~0.0094	138298	+/- 3
G160M	1590	~0.0118	134746	+/- 3
G140L	1400	~0.0865	N/A	+/- 0
G185M	1875	~0.0273	68681	+/- 2
G225M	2250	~0.0342	65789	+/- 2
G285M	2850	~0.0400	71250	+/- 2
G230L	2300	~0.3887	N/A	+/- 0

* Dispersions are based on ray trace models. These values should be updated with the “as built” values, as determined during instrument integration & test.

5.3.2.2 Sub-arrays for Accum Mode Science Observations

Figure 5.3-1 shows the sub-arrays used for Accum mode science observations made with the COS FUV channel. (The sub-arrays that are necessary for target acquisition are discussed in Sec. 5.2.) Sub-arrays are necessary with the FUV detector because the 18MB of on-board memory cannot hold a complete FUV image (containing both detector segments). A single sub-array is used for Accum mode science observations with the NUV channel that includes the entire MAMA detector.

Referring to Fig. 5.3-1, an Accum mode science observation through the PSA would include (for each segment) the lower (blue) sub-array plus the two pink sub-arrays that include the stim pulses. Wavelength calibration observations would include the upper (green) sub-array plus the two stim pulse windows. Thus each type of observation would have six sub-arrays over the two segments. Table 5.3-3 lists the approximate pixel coordinates for the sub-arrays taken with each segment of the FUV detector. Note that buffer memory will be allocated to the smallest rectangle of $2^n \times 2^m$ dimensions that encloses the desired sub-array, even if the sub-array dimensions are not divisible by a power of 2.

Table 5.3-3: Sub-arrays for Accum Exposures with the FUV Detector

Segment and Aperture Region	Sub-array Size (pixels)	Pixel Coordinates of Sub-array Vertices
Segment A:		
PSA/BOA/FCA	16384 x 128	(0,420),(0,548),(13683,548),(13683,420)
WCA	16384 x 128	(0,524),(0,652),(13683,652),(13683,524)
STIM Pulse A1	64 x 32	(313,9),(313,40),(376,40),(376,9)
STIM Pulse A2	64 x 32	(15937,960),(15937,991),(16000,991),(16000,960)
Segment B:		
PSA/BOA/FCA	16384 x 128	(0,476),(0,605),(13683,605),(13683,476)
WCA	16384 x 128	(0,579),(0,707),(13683,707),(13683,579)
STIM Pulse B1	64 x 32	(324,1),(324,32),(388, 32),(388,1)
STIM Pulse B2	64 x 32	(15962,971),(15962,1001),(16025,1002),(16025,971)

Figure 5.3-1: *Schematic of Accum mode sub-arrays for one segment of the FUV detector. The outer gray box represents the 16384 x 1024 pixel region that encloses the active detector area and the inactive region where the stim pulses are projected. The black box represents the full active area of the detector. The middle (blue) window shows the sub-array for science spectra obtained through the PSA, BOA, or FCA apertures; the upper (green) window shows the sub-array for the wavelength calibration (WCA) spectra. Events from the main sub-arrays and two small pink sub-arrays that enclose the stim pulses are accepted and processed; all other events are discarded. (Drawing not to scale.)*

5.3.2.3 Pulse-Height Distribution Data for Accum Mode Observations

A PHD histogram is dumped with every Accum mode image with the FUV detector, consisting of 256 bins (128 bins for each segment) of 32 bits each. The contents of all PHD bins stored in CS memory are cleared at the beginning of an exposure and dumped at the end of an exposure. The PHD data can indicate the health of the detector and whether background events are being properly discriminated. Further details are discussed in Sections 3.2 and 4.1.7. There are no PHD data for the NUV detector.

5.3.3 FUV Gap Coverage

The FUV detector contains two segments whose active areas are separated by a gap approximately 9 mm wide (see Fig. 4.1-3). The optical image of the spectrum is continuous, but the wavelengths that fall on the gap are not recorded. The area between the two segments of the FUV detector causes a 18-20Å gap in the wavelength coverage for the G130M and G160M gratings. Depending upon the science requirements of the observation, these wavelengths can be brought onto the active area of the detector by rotating OSM1 and positioning the z focus. (When a z focus adjustment is made to bring the missing wavelengths into focus, the edges of the spectrum may be somewhat out of focus. A table of OSM1 step numbers for rotation and z focus for each FUV grating position is given in DM-05.) A typical scenario might be that a spectrum of the target is acquired with all mechanisms in their optimum positions. OSM1 is then rotated and repositioned to bring the missing wavelengths onto the detector and into focus. The calibration of the OSM1 positions necessary to observe the wavelengths in the gap will be conducted during instrument calibration and SMOV. Each FUV grating will have three supported setup positions — one is primary, and the other two are secondary (see Table 2-3). Wavelengths that fall on the gap with one of the settings will be visible with at least one of the others. The observer may select one of the settings. If an OSM1 rotation is commanded to bring missing wavelengths onto the detector, after having observed or set up in the nominal focus configuration for a particular grating, the OSM1 rotation must approach the offset step position from the preferred direction positive motor steps.

5.3.4 Selectable Stim Pulse Rates for the FUV Detector

Stim pulse rates are chosen based on exposure time only, and are independent of the acquisition mode (either Time-tag or ACCUM). The stim pulse rates can be commanded, with the object to attain at least several hundred counts in each stim pulse per exposure. Four stim rates are available, at 0, 2, 30, and 2000 counts per second. Observations with long (>100 seconds) commanded exposures will use the 2 Hz rate. Short duration exposures (10-100 s) should use the 30 Hz rate. The highest rate of 2000 Hz will be used for observations <10s and during ground calibration; this rate may also be used as a diagnostic mode on orbit. The stim pulses may be turned off by setting the rate to be 0 Hz. The 0 Hz setting should be used during all phases of target acquisition with the FUV detector, as well as during Local Rate Check (BOP) exposures. (In fact, the 2000 Hz setting could trigger a local rate violation if it were left on during an LRC exposure.) The stim pulses should be turned back on to an appropriate setting for all science exposures.

Since the stim pulse rates can be commanded and the exposure time of an observation is known, the total counts received in the stim pulses can, in principle, be used to calculate the dead-time correction for an exposure.

5.3.5 Detector Lifetime Adjustments

"Detector lifetime adjustments" may be necessary to maintain the performance of the microchannel plate-based COS detectors. After considerable charge extraction at particular locations on the MCP detectors has occurred, the quantum efficiency will drop. This degradation is localized, so moving the locations where science spectra are projected onto the detectors will recover the QE performance. Resiliency to QE degradation is a function of the quality of the flight MCPs. The baseline aperture plate design allows flat-fielding with the internal calibration lamps over the central ~ ± 1.75 mm of the FUV detector. Figure 1.3-8 shows the locations of 5 potential FUV lifetime adjustment positions of the PSA. (Recall that the aberration corrected image projected onto the detector is much smaller than the size of the aperture, hence the overlapping aperture positions in Fig. 1.3-8 deliver point source spectra to distinct detector regions.)

The specification on the FUV detector is that the rate of gain degradation be < $100\%/C/cm^2$. This requirement translates to a 1% loss in detection quantum efficiency with 6.1×10^9 photons across the spectrum or 1.3×10^6 photons/resol. Such a loss would not compromise COS's ability to achieve its science goals, and yet the COS Design Reference Mission indicates that only a few $\times 10^9$ events will be observed *over the entire COS (~7 yr) mission through each channel*. Including events received for flat-field and flux calibration, we may conservatively estimate 10^{10} events observed through each channel during the COS mission. Spreading the predicted 10^{10} events uniformly among the ~4800 total FUV resols results in each resol observing $\sim 2 \times 10^6$ events.

On the FUV detector, there are ~2400 independent spectral resolution elements (resols) per segment (R = 20,000 modes), with each resol occupying ~40×200 microns (≈ 7×10 pixels ≈ $0.008\ mm^2$/resol). As stated above, each resol will be capable of supporting 1.3×10^6 events/resol with only a 1% loss in detection quantum efficiency. Even if some regions (e.g., rest Ly α) receive 10 times more events, only a few fresh detector regions are necessary to maintain the COS FUV performance. We suggest making FUV detector lifetime adjustments as necessary, when noticeable QE loss or gain drop has occurred or as observed in periodic gain maps. Section 5.3.5.1 discusses the physical mechanism responsible for loss in DQE, the diagnostics for monitoring the DQE, recommendations on when to adjust the spectrum location, and strategies for mitigating impacts to instrument operations.

The image at the NUV MAMA quickly degrades as a function of radius from the best focus aperture position. Hence, no detector lifetime adjustments are possible that will retain the full spectral resolution. However, spectra received from each grating will shift position on the MAMA as the gratings are scanned in wavelength. In addition, each grating is expected to be slightly mis-aligned with the other gratings and will use its own detector rows in the dispersion direction. Thus, lifetime adjustments for the NUV detector are not viewed as necessary. Limiting the number of detector lifetime adjustments for the FUV detector minimizes the number of times the new detector regions need to be re-calibrated (in terms of flat-fielding and flux calibration), resulting in a substantial savings in calibration orbits over the mission duration. Indeed, calibration – using bright external sources and internal lamps – may be one of the principal causes of detector performance degradation.

5.3.5.1 Microchannel Plate Gain Diagnostics & Spectral Adjustment Strategies

This section pertains to the repositioning of the spectrum on the FUV detector to compensate for fluence induced gain depression that eventually will lead to a loss of detection quantum efficiency. The purpose of this section is to provide practical guidance in determining when the FUV spectrum should be moved in the cross-dispersion direction on the detector.

It is important to understand the mechanism that results in the loss of detection quantum efficiency to appreciate the diagnostic tools. For each detected event a certain amount of charge is extracted from the microchannel plates. The amount of charge is characterized by the modal gain, A_{e-}, and is $\approx 1X10^7$ e^-/event for the FUV01 detector. This gain will decrease over time with total extracted charge due to physical and chemical reactions in the microchannel walls. For new microchannel plates, the gain decreases rapidly with extracted charge. After sufficient charge has been extracted the rate of the gain sag reaches a plateau. This is why the COS plates are preconditioned (or "scrubbed") with a long exposure to UV radiation in the lab until *the rate of change* of the gain reaches an acceptable level for the mission. This rate of change in gain is quoted in terms of the percent change in modal gain for every coulomb of charge extracted per unit area. The microchannel plates in FUV01 have undergone extensive scrubbing during their processing. Laboratory measurements show that the rate of gain degradation to be < 100%/C/cm^2. Thus, if the modal gain is at channel 10 and then 0.5 C/cm^2 is extracted from the microchannel plates, the modal gain will drop to channel 5 at the location of the charge extraction.

The actual amount of charge extracted per event, or pulse height, is distributed about the modal gain in a pseudo-gaussian distribution, referred to as the pulse-height distribution (see Figure 5.3-2 which shows the measured pulse-height distributions for FUV01 segment A and segment B). The time-to-digital converters have upper- and lower-level thresholds on the charge amplifier output signal. If the pulse height for an event falls between the thresholds, the event is processed and results in a digital event. If the pulse height falls below the lower level threshold or above the upper level threshold the event is rejected.

Now consider the relationship between the lower level threshold and the event pulse height. As the modal gain begins to drop over time (referred to as “gain sag”) then those events at the lower end of the pulse height distribution will fall below the lower level threshold. Thus, while the event did initiate an electron cascade in the microchannel plate stack, the event will go unprocessed by the electronics and is therefore undetected. This effect will lower the detection quantum efficiency of the detector and thus the accuracy of the sensitivity calibration of the instrument will degrade.

There are several ways to monitor the gain sag directly and indirectly. The most informative method for monitoring the gain of the microchannel plates is to acquire a time tag data set and create a pulse height image. The pulse height image is a 2-D array where each pixel contains the average value of gain for that position. To form a high quality gain map requires a minimum of 10 events/pixel. Relative variations in the pulse height image are then direct tracers of gain sag. This technique provides the best information as it tracks the local variations in the gain performance. It is expected that a gain map of the detector will trace the region where the spectrum falls and highlight regions where charge has been preferentially extracted. It is worth noting that the pulse height information contained in time tag data contains only 5-bits of information, or 32 bins.

The second method is to acquire a full pulse height distribution at 7-bit resolution for the entire detector. The full pulse height distribution provides a good measure of the performance of the microchannel plates where the events were detected, but it does not provide the spatial information necessary to fully understand the state of the microchannel plates. For example, if one region of the active area has seen more light than the rest of the detector due to spectral variations, this may not be evident in a pulse height distribution collected from a different spectral distribution. However, it is still a useful tool for monitoring the microchannel plate detector and is the only tool for monitoring an ACCUM image.

A total exposure map can be used to correlate observed variations in gain with measured fluence. However, a total exposure map is a lower limit on the number of events detected, since only those events acquired during an exposure are downloaded from the spacecraft. Thus, an exposure map should be considered a secondary technique for monitoring and managing the fluence through the microchannel plates. Also note

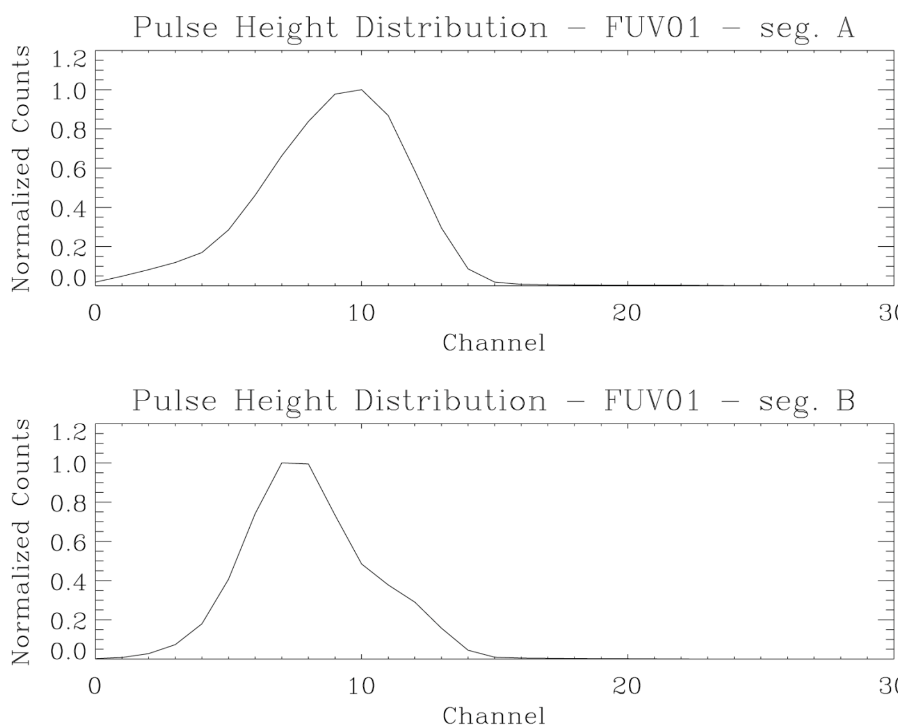

Figure 5.3-2: *This figure presents the pulse-height distribution from FUV01 segments A and B in 5-bit resolution mode, the digitization used in TTAG mode.*

that is a total exposure map is maintained, which the IDT recommends, the FUV detector must be corrected for thermal and geometric distortions prior to being added to the total exposure map.

The absolute photometric accuracy of HST scientific instruments is typically only 2-3%. Based on this accuracy the IDT recommends that the losses of more than 1% in the detection quantum efficiency warrant one of two corrective actions. One, the instrument sensitivity curve can be recalibrated, or two, the spectrum can be moved. Operationally, this first option of recalibrating the sensitivity may prove expedient while preparations are made for moving the spectrum. When the spectrum is moved to a pristine region of the active area, the modal gain will increase to the nominal value, since minimal charge has been extracted at the new location. This means that another 10^7 events/resol can be extracted from the microchannel plates before the detector experiences a 1% loss in detection quantum efficiency. It is also acceptable to choose to not take corrective action until 2 or 3% of the detection quantum efficiency, thus extending the periods between recalibration efforts. However, the decision to extend the charge extraction limit beyond the IDT's recommendation is left to the Space Telescope Science Institute.

Examining Figure 5.5.-3, we see that as more charge is extracted from the plates the rate at which the quantum efficiency drops increases and that each segment exhibits slightly different performance. In fact, in segment A the integrated percentage drops approximately linearly with modal gain out to channel 3. The integrated percentage is essentially a drop in detection quantum efficiency as it represents events falling below the lower level threshold. The integrated percentage for segment B varies more slowly with channel out to channel 3 and then becomes more non-linear.

Based on the measured performance of the FUV01 microchannel plates the IDT recommends the sensitivity of the COS FUV channel be recalibrated for every drop of 1 channel count in the modal gain for observed decreases in the modal gain of <30% (three channel counts) from the in-flight pulse height distribution as measured during SMOV. Once the modal gain has dropped 3 channels or more the spectra should be repositioned and COS FUV channel completely recalibrated. This will insure that the COS calibration remains accurate.

Practically speaking this means that a recalibration is sufficient for up to a 30% change in the modal gain. This corresponds to 0.3 C/cm^2 of charge extracted. Converting this to events/resol we find that 3.8×10^7 events per resolution element can be expected before repositioning the spectrum is required.

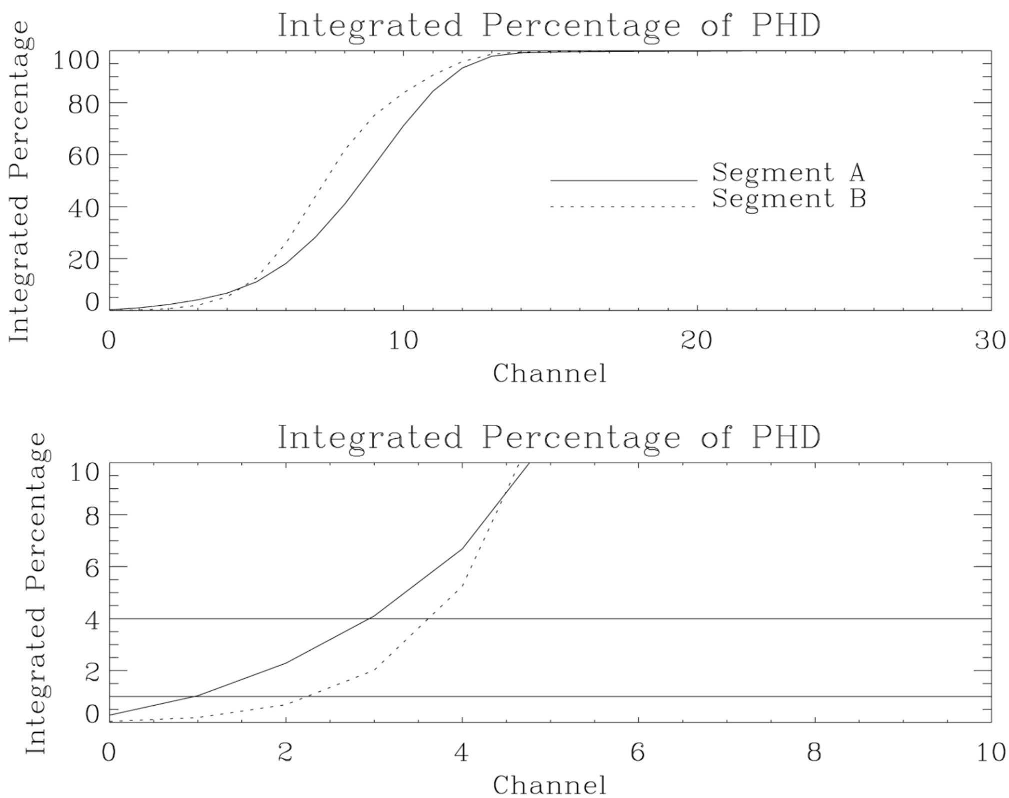

Figure 5.3-3: *The integrated pulse-height distribution for FUV01 segments A and B. The top panel is full scale and the lower panel shows the same data, but with an expanded y-scale. The horizontal lines in the lower panel represent 1% and 4% loss of detection quantum efficiency. The vertical line denotes the maximum allowable change in the modal gain before the spectra must be repositioned on the detector.*

5.3.6 Aperture Mechanism Motions when Using the BOA

Figure 1.3-8 shows the layout of the aperture plate. As noted in Sec. 1.3.4, two design requirements place constraints on the usage of the BOA: (1) the flat-field calibration aperture (FCA) must be masked from transmitting wavelength calibration lamp photons during wave cal exposures; and (2) severe off-axis aberrations in the NUV channel require that a single, preferred position in the HST focal plane for placement of the science aperture be used. Hence, the BOA must be moved to the preferred PSA position for science observations. For example, if PSA position 2 in Fig. 1.3-8 were the preferred aperture position for FUV observations, then the BOA would be moved to PSA position 2 to obtain science data. Assuming that wavelength calibration spectra would be obtained before and after the BOA science exposure, the first wave cal exposure would be taken prior to moving the BOA to PSA position 2 (while the FCA is still masked), and the subsequent wave cal exposure would be taken after moving the BOA back to its stowed position (with the PSA back at PSA position 2 and the FCA once again masked).

5.3.7 FUV Single Segment Operational Scenarios

The COS FUV detector consists of two distinct segments which are, at the lowest commanding level, operated and read out independently. There are three FUV states available for science observations: both segments on (HVNOM), or one or the other segments at a low HV level, where the HV is not high enough to initiate electron cascades (HVNOMA or HVNOMB). For most FUV observations, both detector segments will be utilized. However, there are circumstances where operating with one detector segment at the nominal HV and the other in the “low” (or SAA) HV level can benefit the science program. Such programs include, but are not limited to:

1) One of the detector segments suffers a failure (e.g., of an HVPS) and becomes inoperable. Science could continue to be conducted with the other segment. In this case, one segment operates as usual and the other segment is not powered.
2) Sources with unusual spectral energy distributions at FUV wavelengths (bright emission lines or rapidly increasing/decreasing continuum slopes), where the count rate on one detector segment may be over-illuminated and would exceed the bright object protection, but the other segment would be safe for observing.
3) Sources with unusual spectral energy distributions at FUV wavelengths (bright emission lines or rapidly increasing/decreasing continuum slopes), where the count rate on one detector segment would be high but safe, and the other segment would have a relatively low count rate. In this case, if the science to be done were on the low count-rate segment, operating just that segment may result in a substantially reduced dead-time correction.
4) Observing the very far-UV (VFUV; i.e., “FUSE band”) wavelength region between <900 – 1100 Å on the short wavelength segment B with the G140L grating. The effective area is predicted to be ~100 times lower at VFUV

wavelengths, and so any source producing reasonable count rates in the VFUV may over-illuminate segment A.

Note that there should be no special calibration requirements for single-segment operations. Wavelength and flat-field calibration procedures will remain the same for a particular segment whether the other segment is operating or not.

5.3.8 FP-SPLITs

FP-SPLITs may be used to enhance signal-to-noise in spectroscopic data by allowing the observer to correct for fixed pattern detector features through a sequence of exposures taken at slight offsets in the dispersion direction. On the exposure logsheet the observer will specify either FP-SPLIT = YES or FP-SPLIT = NO; "YES" will be the default mode. The baseline is to use 4 FP-SPLIT positions: a nominal position, 1 position toward shorter wavelengths, and 2 positions toward longer wavelengths. Depending on which channel is being used, OSM1 or OSM2 will be adjusted slightly in rotation to achieve the offset wavelength positions. It is not necessary to adjust the ApM, the sub-arrays, or the z-focus position of OSM1 for FP-SPLIT exposures. However, it is necessary that the OSM1 or OSM2 rotation to each FP-SPLIT position approach the desired step number from the preferred direction positive motor steps. The number of steps to rotate the mechanisms is one (1) for each adjacent FP-SPLIT position. Tables 5.3-4 and 5.3-5 indicate the amount that a particular wavelength moves in the dispersion direction on the detector due to one rotation step of the appropriate mechanism. The subsequent spectra will be aligned and co-added on the ground. Wavelength calibration spectra should be obtained for at least one of the FP-SPLIT exposures, and possibly for each FP-SPLIT position, especially if the 4 exposures take longer than one orbit to complete. (In general, at least one wavelength calibration spectrum should be obtained per orbit.)

Table 5.3-4: Image Movement Due to One OSM1 Rotation Step

	Image Movement in Dispersion Direction		
FUV Optic	**mm**	**pixels**	**Å**
G130M	1.45	240	2.4
G160M	1.45	240	2.4
G140L	1.45	240	19.2

Table 5.3-5: Image Movement Due to One OSM2 Rotation Step

	Image Movement in Dispersion Direction		
NUV Optic	**mm**	**pixels**	**Å**
G185M	1.23	49	1.8
G225M	1.23	49	1.7
G285M	1.23	49	2.0
G230L	1.23	49	18.6

5.3.9 NUV Imaging Observations

Some elements of the discussion in this section are based on material presented in the CU TER's COS-11-0024 ("TAACOS: NUV Phase I Report") and COS-11-0027 ("TAACOS: Target Acquisition with the TA1 Mirror"). In areas of discrepancy, this document shall take precedence.

The NUV optics mounted on OSM2 include a flat mirror (TA1) that produces an image of the sky with a field of view slightly larger than the diameter of the aperture. It will have several uses. During SMOV it will be used to verify alignment and the NUV plate scale – e.g., checking the distance from the calibration aperture to the target in the science aperture when it is properly centered. During normal science operations, it will be used for NUV imaging target acquisition, to measure the offset of the target in the aperture in the dispersion direction in order to improve the precision of the wavelength scale, or to map the field as an early acquisition image as described in Sec. 5.2.3. There will be no Doppler corrections made during NUV imaging observations, nor will FP-SPLITs be allowed.

The field of view imaged by TA1 is circular, essentially limited by the size of the aperture. Sources located within ~0.3 arcseconds of on-axis will transmit essentially their total flux and will be in focus. Sources located further off-axis will begin to vignette, because flux from the aberrated halo is lost outside the aperture, and will be out of focus due to off-axis aberrations (e.g., coma). Sources can be detected out to a radius of ~2 arcseconds off-axis, for a total circular field of view of ~4 arcseconds diameter.

The mirror will have two values of reflectivity: a primary reflection off the mirror surface (designated TA1) to be used for faint sources, and an attenuated reflection (designated "TA1-Rear-View-Mirror-Mode" or TA1-RVMM) for bright targets. The spectral coverage includes the entire NUV bandpass from ~1650-3200Å, limited at the short wavelength end by the order separation filter. The attenuated TA1-RVMM is achieved by using the front surface reflection of the order separation filter, which is mounted at a slight angle from normal incidence. The TA1-RVMM will have roughly 4% of the throughput of the primary TA1 imaging mode. Each reflectivity mode (TA1 and TA1-RVMM) can be accessed by commanding different step numbers of OSM2. There will not be any selectable filters.

The images produced by the TA1 and TA1-RVMM reflections are located on the NUV MAMA detector as shown in Figure 5.3-3. The TA1 reflective surfaces are tilted slightly (relative to the NUV gratings) so that the images appear between the stripes. This helps to mitigate charge extraction at the locations of the science and wavelength calibration spectral stripes. The images are formed by the NCM3b camera mirror.

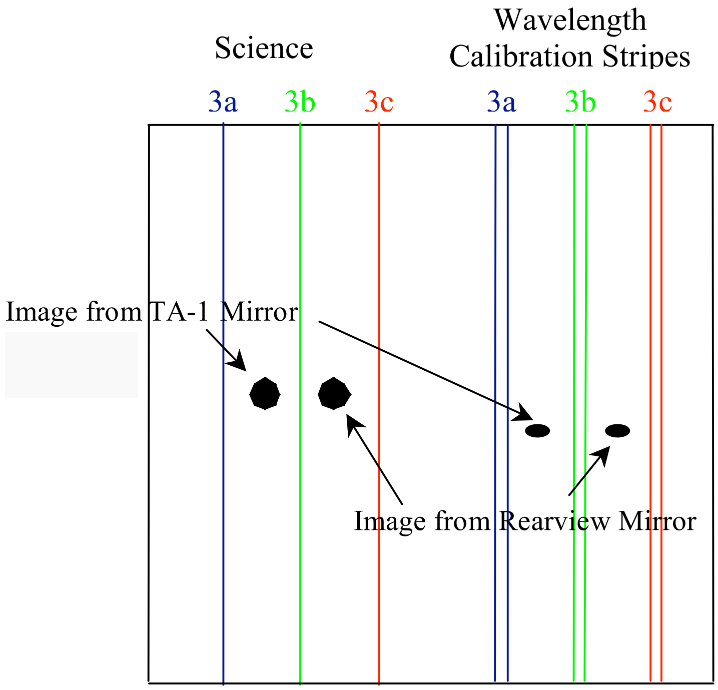

Figure 5.3-3*: Depiction of the locations of the TA1 images on the NUV MAMA detector. The science and wavelength calibration images from the primary TA1 mirror reflection are displaced 1.375 mm (= 55 pixels) toward the left (higher column numbers), and the TA1-RVMM images are displaced –1.375 mm (= -55 pixels) toward the right (lower column numbers) of the associated science and wavelength calibration stripe B (i.e., NCM3b stripe).*

The dynamic range for a given reflectivity mode will essentially be limited by the count rate capability of the MAMA detector, combined with the throughputs attained through the PSA and BOA for science targets and WCA for the wavelength calibration lamp. A major concern when using the TA1 imaging mode is over-illumination of the NUV MAMA. The local count rate limit is ~200 counts/s/pixel. The central pixel of a TA1 image of a sample QSO spectral source achieves this count rate at a mean flux level of approximately F_λ=1.3×10^{-14} ergs/cm^2/s/Å. Because of the uncertain flux and variability of astrophysical targets, the exposure times used for TA1 imaging should be conservative. For targets brighter than F_λ=1.3×10^{-14} ergs/cm^2/s/Å, two methods of flux attenuation are possible. The first is to use the TA1-RVMM mode, which attenuates the flux by a factor of ~25. The second is to use the BOA, which attenuates flux by a factor of 100. Very bright targets could be attenuated with both the BOA and TA1-RVMM. Simulations show that sources with mean F_λ > ~6 × 10^{-11} ergs/cm^2/s/Å would not be observable with the TA1 mirror.

Exposure time estimates for each of the TA1 imaging modes are shown in Figure 5.3-4. The solid lines plot the exposure times that attain S/N = 14 (~200 total counts) in the brightest pixel in a NUV+TA1 image, whereas the dashed lines show the exposure times to achieve S/N = 100 in the brightest pixel. The shortest exposure times shown for each imaging mode assume a maximum local count rate of 100 counts/s/pixel. Exposure times in green are un-attenuated (through the PSA); those in red, blue, and magenta have been attenuated by the RVMM, BOA, and BOA+RVMM, respectively.

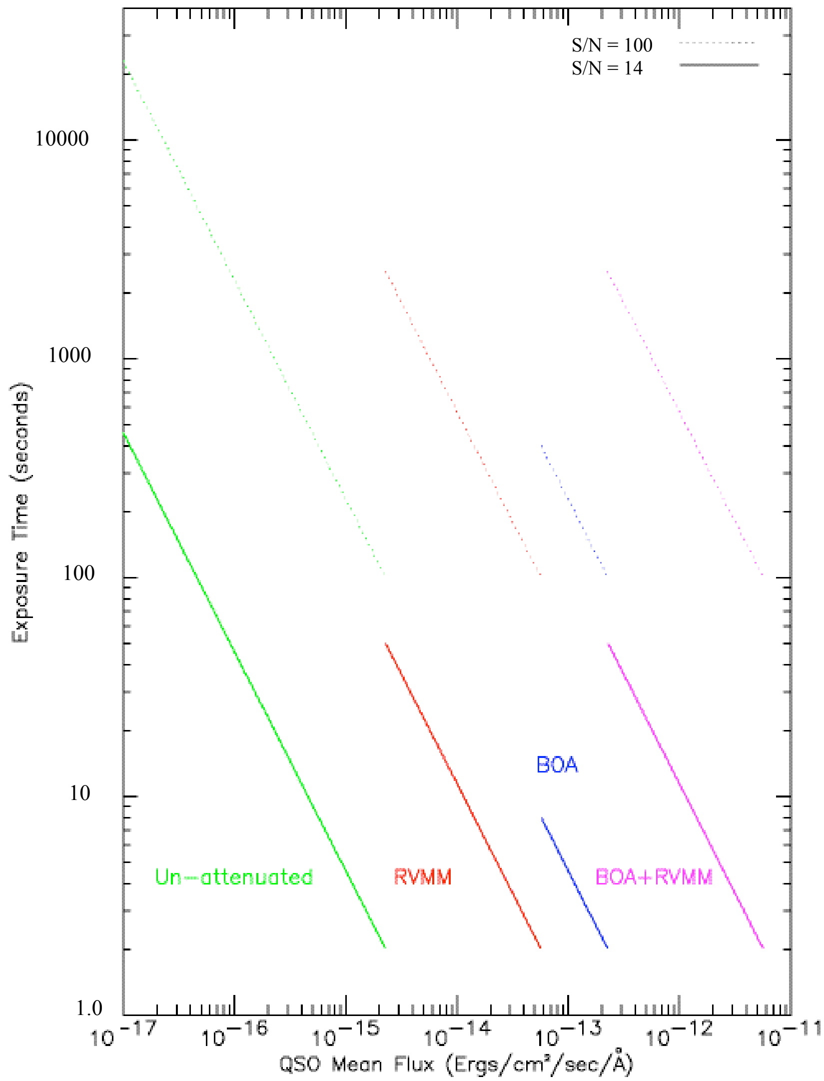

Figure 5.3-4: *Estimated exposure times* versus *QSO mean flux for each of the TA1 imaging modes. Green curves are for the un-attenuated TA1 images through the PSA, red curves are through the PSA with the TA1-RVMM, blue curves are for TA1 images using the BOA, and magenta curves are for TA1-RVMM images through the BOA. The lower set of solid-line curves achieve S/N = 14 in the brightest pixel, while the upper dashed-line curves achieve S/N = 100 in the brightest pixel.*

5.4 CALIBRATIONS

This section discusses calibration data that may be obtained in orbit to support routine reduction of science observations. Both wavelength and flat-field calibration data should be obtained in Time-tag mode to maximize the scientific content. Doppler corrections should not be made to calibration data, either on the ground for Time-tag exposures or on orbit if for some reason Accum mode had to be used to collect the calibration data.

5.4.1 Wavelength Calibration

Late in the development of the COS instrument it was discovered that the OSM1 and OSM2 mechanisms were exhibiting drift, where the magnitude of the drift depended upon the size of the mechanism motion. For example, for single step motions there was essentially no drift but for large motions between gratings there could be up to tens of pixels of drift over 20 minutes. A preliminary algorithm was assembled and tested using data acquired during final calibration that tracked and corrected the mechanism drift. In short, the wavelength calibration lamps would be flashed up to six times per exposure with the external shutter OPEN. The wavelength calibration spectra would then be embedded in the science data. A cross-correlation technique was used to track the drift using the wavelength calibration spectra. Once the time dependent drift was characterized it was then removed from the science data stream. The actual number of embedded wavelength calibration spectra depends upon the exposure time and in shown in Table 5.4-1 below. The number of wavelength calibration spectra were chosen to accurately sample the observed drift motion. The wavelength spectra are not expected to be equally spaced in time, however, the final sampling frequencies have yet to be defined. The exposure times for the embedded wavelength calibration spectra are presented in Table 2.2-2.

Table 5.4-1

Exposure Time	# of Wavelength Spectra
0 – 60 sec	1
60 – 300 seconds	2
300 – 600 seconds	3
600 – 1200 seconds	4
1200 – 3000 seconds	5
3000 – 6500 seconds	6

5.4.2 Flat-field Calibration

The basic flat-field calibrations will be obtained during the ground-based calibration of COS. These data should be applicable to either single exposures or multiple exposures made with the FP-SPLIT procedure. We expect them to remain valid until charge depletion causes the pixel-to-pixel variations in the detector response to change significantly. COS will include redundant flat-field lamps as part of the on-board calibration subsystem. It will be a spectrally dispersed calibration signal. Observations of the lamp will be used to monitor changes in the detector flat-field response, and to derive updates to keep the calibration data in the pipeline database relevant and useful. We expect that these updates will be infrequent. A calibration maintenance proposal that runs once a month or so should be adequate.

5.4.3 Signal-to-Noise Ratio

There are three basic approaches to obtaining and processing COS spectra. They are described here in order of increasing complexity, which is also the order of potentially increasing S/N in the final product. We believe that the first two may meet our requirement to achieve S/N = 100, and the third may be an option for reaching higher values. The quality of the flat-field data will determine the range of S/N in the resultant spectrum that can be achieved with the first two options.

Single exposure with flat-field.

The simplest approach is to obtain a spectrum at a single setup position, normalize the two dimensional data with a flat-field map, then extract the one-dimensional spectrum. The resultant S/N will be limited by statistical noise in both the spectrum and flat-field data. The flat-field data may have been obtained during a previous calibration measurement, perhaps even during the ground-based test program. It is not necessarily a contemporaneous exposure.

Multiple exposures with flat-field.

A slightly more complex procedure will be to break the exposure into four or more subexposures, and record the raw data at different positions on the detector. Each subexposure is normalized with the same flat-field data. The spectral data are aligned in wavelength and added together. This merging could be done either in the adjusted two-dimensional data or in the adjusted and extracted one-dimensional spectra. This procedure will reduce the effect of the statistical noise in the flat-field data, and will allow higher S/N to be achieved in the resultant spectrum for the same data quality. The simplest approach will be to use the FP-SPLIT procedure, which rotates the grating slightly between subexposures, and displaces the spectra parallel to the direction of dispersion. However this approach does not demand that the subexposures be displaced purely in dispersion.

FP-SPLITs with granularity vector.

From an operational point of view this is identical to paragraph 5.3.8. A different data reduction approach may allow higher signal-to-noise ratios. COS may be used to observe stars that are near the bright end of its range. The counting statistics may allow S/N higher than the available flat-field data can support. In this case a procedure for using FP-SPLITs to derive the spectrum and granularity vector directly from the same data set can be used. This algorithm does demand that the offsets be purely in the dispersion direction. No flat-field data are required, and the S/N of the resultant will be very close to the Poisson limit of counting statistics in the raw spectrum data. This will be an optional data processing path, which an observer may choose. It will not be the standard result of the pipeline processing.

5.4.4 Sensitivity Calibration

The sensitivity calibration is the relationship between observed count rates and astrophysical flux. It has been predicted from the instrument design, will be measured during pre-launch Thermal-Vacuum testing, and will be calibrated definitively using standard stars early in the mission. The sensitivity may be checked once a year or so to track changes. It is not a calibration that is repeated frequently.

5.4.5 Dark Count Rates

Background dark counts will be subtracted from every observation during the reduction process. The dark count rate can either be estimated from a region of the detector far from the optical spectrum in the cross-dispersion direction, or from dedicated calibration exposures taken with the shutter closed and all sources of light off. Dark count observations are usually part of a routine calibration proposal that can be run frequently.